UCLA
UCLA Electronic Theses and Dissertations

Title
The structure of the hydrated electron in bulk and at interfaces: Does the hydrated electron occupy a cavity?

Permalink
https://escholarship.org/uc/item/26r2n6rb

Author
Casey, Jennifer Ryan

Publication Date
2014

Peer reviewed|Thesis/dissertation

eScholarship.org Powered by the California Digital Library
University of California

University of California

Los Angeles

The structure of the hydrated electron in bulk and at interfaces: Does the hydrated electron occupy a cavity?

A dissertation submitted in partial satisfaction

of the requirements for the degree

Doctor of Philosophy in Chemistry

by

Jennifer Ryan Casey

2014

© Copyright by
Jennifer Ryan Casey
2014

Abstract of the Dissertation

The structure of the hydrated electron in bulk and at interfaces: Does the hydrated electron occupy a cavity?

by

Jennifer Ryan Casey

Doctor of Philosophy in Chemistry

University of California, Los Angeles, 2014

Professor Benjamin J. Schwartz, Chair

Since its discovery over fifty years ago, the hydrated electron has been the subject of much interest. Hydrated electrons, which are free electrons in water, are found in fields ranging from biochemistry to radiation chemistry, so it is important that we understand the structure and dynamics of this species. Because of its high reactivity, the hydrated electron's structure has proven difficult to pin down, especially its molecular details. One-electron mixed quantum/classical molecular dynamics simulations have proven useful in helping elucidate the structure of the hydrated electron. The picture most commonly presented from these studies is one of the electron residing in a cavity, disrupting the local water structure much like an anion the size of bromide. Our group has recently proposed a completely different structure for the hydrated electron, which arose from rigorous calculations of a new electron-water potential. The picture that emerged was of an electron that does not occupy a cavity but instead draws water within itself; this non-cavity electron resides in a region of enhanced water density. The one-electron cavity and non-cavity models all predict similar experimental observables that probe the electronic structure of the hydrated electron, such as the optical absorption spectrum, which makes it difficult to determine which model most accurately describes

the true structure of the hydrated electron.

In this thesis, we work to calculate experimental observables for various simulated cavity and non-cavity models that are particularly sensitive to the local water structure near the electron, in an effort to distinguish the various models from each other. Two particular observables we are interested in are the resonance Raman spectrum and the temperature dependent optical absorption spectrum of the hydrated electron. We find that for both of these experiments, only the non-cavity model has qualitative agreement with experiment; the cavity models miss the experimental temperature dependence in the optical absorption spectrum and show the wrong trends in the resonance Raman spectrum. We also explore the differences between non-cavity and cavity models by quantifying the electron-water overlap, referring to the non-cavity model as an 'inverse plum pudding,' where the water molecules are embedded within the electron density.

Finally, we examine hydrated electrons in the presence of an air/water interface. Experiments indicate that most likely electrons do not reside at the surface, and if they do, they have structural and dynamical properties reminiscent of the bulk. Our calculated Potentials of Mean Force indicate that both cavity and non-cavity electrons prefer to be solvated by the bulk, but that the cavity electron has a local free energy minimum near the surface. These calculated interfacial cavity electrons behave very differently than cavity electrons in the bulk, in direct contrast to experimental evidence. From the work presented in this thesis, it is clear that the non-cavity electron is the most appropriate one-electron model we have for the structure of the hydrated electron.

The dissertation of Jennifer Ryan Casey is approved.

Peter M. Felker

Vidvuds Ozolins

Benjamin J. Schwartz, Committee Chair

University of California, Los Angeles

2014

To my family and friends. Your love and support mean everything to me.

Table of Contents

List of Figures

List of Tables

Acknowledgments

I have grown and changed considerably during my time at UCLA, and I have many people to thank for their support and encouragement throughout the years. First and foremost I want to thank my advisor, Professor Benjamin Schwartz. I admire Ben's enthusiasm for science, and he has taught me the importance of the big picture. Ben has always proven to be full of good ideas and inspiration, which I appreciate. I also want to thank other faculty members at UCLA, especially Dr. Lavelle and Dr. Pang. I have a great respect for their teaching philosophies, and they have provided me with incredible insight into teaching at a university.

I was fortunate enough to have a wonderful group of peers during my first year as a graduate student. I still think about that year with fondness, as we had such ridiculous experiences navigating graduate school together. I have never had such a close-knit group of friends, and the experience was wonderful. One friend in particular that I want to thank is Xiaoming Zhu. Despite my inferior math skills, Xioaming and I became great friends. I appreciate all of the fruit she made me eat and all of the encouragement she shared.

The Schwartz group has changed quite a bit since I joined, so I thank both former and current members. There are a few group members whom I would like to thank in particular. First is Argyris Kahros. Argyris has been my close friend since that fateful first year and his friendship and advice have proven to be invaluable to me, both inside and outside of UCLA. I also want to thank Will Glover, who has been infinitely patient with me. I have learned so much from Will (such as the importance of error bars) and it has been my pleasure to work with him. Godwin Kanu also deserves a special thank you for his continual encouragement. I couldn't ask for a better officemate. Although I have not worked directly with Lekshmi Sudha Devi, I did have the pleasure of sharing an office with her. Lekshmi believed in me even during my darker times of graduate school, and

I cannot thank her enough for all of the encouraging pep talks.

I would like to acknowledge the co-authors of papers on which this Dissertation is based. Chapter 2 is a version of the article "J. R. Casey, R. E. Larsen, and B. J. Schwartz, "Testing Cavity and Non-Cavity models of the Hydrated Electron Against Experiment: The Raman and Temperature-Dependent Electronic Absorption Spectra," *Proc. Nat. Acad. Sci. USA* **110**(8), 2712-2717 (2013)." Chapter 3 is a version of the article "J. R. Casey, A. Kahros, and B. J. Schwartz, "To Be or Not to Be in a Cavity? The Hydrated Electron Dilemma," *J. Phys. Chem. B* **117**(46), 14173-82 (2013)."

I also want to thank Laura Rossi. Laura is incredibly kind and compassionate, and I am thankful that she and I had the opportunity to meet at UCLA. I thank Laura for all of the flowers and ice cream, but more importantly I thank Laura for always listening and cheering me on. I also want to thank Janeal Speight, a long-time friend of mine. Janeal has always been supportive and I thank her for her constant friendship. And I of course want to thank my wonderful boyfriend, Kenny Mayoral, another friend from that first year of graduate school. Kenny is one of the most patient, generous, and loving people I know and I don't know where I would be without him. I thank him for his endless support and his enduring belief that I am capable, even when I feel less so.

And finally, I want to thank all of my family. My family members have all played an important role in my life. I especially want to thank my brothers, Kyle Landin and Shawn Landin, and my sister-in-law, Cheryl Landin, who all continually inspire me. They are amazing people, and I am fortunate to call them family. Then there are my wonderful parents, Annie and Tom Casey, to whom I owe everything. I thank them for their constant support and love. They never belittled my dreams, no matter how crazy my dreams were. I am fortunate to have such encouraging parents, and I thank them for being with me every step of the way.

Vita

2005-2007	Undergraduate Student Researcher, Chemistry Department, California State University, Long Beach.
2007	B.S. (Chemistry) and Minor (Mathematics), California State University, Long Beach.
2007-2012	Teaching Assistant, Chemistry and Biochemistry Department, University of California, Los Angeles.
2007-2014	Graduate Student Researcher, Chemistry and Biochemistry Department, University of California, Los Angeles.
2010-2011	National Science Foundation GK-12 Fellow, University of California, Los Angeles.

CHAPTER 1

Introduction

1.1 The importance of solvation

Most of the chemistry happening around us does not occur in a vacuum. In fact, the majority of important chemical reactions occur in the presence of a solvent, such as water. We ourselves are made up of about 60% water, while the Earth we inhabit is about 70% water. If we truly want to understand the chemistry of our world, we need to account for the solvent's role in chemistry. Things change considerably in the confined space of a liquid; for instance solutes become caged and trapped by surrounding solvent molecules, making diffusion slower. There is also a lot of jostling as close-packed molecules try to diffuse, leading to a wide range of interactions, rotations, and vibrations and hence much more complicated spectra. The presence of a solvent also can make a reaction faster in the case of solvent supported transition states. In an S_N1 reaction, for example the carbocation intermediate is heavily stabilized by the surrounding solvent molecules, so much so that the reaction rate can change by orders of magnitude based on the solvent used. The presence of a solvent can even open up entirely new reaction pathways. If gaseous Sodium Chloride (NaCl) is excited, the bond breaks to form neutral Na and Cl. If this same molecule is excited in the presence of a polar aprotic solvent such as tetrahydrofuran, we form the cation Na^+, neutral Cl, and a free electron. This formation of a solvent-supported free electron is known as a charge transfer to solvent (CTTS) reaction (even though the electron does not reside on any specific solvent molecule) and these reactions

play an important role in many fields of chemistry, as discussed further below. From the examples, it becomes clear just how important the condensed phase is - entirely new behaviors emerge when we consider the effects of the surrounding solvent.

1.2 A brief review of the hydrated electron

When studying something as complex as dynamics in a liquid, it is ideal to keep the system simple so we can better understand the solvent's role. It is for this reason that the hydrated electron, which is an excess free electron solvated by liquid water, is a particularly appealing system. The hydrated electron is the simplest quantum mechanical object we can study as it is just one single electron in the presence of many water molecules. The hydrated electron provides a great probe of solvation as the electron is entirely solvent supported. By studying the hydrated electron system, we can further understand the complex role the solvent plays in stabilizing a quantum mechanical solute.

There are multiple ways to generate solvated electrons in liquid water, such as two-photon excitation of water, direct ionization of bulk water, or ionization of an electron donating solute (such as iodide) in an aqueous environment.[1] The hydrated electron, which is larger than a water molecule, is a powerful reducing agent, and so it has a lifetime on the order of microseconds even in pure water. Because it is so reactive, the hydrated electron is an extremely important species in chemical reactions occurring in such diverse fields as biochemistry and atmospheric chemistry. For example, radiation is not solely responsible for damage to the human body; radiation ionizes the water in our body, which results in free radicals and free electrons that can then damage the genetic material in cells.[2, 3]

The hydrated electron's prevalence has made it a heavily studied system for over the last fifty years, yet despite the intense interest, it has proven difficult

to pin down its chemical nature. There is very little direct experimental evidence of the hydrated electron's structure because it is such an unstable species. One experimental result we have that does provide a look at the hydrated electron's structure comes from electron-spin resonance (ESR) experiments performed on alkaline, glassy matrices at extremely low temperatures.[4] The structure determined from ESR consists of a free electron occupying a cavity, with six water molecules surrounding the electron in an octahedral fashion (see Figure 1.1). This cavity structure has become known as the 'Kevan structure,' and it is the picture most scientists turn to when thinking about the hydrated electron, despite the fact that the conditions of the experiment are very different from the conditions of the ambient water we are most interested in. Other experimental evidence we have characterizing the hydrated electron only indirectly tells us about structure, including the optical absorption spectrum, ionization energy, and resonance Raman spectrum. Although none of these experiments provide us with an actual structure of the hydrated electron, they do provide us with clues that can then be further investigated through theoretical studies.

1.3 Theoretical studies on the hydrated electron

Much theoretical work has been done to help elucidate the true structure of the hydrated electron, yet there is heated controversy over what the true structure actually is. Early theoretical work performed by Schnitker and Rossky (SR) found that the electron resided in a cavity much like that presented by Kevan in the ESR experiments (see Figure 1.2A).[5, 6, 7] Later theoretical work performed by Turi and Borgis (TB) also found a cavity electron, although the TB hydrated electron is slightly smaller than the SR hydrated electron and has an average coordination number of four rather than six water molecules (see Figure 1.2B).[8, 9] The two models both found good agreement with experimental observables (such

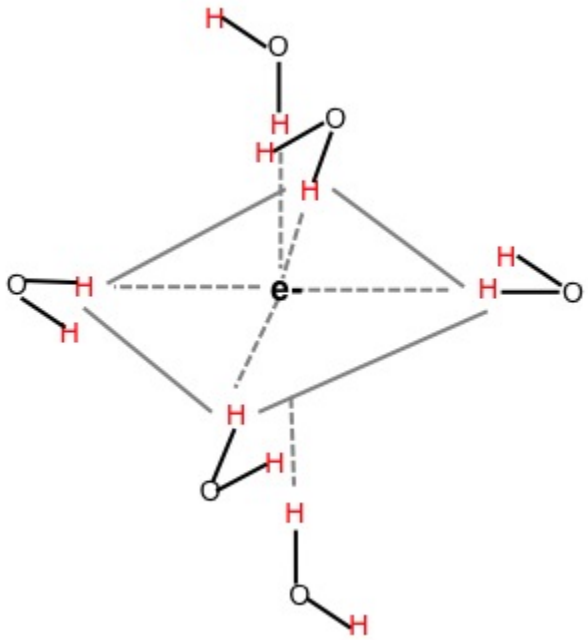

Figure 1.1: Cartoon of the Kevan structure of the hydrated electron.

as the optical absorption spectrum), thus providing a seemingly good model for the hydrated electron. Modifications were made, such as using polarizable water molecules, but the same general picture of a cavity electron kept emerging.[10, 11]

It was not until 2010 that theoretical calculations observed a different structure for the hydrated electron, a structure where the electron no longer occupied a cavity but instead occupied a region of enhanced water density (see Figure 1.2D).[12] This non-cavity model, which has since been named the LGS electron after Larsen, Glover, and Schwartz, also shows good agreement with experimental observables such as the radius of gyration and optical absorption spectrum, yet it met with strong resistance[13, 14, 15]. The debate arises mainly from the fact that the hydrated electron seems to be highly sensitive to the electron-water interaction used in simulations, a topic we will discuss further in the next section and in Chapter 3 of this thesis.

Interestingly, the idea of a non-cavity electron is not new, and in fact was presented by Golden and Tuttle in the early 1990s when they observed that solvated

electrons' optical absorption spectra shift with changing temperature and/or pressure yet have shape stability, while the optical absorption spectra of solvated anions such as iodide do not.[16] These authors concluded that the hydrated electron is extremely sensitive to the solvent, something not normally seen with cavity-like species. This brings up an interesting point, as the experiments simulated thus far have all been sensitive only to the electronic structure of the hydrated electron, and since the wavefunction is similar in the SR, TB, and LGS models, it is not surprising that all models have shown good agreement with experiment. In order to distinguish between the cavity and non-cavity models, we need to examine experiments that are sensitive to the local water structure near the electron, as that is what distinguishes the cavity and non-cavity models from each other. The focus of this thesis is to determine how well various models do at predicting observables associated with experiments that are particularly sensitive to the local solvation structure near the hydrated electron.

All of the models presented above use a one electron mixed quantum/classical molecular dynamics approach, which we will describe further in the next section. It should be mentioned, however, that some work has been done on the hydrated electron using *ab initio* molecular dynamics (AIMD). This work, performed by Jungwirth and co-workers, found a hydrated electron that had a small interior cavity, yet over 50% of the electron density overlapped with the water density in a manner similar to the non-cavity LGS electron.[17] This hybrid electron, referred to as the UMJ model, has characteristics of both cavity and non-cavity models as seen in Figure 1.2C, yet it is not the final word on the hydrated electron. The UMJ model is based on density functional theory (DFT) calculations, and it is still very difficult to determine which density functional is most appropriate to use, especially for cases where the electron is not localized. The vast number of water molecules that are required for the hydrated electron system also puts the hydrated electron at the bounds of what is feasible for *ab initio* calculations. It

is especially difficult for these all-electron calculations to replicate experimental observables that require excited states of the electron. Throughout this work, we will be testing the UMJ model when possible, as it provides a very useful middle ground between a simulated cavity and non-cavity electron.

1.4 Simulation techniques

1.4.1 Mixed quantum/classical molecular dynamics

As mentioned previously, much theoretical work has been done on the hydrated electron, and the primary means of studying this system consists of mixed quantum/classical (MQC) molecular dynamics (MD) simulations. Ideally, we would be able to treat every electron in the system quantum mechanically, but because we are interested in bulk water, many hundreds of water molecules (and hence thousands of electrons) need to be included in these simulations. It has been shown that spectroscopic properties, such as the optical absorption spectrum of the hydrated electron, are sensitive to the number of water molecules used in the simulation cell.[12] It seems that long-range Coulomb forces play an integral role in stabilizing the electron, which is particularly true for the LGS non-cavity electron. Because we need $\sim$500 water molecules in our hydrated electron simulations, we decided to treat only the valence electron quantum mechanically instead.

The main idea behind MQC MD is that we want to minimize the number of quantum degrees of freedom. Rather than treat all of the electrons in the system quantum mechanically, we treat only certain parts of our system quantum mechanically. In a system such as the hydrated electron, it is simple to separate the classical and quantum degrees of freedom: we treat the free electron quantum mechanically while all of the water molecules are treated with classical Newtonian physics. The water molecules' interactions are governed by a Lennard-Jones short-range potential and a Coulombic long-range potential, the parameters of which

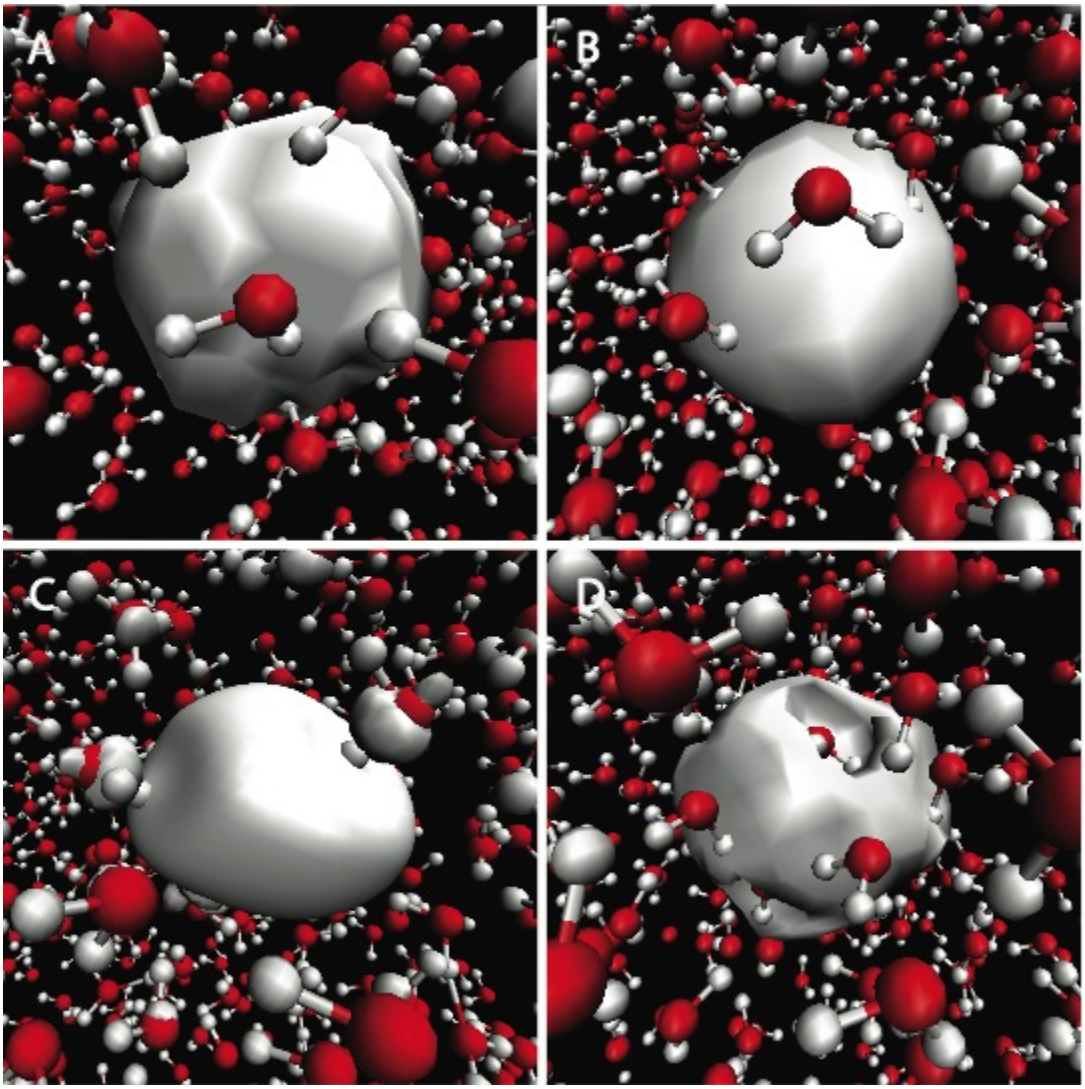

Figure 1.2: Illustrations of the SR (A), TB (B), UMJ (C), and LGS (D) hydrated electron models.

are governed by the type of water model chosen.

Because we usually deal with periodic boundary conditions, the long-range potential is conditionally convergent. There are a few ways to get around this problem. The first is to use a spherical truncation scheme, where we only include long-range interactions within a certain cutoff distance r_c of each molecule. To guarantee that there are no discontinuities in the forces, we smoothly taper the potential to zero past r_c. Although this method provides a fast computational solution, it does not fully account for all long-range forces between periodic images. Ewald summation, however, does provide a means to accurately account for long-range forces by splitting the Coulombic potential into a quickly decaying short range part and a smooth long-range part. Utilizing the fact there is periodicity in the simulation cell lattice, Fourier transforms can be used to complete the calculation.[18] Unfortunately, Ewald summation is more computationally expensive than spherical truncation. The choice of one method over the other will be discussed further in Chapter 4.

1.4.2 Pseudopotential development

One of the most difficult parts of an MQC MD simulation is determining how a quantum electron will interact with a classical water molecule. We want to implicitly include the effects of the water molecule's core electrons on the wavefunction of the free electron, which can be done through the construction of a pseudopotential. The Phillips-Kleinman (PK) pseudopotential theory provides a rigorous quantum-mechanical formalism for constructing an electron-water interaction[19, 20]. The general idea is that a local potential (the pseudopotential) is added to the Hamiltonian so that the valence electron's wavefunction is forced to be orthogonal to the implicit core electrons of the water molecules.

In practice, the hydrated electron pseudopotential is constructed by performing

an *ab initio* calculation on a gas phase water molecule and an excess electron in order to obtain the core and valence orbitals for the water molecule. It should be noted that the method of deriving an electron-water potential from the gas phase for use in the condensed phase may not be ideal, as the properties of a gaseous water molecule are quite different from those of a water molecule in the condensed phase (i.e. the dipole moment and O-H stretch frequency). Despite this fact, it is a standard procedure in the field. From this calculation, the pseudopotential can be derived as illustrated in Ref. [20]. The raw numerical pseudopotential is too complicated to be utilized in MQC MD simulations directly, so it must be both smoothed and fitted to an analytical expression so that energies and forces can easily be calculated.

Despite the fact that the pseudopotential can be rigorously derived, the subsequent smoothing and fitting of the raw pseudopotential leads to subtle differences in the electron-water interactions, which in turn can lead to vastly different hydrated electron behavior.[13, 15] The fact that the hydrated electron is so sensitive to the electron-water interaction is one of the main focuses of the controversy surrounding the hydrated electron. In Chapter 3, we will spend some time exploring the origins of this sensitivity. Ultimately, it is unclear as to what is the best way to smooth and fit the pseudopotential, with each group having their own set of justifications and suggestions. Despite this difficulty, the various hydrated electron models presented provide us with a unique opportunity to connect experiment and theory. If one of the hydrated electron models is able to predict experimental observables more reliably than the others, we can then begin to understand what aspects of the pseudopotential are critical for experimental agreement.

1.5 Summary

Understanding the role of the solvent is essential in determining the true structure of the hydrated electron. These cavity, non-cavity, and hybrid models are all defined by the behavior of the local water structure near the electron. By probing these water molecules, we can add valuable insight to the controversy that has recently arisen in the field. Most experiments probe the hydrated electron's structure indirectly, thus precluding us from having a clear understanding of what is happening at the molecular level. Theoretical studies do allow us to probe the hydrated electron at the molecular level, giving us a glimpse as to what the true structure of the hydrated electron might be. Unfortunately, previous simulations have focused on experiments that are sensitive only to the electronic wavefunction, which is similar in all models. Throughout this thesis, we will be connecting these various models with experimental observables that are sensitive to the local water structure near the electron, as this is what sets each model apart. As a result, we can determine which model provides the best representation of the hydrated electron.

In Chapter 2 of this thesis, we specifically explore how well the SR, TB, and LGS hydrated electron models do at predicting experimental observables such as the temperature-dependent optical absorption spectrum and resonance Raman spectrum of the hydrated electron. These experiments are extremely sensitive to the local water structure near the electron, thus providing an excellent probe as to what type of solvation is required in order to find agreement with experiment. We find that the SR and TB cavity electrons' optical absorption spectrum does not have the experimentally seen temperature-dependent shift and their resonance Raman spectra have the opposite behavior of the experimental resonance Raman spectrum due to the disruption of the hydrogen-bonding network. The LGS non-cavity model is the only model we tested that had qualitative agreement with

both experiments, as it seems critical that the local water structure remain intact in order to correctly predict these experimental observables.

In Chapter 3, we continue to explore the resonance Raman experiment, this time examining the UMJ hybrid model as well. We also take a closer look at the specific differences in water structure found in the various hydrated electron models, focusing primarily on the amount of electron-water overlap present in each model. The LGS model has complete radial overlap between the water density and the electron density, but only $\sim$17% of the water molecules directly overlap with the electron density, leading to a new 'inverse plum pudding' picture of the hydrated electron. The direct overlap is similar to that found in the UMJ *ab initio* study, while the SR and TB models have relatively little direct overlap. We also explore the effects of smoothing on the electron-water pseudopotential. From this, we get a clear picture of how differences in the pseudopotentials arise, as well as what features are responsible for the various structures of the hydrated electron. For instance, the TB pseudopotential is reminiscent of an overly smoothed LGS pseudopotential, which captures many of the detailed features of the original PK pseudopotential.

Finally in Chapter 4, we explore the behavior of various hydrated electron models at the air/water interface, as this once again provides us with a way to distinguish between the various hydrated electron models through connection with experiment. Based on previous work done on anions at the air/water surface, it seems that the behavior of cavity and non-cavity electrons would be very different for this system. We calculate Potentials of Mean Force for the SR, TB, and LGS hydrated electron models relative to the instantaneous interface, providing us with a complete picture of hydrated electron solvation in the presence of an air/water interface. We find that although all of the models prefer bulk solvation, the TB electron has a local free energy minimum 1 Å below the interface, while the LGS electron avoids the interface entirely. Interestingly, the TB interfacial electron's

properties vary from those of the bulk, although most experiments indicate that if there are interfacial electrons (which is currently under debate), they should have properties similar to the bulk. Overall, this work provides us with new perspective on the hydrated electron, as well gives us significant insight into the controversy surrounding the hydrated electron.

CHAPTER 2

Resonance Raman and temperature-dependent electronic absorption spectra of cavity and non-cavity models of the hydrated electron

2.1 Abstract

Most of what is known about the structure of the hydrated electron comes from mixed quantum/classical simulations, which depend on the pseudopotential that couples the quantum electron to the classical water molecules. These potentials are usually highly repulsive, producing cavity-bound hydrated electrons that break the local water H-bonding structure. However, we recently developed a more attractive potential, which produces a hydrated electron that encompasses a region of enhanced water density. Both our non-cavity and the various cavity models predict similar experimental observables. In this paper, we work to distinguish between these models by studying both the temperature dependence of the optical absorption spectrum, which provides insight into the balance of the attractive and repulsive terms in the potential, and the resonance Raman spectrum, which provides a direct measure of the local H-bonding environment near the electron. We find that only our non-cavity model is able to capture the experimental redshift of the hydrated electron's absorption spectrum with increasing temperature at constant density. Cavity models of the hydrated electron predict a solvation structure that is similar to that of the larger aqueous halides, leading to a Raman O–H stretching band that is blue-shifted and narrower than that of bulk

water. In contrast, experiments show the hydrated electron has a broader and red-shifted O–H stretching band than bulk water, a feature recovered by our non-cavity model. We conclude that even though our non-cavity model does not provide perfect quantitative agreement with experiment, the hydrated electron must have a significant degree of non-cavity character.

2.2 Introduction

The hydrated electron is the simplest quantum mechanical solute, consisting of an excess electron in liquid water. Because of its apparent simplicity, the hydrated electron provides a unique opportunity for confrontation between experiments and quantum simulations. Yet, despite nearly five decades of interest in the hydrated electron, there is still controversy over the nature of its molecular structure.[4, 6, 5, 21, 16, 22, 8, 23, 9, 24, 25, 26, 27, 12] Experimental observables, such as the absorption spectrum of the hydrated electron at different temperatures and pressures[26, 27] or the results of ultrafast pump-probe experiments on the hydrated electron, only provide indirect clues to the electron's molecular structure. One of the few experiments that has offered a definite possible structure was electron spin-echo envelope modulation (ESEEM) measurements on excess electrons in aqueous alkaline glassy matrices at 77 K.[4] These experiments suggested that the electron is localized in a cavity that contains no water molecules, and that there are six surrounding water molecules in an octahedral geometry around the cavity, each with an O–H bond oriented toward the electron; this arrangement has been referred to as the 'Kevan structure.' It is not clear, however, how transferrable results from frozen aqueous alkaline glasses are to hydrated electrons in room-temperature liquid water, and there is surprisingly little structural information that can be inferred directly from most other experiments.

Thus, most of the evidence for assigning particular structures to the hydrated

electron has come from quantum molecular dynamics (MD) simulations. One of the earliest mixed-quantum/classical (MQC) simulations of the hydrated electron was performed by Schnitker and Rossky (SR), who used a pseudopotential whose derivation was later shown to contain an error, albeit one that did not qualitatively change the nature of their results.[28] With their potential, SR found that the hydrated electron had, on average, the Kevan structure, with the electron in a cavity and roughly octahedrally coordinated by six bond-oriented water molecules.[5, 7] A few years later, Turi, Borgis and their co-workers (TB) developed a more rigorous electron-water interaction potential and also found a simulated hydrated electron that occupied a cavity in the solvent, but the water structure around the cavity was somewhat less defined than seen with the SR model and the first solvent shell contained only roughly four water molecules instead of six.[9] Jacobson and Herbert recently have extended the TB model to incorporate electronically polarizable water, but found little difference in structure from that seen by TB.[11] Fully *ab initio* simulations of the hydrated electron largely have been limited to just a few explicitly-treated water molecules and have been based on DFT functionals that may not be appropriate for treating an unbound electron;[29] these simulations have also suggested that the electron occupies a cavity, albeit highly fluxional and distorted. There also has been a large variety of both experimental and theoretical work studying the structure of gas-phase water anion clusters, but the way that the behavior of such clusters extrapolates to that of the hydrated electron in bulk water with cluster size has been highly controversial.[30]

Although almost all of the theoretical work to date suggests that the hydrated electron occupies a cavity, we recently challenged this idea by suggesting a picture in which the hydrated electron is associated with a region of enhanced water density.[12] Even though there are roughly 30 water molecules occupying the space inside the majority of the hydrated electron's wavefunction, this picture also appears consistent with experiment. We found this unusual non-cavity behavior

when developing a new pseudopotential that includes repulsive terms between the water H atoms and attractive terms behind the water O atom that were not included in previous potentials but are necessary to guarantee orthogonality between the excess electron's wavefunction and the electrons in the occupied water molecular orbitals; our new potential has since been referred to as the LGS model. Our proposal that a non-cavity model should be considered on par with the various cavity models, however, has met with some resistance.[13, 14, 31] Part of the objections to our proposed possible non-cavity picture stem from technical issues such as whether or not the electron–water pseudopotential should be analytically fitted to better represent the physical features found in the true potential or to better reproduce the eigenenergy for a single water anion.[15] In addition, Turi and Madarasz found that small changes in the balance of attractive and repulsive terms in the pseudopotential can change whether or not the resulting hydrated electron occupies a cavity;[13] this extreme sensitivity to minute details in the potential suggests that caution is warranted when inferring *any* structural model from the details of a mixed quantum/classical simulation.[15]

It is worth noting that our group was certainly not the first to suggest that the hydrated electron may not reside in a cavity,[16] and the idea that there may be water molecules interior to the wavefunction of the hydrated electron also recently has been extended by Jungwirth and co-workers.[17] These workers performed DFT-based *ab initio* MD simulations of the hydrated electron with 64 waters treated quantum mechanically and hundreds more treated classically, and found that the resulting hydrated electron had both cavity and non-cavity features: the central cavity was significantly smaller than that predicted by either the SR or TB models, and well over half of the electron density resided outside of the central cavity and overlapped with the surrounding water.[17] Thus, even *ab initio* work suggests that it is not unreasonable for the hydrated electron to have interior water molecules, leaving open the question as to whether a cavity,

non-cavity or possibly a hybrid picture is the best for describing the molecular structure of the hydrated electron.

In this paper, we work to better understand the structure of the hydrated electron by making some more rigorous comparisons between experiment and the simulated cavity and non-cavity pictures of the hydrated electron. First, we examine the temperature and density dependence of the hydrated electron's absorption spectrum, since this provides an exquisite measure of the balance between the attractive and repulsive terms in the underlying potential. What we find is that the SR and TB cavity models of the hydrated electron are unable to produce the experimental linear red-shift of the hydrated electron's absorption spectrum with increasing temperature at constant density. In contrast, our non-cavity LGS model does show a linear red-shift, but the slope is roughly twice as large as experiment. This suggests that cavity models underestimate the attractive terms in the potential, while our non-cavity model overestimates these terms. Second, we focus on connections between simulations and the experimental resonance Raman spectrum of the hydrated electron. We find that the TB and SR cavity models of the hydrated electron predict O–H stretching bands for the nearby water molecules that are narrower than that of bulk water, with most of the enhanced intensity on the blue side of the bulk water band, a result that is in poor qualitative agreement with experiment. In contrast, our non-cavity LGS potential predicts an O–H stretching band that is broader than that of bulk water and enhanced on the low-frequency side, in excellent qualitative agreement with experiment. Together, the results indicate that the correct picture of the hydrated electron must include significant overlap between the hydrated electron and the solvating water molecules in order to obtain qualitative agreement with experiment.

2.3 Results

To compare various simulation models of the hydrated electron to experiment, we performed MQC MD simulations of one quantum mechanical electron and 499 classical SPC Flex[32] water molecules. Like all of the previous work done in this area,[6, 21, 9, 24, 12] we chose to perform our MQC simulations in the microcanonical ensemble, which provided an average temperature with ∼5 K fluctuations (see Section 2.5.1 for details). The system was confined to a cubic box of length 24.64 Å with periodic boundary conditions, and all interactions were tapered using a spherical cutoff centered at the oxygen atom. The quantum mechanical wavefunction of the excess electron was expressed on a cubic grid of length 18.17 Å; we found that 16^3 grid points were satisfactory to describe the electron with the SR and TB potentials but that our non-cavity LGS potential required 32^3 grid points. The adiabatic eigenstates were found at every time step using the Lanczos algorithm, and the quantum forces were evaluated using the Hellmann-Feynman Theorem with the Verlet algorithm used to propagate dynamics with a 0.5-fs time step. Additional computational details, including the way we construct the optical absorption and resonance Raman spectra of the various hydrated electron models, are presented in Section 2.5.1.

Before discussing how the fundamental differences in the SR, TB, and LGS models lead to differences in predicted experimental observables, we begin by quickly reviewing the structural properties of the three models. In all three models, the electron has a roughly spherical wavefunction with a radius of gyration of ∼2.2 to 2.4 Å, in reasonable agreement with experimental estimates based on spectral moment analysis.[26] This explains why all three models do a satisfactory job of reproducing the experimental absorption spectrum. Despite the similarities in charge density, however, the three models predict very different molecular structures for the hydrated electron. In Figure 2.1, we have plotted radial distribution

functions to gauge the positions of both the water O atom (black solid curves) and H atom (red dotted curves) sites relative to the hydrated electron's center of mass (COM) for each of the three models. The SR model and the TB models (panel a) both show a cavity-bound electron with the SR cavity being marginally larger than the TB cavity. The SR and TB radial distribution functions resemble those of the halides in water, [33, 34] except that the structure around the electron is somewhat less well defined. In contrast, the radial distribution functions for the LGS electron (panel b) show water molecules residing well inside of the electron density due to the inclusion of attractive forces that were neglected in the SR and TB models.[12] With the "first shell" water molecules experiencing such fundamentally different environments for the cavity and non-cavity models, it seems that it would be simple to determine which picture is more accurate via experiment, but thus far comparison with experiment supports both models about equally well.[12] Fortunately, the differences in attraction between the electron and the local water environment can be probed by the temperature-dependence of the electronic absorption spectrum and the resonance Raman spectrum provides a measure of the local water H-bonding structure around the hydrated electron.

2.3.1 Temperature-dependent absorption spectra of different models of the hydrated electron

Since many of the questions concerning the different models of the hydrated electron revolve around the balance of attractive and repulsive terms in the electron-water pseudopotential,[13] we begin our discussion by focusing on calculating the properties of different models of the hydrated electron as a function of temperature. This is because at constant density, solutes that have predominantly repulsive interactions with solvent molecules will have properties that are highly insensitive to temperature, whereas solutes that have predominantly attractive interactions with solvent molecules will have highly temperature-dependent properties.[35]

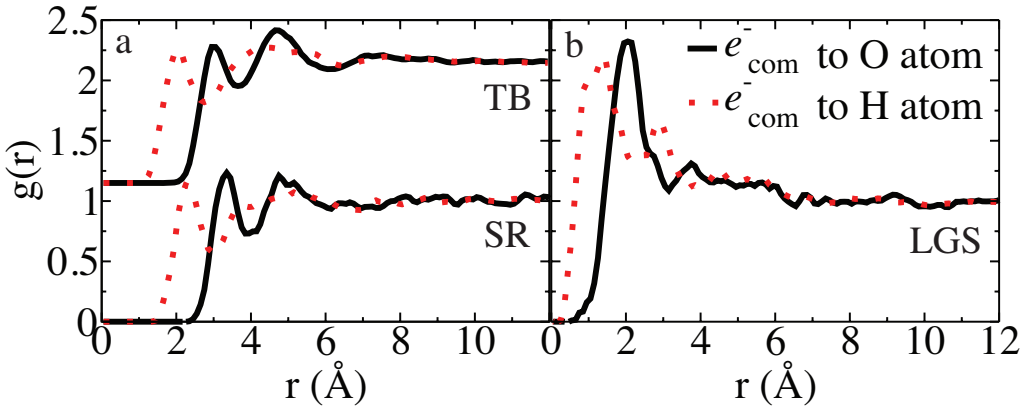

Figure 2.1: The radial distribution function of the electron COM to both O atom (black solid curves) and H atom sites (red dotted curves) for the (a) SR and TB (offset by 1.15 for clarity) and (b) LGS models of the hydrated electron at ∼298 K and a density of 0.997 g/mL. The SR and TB models show a distinct cavity while the LGS model shows water molecules residing near the electron center of mass.

After all, systems that are dominated entirely by repulsive forces (*e.g.*, the hard sphere fluid) do not even have a well-defined temperature, but their structure is highly sensitive to the density. In contrast, temperature starts to make a difference in structure at fixed density when repulsive interactions are softened and/or attractive interactions are introduced. Thus, the temperature-dependence of the hydrated electron's absorption spectrum at constant density should provide an excellent metric of the correct balance between the attractive and repulsive terms in any given model for electron–water interactions.

The absorption spectrum of the hydrated electron at room temperature and density consists of a broad, featureless band that spans the visible and near-IR wavelength ranges with an absorption maximum ($E_{\max}$) of 1.72 eV. The spectrum is known to fit empirically to a Gaussian function on the low-energy side of $E_{\max}$ and a Lorentzian function on the high-energy side.[36] Both the TB and the LGS potentials predict absorption spectra for the hydrated electron that are in generally good agreement with experiment, although the TB model predicts a

spectrum that is slightly blue-shifted from experiment[9] while the LGS-predicted spectrum is slightly red-shifted.[12] The original SR potential produces an optical absorption band for the hydrated electron that is quite blue-shifted (by $\sim$0.7 eV) relative to experiment,[7] although the SR model's absorption spectrum shifts into better agreement with experiment when the mathematical error in its derivation is corrected.[28] Of greater interest for the present purpose is the fact that the hydrated electron's optical absorption band undergoes a roughly linear red-shift with increasing temperature; this red-shift happens at both atmospheric pressure[27] and at pressures into the supercritical regime,[26] with a noticeable change in $E_{\max}$ of the electron's spectrum even for relatively small (a few K) changes in T.

Several groups have attempted to understand this temperature dependence of the hydrated electron's absorption spectrum on the basis of MQC simulation models. Berne and co-workers developed a repulsive electron-water interaction potential that produced a cavity hydrated electron, and found that although the calculated absorption spectrum of the electron with this potential was in reasonable agreement with experiment at room temperature, this model produced no shift in the electron's spectrum even after the temperature was increased 73 K.[21] Golden and Tuttle commented on the inability of early cavity models to capture the essence of the experimental optical absorption spectrum of the hydrated electron and suggested that a solvent-anion complex might prove to be more consistent with experiment.[16] Subsequently, Borgis and co-workers performed temperature-dependent simulations of the hydrated electron using the cavity-forming TB model, and found that the electron's spectrum shifted slightly to the blue with increasing temperature at constant density,[24] the opposite of what is seen experimentally. These authors noted, however, that real water undergoes a density change when the temperature is varied at constant pressure, and that some of the observed red-shift of the electron's spectrum could be recovered when the constant-volume simulations were constructed to allow the water

density to vary in a manner similar to experiment. Thus, Borgis and co-workers concluded that the observed redshift of the electron's spectrum with temperature is not actually a temperature effect but is instead a density effect.[24]

Although this conclusion appeared to make sense, subsequent experiments showed that the observed red-shift of the electron's spectrum is indeed truly a temperature effect. First, Bartels and co-workers examined the spectrum of the hydrated electron in supercritical water at constant temperature and found only a small change in $E_{\max}$ over a 0.5 g/mL change in density.[26] Second, another experiment from this same group took advantage of the facts that water has a density maximum at 4°C and that water can easily be supercooled; this allowed these authors to examine the spectrum of the hydrated electron at pairs of points on opposite sides of the density maximum that have the same density but different temperatures. These workers found that the absorption spectrum of the hydrated electron red-shifted by 0.12 eV between -18°C and 32.6°C, state points at atmospheric pressure where water has a density of 0.9947 g/mL.[27] Additional experiments led Bartels and co-workers to conclude that the absorption maximum of the hydrated electron's spectrum shifts by 0.0022 eV/K, independent of the water density;[27] this comprises a fairly substantial constant-density temperature dependence.

To better understand how different simulation models reproduce the experimental temperature dependence of the hydrated electron's absorption spectrum, we ran MQC simulations of the SR, TB and LGS models of the hydrated electron in the microcanonical ensemble at temperatures of approximately 300 K, 325 K, 350 K, and 370 K at a constant density of 0.997 g/mL, and also at the experimental densities for each temperature for water at 1 atm pressure (see Section 2.5.1). The calculated absorption spectra of the hydrated electron from the constant density simulations are shown in Figure 2.2; the changes in $E_{\max}$ with temperature found from fitting the calculated spectra to the standard Gauss-Lorentzian form

are summarized in Figure 2.3, with least-squares fitted lines drawn through the data points. For these constant-density simulations, both the cavity-forming SR (green line, shifted into better agreement with experiment by 0.5 eV) and TB (blue line, shifted into better agreement with experiment by 0.25 eV) potentials predict that the maximum of the hydrated electron's absorption spectrum effectively does not change with increasing temperature, in contrast to experiment (black curve, see Ref. [27]), which shows a clear red-shift with increasing temperature at constant density. Our non-cavity LGS model (purple line, data not shifted), in contrast, is able to correctly predict a substantial red-shift in the optical absorption spectrum of the hydrated electron with increasing temperature at constant density. Moreover, the shift of $E_{\max}$ with T for the LGS model is indeed quite linear, also in good agreement with experiment, but the slope of the shift for the LGS-calculated spectrum is 0.0052 eV/K, about a factor of 2.4 larger than what is observed experimentally.

Taken together, the data in Figure 2.3 allow us to conclude that cavity-forming hydrated electron models, such as Berne's,[21] SR and TB, contain electron–water interactions that are too repulsive: none of these three models shows a significant T-dependence for the hydrated electron's spectrum at constant density, a result that is in direct contrast to experiment. This means that all of these models significantly underestimate the role of attractive interactions in the electron–water interaction, and it is these attractive interactions that are responsible for the non-cavity behavior seen with the LGS model.[13, 15] The LGS potential appears to provide a qualitatively correct prediction of the behavior of the experimental hydrated electron, but the fact that the T-dependence is overestimated suggests that the LGS potential somewhat overemphasizes the attractive terms in the electron–water interaction. This observation is consistent with the fact that the LGS potential slightly overbinds the electron both to a single water molecule[13] and to small water anion clusters.[14] Thus, our conclusion from this section is that none

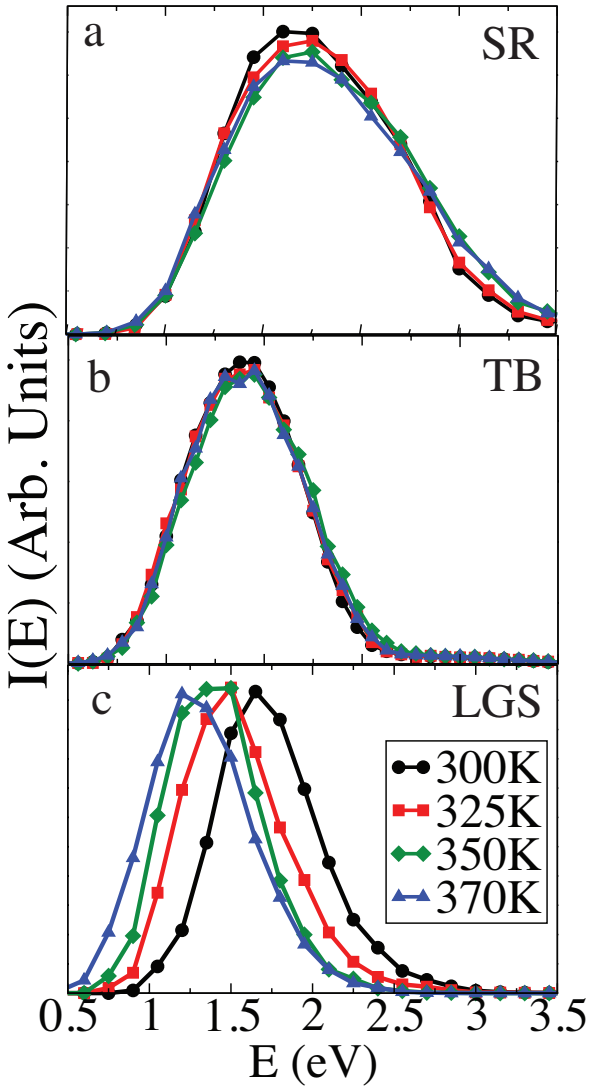

Figure 2.2: Calculated absorption spectra for the (a) SR, (b) TB, and (c) LGS models of the hydrated electron at ∼300 K (black circles), ∼325 K (red squares), ∼350 K (green diamonds), and ∼370 K (blue triangles) at a constant density of 0.997 g/mL. Only the LGS non-cavity model captures the experimentally-observed red-shift with increasing temperature at constant density; see also Fig. 2.3.

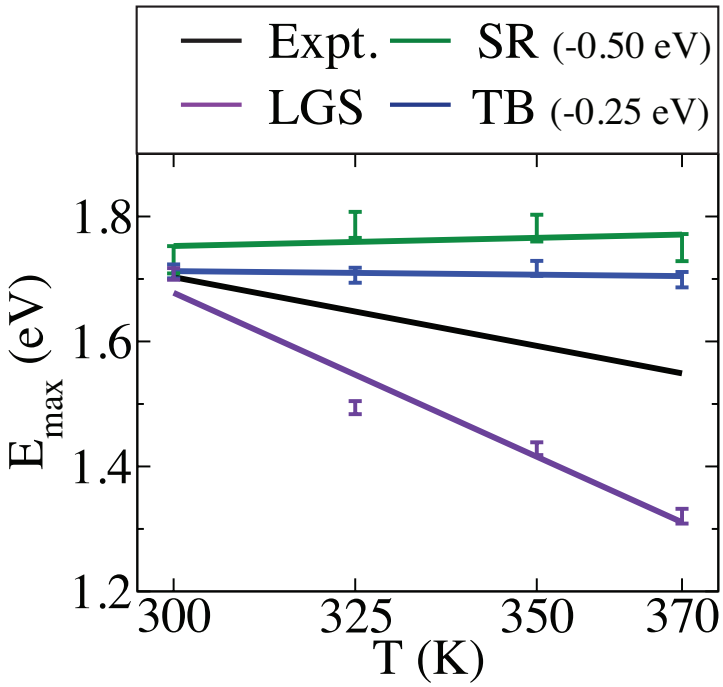

Figure 2.3: The peak of the hydrated electron's absorption spectrum, $E_{\max}$, plotted against T for water held at a fixed density of 0.997 g/mL. The black line shows the experimentally measured results, see Ref. [27]. For the different simulation models, $E_{\max}$ and the error bars (representing the 95% confidence interval) were determined by fitting the data in Fig.2.2 to the standard Gauss-Lorentz form, yielding values for the SR model (green points, $E_{\max}$ shifted by 0.5 eV into better agreement with experiment), TB model (blue points, $E_{\max}$ shifted by 0.25 eV into better agreement with experiment) and LGS model (purple points, data not shifted); the colored lines drawn through the points are linear least-squares fits to the data.

of the water–electron pseudopotentials that have been produced to date have done a proper job of balancing the attractive and repulsive interactions,[15] but that the LGS potential is the only one tested for temperature- and density-dependence thus far that includes attractive terms that are sufficient to provide a meaningful connection with experiment.

2.3.2 Modeling the resonance Raman spectrum of the hydrated electron

Resonance Raman spectroscopy is one of the few experiments that directly addresses the structure of the hydrated electron in room-temperature liquid water. The experiments by Tauber and Mathies[22, 23] and Tahara and coworkers[37] found that the water vibrations that were resonantly enhanced upon excitation of the hydrated electron were virtually identical to those of bulk liquid water, indicating that the hydrated electron's wavefunction resides predominantly between water molecules and does not significantly perturb the water's electronic structure. The resonance Raman spectrum of water associated with the hydrated electron does show a slight red-shift of the bending vibration and a broadening and enhancement on the red side of the O–H stretching vibration; the experimental data from Ref. [25] are reproduced as the circles/black curve in Figure 2.4. In addition, resonance Raman studies of hydrated electrons in isotopically labeled water have shown a splitting of the water bending vibration. This indicates that the H atoms on any given molecule surrounding the hydrated electron experience different local environments, so that there must be some net H-bond orientation towards the electron.[25] For liquid water, it is well established that water molecules that make strong hydrogen bonds have lower O–H stretching frequencies whereas water molecules that make weaker H-bonds have higher O–H stretching frequencies. The fact that the O–H stretches of the water molecules closest to the hydrated electron are broadened compared to those of bulk water thus suggests that these

molecules experience a wider variety of H-bonding environments than when no electron is present, and the enhancement seen at lower frequencies indicates that most of the water molecules nearest the electron experience H-bonds that are stronger than those experienced by water molecules in the bulk.

Given that the resonance Raman spectrum contains information about the local water H-bonding and thus the structure of the hydrated electron, we extended the semiclassical method developed by Skinner and co-workers[38, 39, 40] to calculate the resonance Raman spectrum of the SR, TB and LGS models of the hydrated electron; the details of how we calculated the resonance Raman spectra are given in Section 2.5.1. Figure 2.4 shows that the SR (green squares/curve) cavity model of the hydrated electron predicts a resonance Raman spectrum for the O–H stretch that is both narrower and preferentially enhanced on the blue side relative to the spectrum in bulk flexible SPC water (red plus signs/curve). This predicted narrowing of the spectrum, which is in contrast to experiment, is perhaps not surprising. Our calculations shows that for the SR model, which predicts the Kevan structure for the hydrated electron, the closest six waters contribute most significantly to the resonance Raman spectrum (see Section 2.5.2), and these six waters are all in roughly equivalent environments given the near-octahedral symmetry of the structure predicted by this model. This homogeneity of the first-shell water environments explains why the predicted resonance Raman spectrum for the SR electron is narrower than for the bulk. That the six closest water molecules in the SR model have a blue-shifted Raman spectrum is a consequence of the fact that these water molecules interact more weakly with the hydrated electron than they would to another H-bonding water molecule. This is because for SPC water, the O atom from a water molecule that makes an H-bond to another water molecule carries a charge of $-0.8\ e$ at a distance of $\sim$1.6 Å, whereas if one uses Gauss' law and assumes that a cavity hydrated electron can be treated as a point charge at its center of mass, then the electron carries

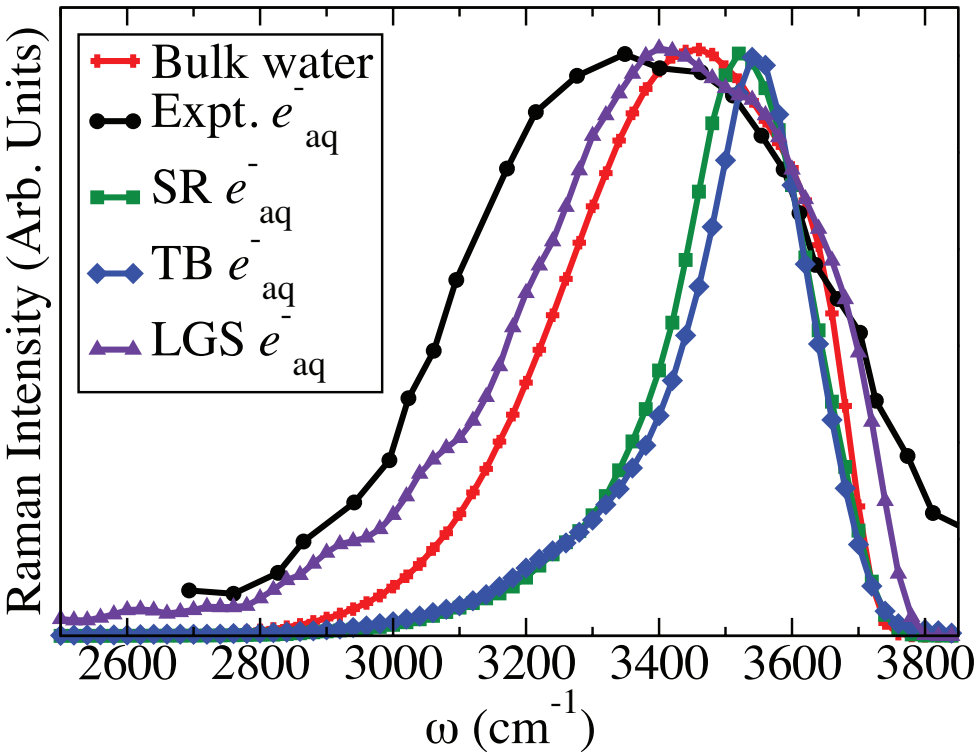

Figure 2.4: The experimental resonance Raman spectrum of the hydrated electron (black circles/curve, from Ref. [25]) compared to the calculated Raman spectrum of bulk SPC/Flex water (red plus signs/curve) and the force-weighted calculated resonance Raman spectra of the SR (green squares/curve), TB (blue diamonds/curve), and LGS (purple triangles/curve) models of the hydrated electron. Both the SR and TB models produce Raman spectra that are blue-shifted and narrowed compared to the bulk, in stark contrast to the experiment, while the LGS model correctly predicts that the Raman spectrum of the hydrated electron should be both broader and red-shifted relative to that of bulk water.

a charge of -1 e at a distance of $\sim$2.1 Å from the nearest H atoms. Since the electric field goes inversely with the square of the distance (see Eq.2.3 in Section 2.5.1), this simple argument explains why the cavity electron is a poorer H-bonder than water, and thus why the SR model predicts a narrowed, blue-shifted O–H stretching spectrum that is in contrast to experiment.

A similar argument can be used to explain the poor agreement between the predicted O–H Raman stretch for the TB model (Fig. 2.4, blue diamonds/curve) and experiment. Like the SR model, the roughly four first-shell water molecules in the TB model make poorer H-bonds to the electron in the cavity compared to the H-bonds they would make with other water molecules. These molecules are the ones that experience the largest force difference upon excitation of the electron (see Section 2.5.2), so they are the molecules that dominate the observed resonance-enhanced O–H stretch, explaining the blue-shifted and narrowed predicted spectrum. We note that the water molecules in the TB electron are slightly closer to the electron's center of mass than those in the SR model, but more of the electron's wavefunction lies outside of the first-shell H atoms in the TB model relative to the SR model, so the electron makes roughly equally poor H-bonds to the four first-shell molecules around the TB cavity as to the six molecules around the SR cavity. In essence, cavity models of the hydrated electron intrinsically assume that the electron significantly breaks the local structure of water's H-bonding network,[23] and this disruption of the network is not consistent with the broadening and enhancement of lower-frequency O–H stretches seen experimentally.

In retrospect, the blue-shift and narrowing of the resonance Raman spectra predicted by the SR and TB cavity models is not all that surprising. A cavity electron is similar in shape and intermediate in size to halide ions such as Cl^- and Br^-; indeed, as mentioned above, the radial distribution functions of the water around the SR and TB electrons are quite similar to those of the larger halides.[6]

It is well known that the presence of halides in water alters the Raman spectrum of the water's O–H stretch, with O–H Raman spectra of the larger aqueous halides that are blue-shifted and narrowed compared to that of bulk water.[33, 34] This effect has been ascribed to the fact that halide ions break the local H-bonding structure of the surrounding water molecules: the water molecules in the halide's first solvation shell orient an O-H bond towards the anion, so that both the first- and second-shell water molecules make weaker H-bonds (both to the halide ion and to the neighboring water molecules), thus raising the average frequency of the O-H stretch in a manner that increases with the size of the halide ion.[33] Since a cavity hydrated electron is intermediate in size to Cl^- and Br^- and breaks the local water structure the same way, it is thus not surprising that it should have a Raman spectrum of the O–H stretch that is similar to that of the larger halides. Interestingly, however, aqueous F^- (and also aqueous hydroxide) have an O–H Raman spectrum that is red-shifted and broadened relative to that of bulk water,[33, 34, 41] very similar to that observed for the hydrated electron. The Raman spectra of F^- and OH^- have been explained as resulting from significant electron transfer from the anion to the surrounding water molecules, so that the anionic charge distribution encompasses the first-shell waters. Thus, based on the Raman spectrum of the water O–H stretch, one might expect the hydrated electron to have a structure that resembles F^- or OH^- rather than the larger halides, with little breaking of the local H-bonding and a delocalized charge distribution,[42] both of which are better represented by a non-cavity model than by a cavity model for the hydrated electron.

Thus, in contrast to the cavity models, our LGS potential is able to capture both the broadening and the enhancement on the lower frequency side of the hydrated electron's O–H stretch resonance Raman spectrum, as seen in Figure 2.4 (purple triangles/curve). The predicted O–H stretching band for the LGS model can be rationalized by the fact that most of the water molecules inside the hy-

drated electron's wavefunction contribute to the resonance Raman spectrum (see Section 2.5.2). Since these water molecules in the LGS electron are compressed by electrostriction to a higher density than the bulk,[12] these water molecules have stronger H-bonds, on average, than water in the bulk, explaining the low-frequency enhancement of their O–H stretches. In addition, the water molecules inside the non-cavity LGS hydrated electron maintain their H-bonding network,[12] explaining why, unlike the structure-breaking cavity models, the full width of the O–H stretching band is preserved in the predicted LGS resonance Raman spectrum. Moreover, the fact that the LGS hydrated electron's wavefunction decays from the center outward means that the water molecules inside the electron experience a significant electric field gradient. A majority of these interior waters are oriented with H-bonds pointing toward the electron's center of mass,[12] so for these waters, the electric field gradient from the electron enhances their O–H bonding and thus further lowers the O–H stretching frequency, providing an additional reason why the predicted spectrum is enhanced on the low-frequency side. But unlike the cavity models, some of the waters in the interior of the LGS electron have O–H bonds oriented against the electric field gradient, so these waters experience effectively weaker H-bonds and thus show blue-shifted O–H stretching frequencies, explaining why the predicted O–H stretching band for the LGS electron is slightly broader than that in bulk water.

In summary, the data in Fig. 2.4 show that the cavity models of the hydrated electron tested here do not predict resonance Raman spectra for the O–H stretch that are consistent with experiment: the experimentally observed red-shift of the O–H stretch is simply inconsistent with the disrupted H-bond network that would accompany confinement of the hydrated electron in a cavity. Moreover, the homogeneous environment of the first-shell waters that make H-bonds to the electron in cavity models would predict a narrowing of the Raman O–H stretching spectrum, a result that is again in contrast to experiment. Our non-cavity LGS

electron, on the other hand, predicts a resonance Raman spectrum for the O–H stretch that is in excellent qualitative agreement with experiment, explaining both the broadening of the band and the preferential enhancement of intensity on the low-frequency side. We note that $(H_2O)_2^-$ also shows a similar broadening and red-shift of the O–H stretch,[43] suggesting that overlap between the electron and water wavefunctions also might be responsible for the redshift, an idea we plan to investigate in the future. Thus, even though the predicted resonance Raman spectrum for our LGS model is not in quantitative agreement with experiment, the results presented above suggest that a non-cavity model is in much better line with the experimentally observed vibrational structure of the hydrated electron than a cavity model.

2.4 Conclusions

From the studies we have done on both the temperature-dependence of the absorption spectrum and the resonance Raman spectrum of the hydrated electron, it seems clear that our non-cavity picture is superior in making contact with experiment relative to the cavity models tested here. In the SR and TB cavity models, the electron resides in a repulsive and rigid cavity, leading to a lack of temperature dependence of the absorption spectrum and a narrowed and blue-shifted O–H stretch in the resonance Raman spectrum, both of which are in contrast to experiment. Our LGS potential is found to be somewhat too attractive, as had been previously pointed out,[13, 14, 15] in that it overestimates the temperature dependence of the hydrated electron's absorption spectrum, but at least it shows a temperature dependence with the correct sign and order of magnitude, and thus we consider the general agreement to be satisfactory. Perhaps more importantly, the fact that a non-cavity model such as LGS can predict a resonance Raman spectrum that is consistent with experiment while cavity-forming models cannot is to

us a clear sign that the structure of the hydrated electron must have significant non-cavity character.

As mentioned in the introduction, recent *ab initio* MD simulations by Jungwirth and co-workers have suggested a structure that is something of a compromise between the cavity and non-cavity pictures of the hydrated electron.[17] The computational expense of this type of model makes calculating the temperature dependence of the absorption spectrum computationally prohibitive. However, for this hybrid structural picture, the facts that the electron density overlaps with the closest water molecules (as with our LGS model) and that the structure of the surrounding water is less broken than the cavity models suggests that such a hybrid structure might be more consistent with the experimental resonance Raman spectrum than the cavity models. On the other hand, the fact that only a fraction of the electron's charge density overlaps with the nearby waters also suggests that there may not be enough of an electric field gradient to produce the broadening of the spectrum seen both experimentally and with the LGS model. Calculations of the Raman spectrum for this hybrid model of the hydrated electron are presently underway.

Finally, we note that as long as we are restricted to a one-electron picture to do extensive calculations to compare with experiment, the structure of the hydrated electron we predict from such models will be determined by subtleties in the pseudopotential that may be difficult to capture. Clearly potentials that are too repulsive lead to cavity hydrated electrons whose Raman spectra do not agree well with experiment, while potentials that are too attractive lead to an overbound electron for which the temperature dependence of the absorption spectrum is overstated relative to experiment. The 'true' one-electron potential, if any such thing exists, is clearly somewhere in the middle, right at the tipping point between cavity and non-cavity behavior.[13, 15] We believe that a problem with all one-electron models lies in the fact that they generally are derived for the

interaction between an electron and an isolated gas-phase water molecule. Yes, corrections for polarizability and other condensed-phase effects can be grafted on afterwards,[31] but this still does not change the intrinsic problem that the electron's wavefunction is being forced by such potentials to be orthogonal to those of a gas-phase water molecule's molecular orbitals (MO's), even though the MO's of water molecules in liquid water are quite different from those in the gas phase (as evidenced by the change in dipole moment and vibrational frequencies of a gas-phase water molecule upon entering the condensed phase). Moreover, the MO's of a water molecule in liquid water also depend on the molecule's local environment, which means that any pseudopotential describing the electron–water interaction should be different for every water molecule. We recently have developed a new pseudopotential formalism that allows the potential to vary as the local environment changes,[44] and we hope to understand how this removal of the so-called frozen core approximation affects the predicted properties of the hydrated electron in future work.

2.5 Appendix

2.5.1 Methodological Details

The simulations performed in this work were all under the condition of constant volume rather than constant pressure. There are several reasons why we and others [12, 6, 21, 9, 24] have chosen to perform these mixed quantum/classical (MQC) simulations in the microcanonical or canonical ensemble. The SPC water model was parameterized to provide the correct water structure and dynamics for the experimental volume near room temperature, which is why SPC water freezes around 200K and 1 atm. If these simulations were performed under the condition of constant pressure, the average water density would not be comparable to experiment. Because we are trying to untangle density and temperature effects on the

absorption spectrum of the hydrated electron, it is crucial that we simulate the proper density. In order to get the proper density for a constant pressure simulation, we could need to perform simulations at very unrealistic pressures. Another reason why these MQC simulations are performed under constant volume arises from technical difficulties associated with system volume changes. For instance, the quantum basis set cannot easily fluctuate when the volume of the simulation box changes and it would be difficult to determine the way the electron interacts with its periodic image as the box size fluctuates. These are just some of the reasons why all of the hydrated electron simulations performed thus far have not been isobaric. In fact, because all other previous work on the hydrated electron has been performed in the microcanonical or canonical ensemble, we can only compare our results on equal footing to those of previous work by also performing constant volume simulations. Constant volume simulations of the hydrated electron have also proven themselves to be very robust [45, 46] and so we have no doubt that the microcanonical ensemble is appropriate to use when simulating the hydrated electron.

2.5.1.1 Obtaining Temperature-Dependent Absorption Spectra

In order to obtain the hydrated electron absorption spectra at various temperatures (∼300 K, ∼325 K, ∼350 K, and ∼370 K), we took an equilibrium configuration at a temperature of ∼300 K and a water density of 0.997 g/mL for each model potential and ran a simulation where we periodically rescaled the water site velocities for at least 10 ps. Once the simulation temperature reached the desired average temperature, we ceased velocity rescaling and ran the simulation for an additional 10 ps to ensure that the system was equilibrated at the desired average temperature. Finally, we ran 40-ps production runs, where the transition dipole moments between the ground and first 7 excited states were output every 10 fs. Absorption spectra were calculated in the inhomogeneous limit for each

model using the transition dipoles between the ground and first seven electronic excited states according to:

$$A(\epsilon) = 4\pi^2\alpha \sum_{i=1}^{7} \epsilon_{0i} |\langle 0|r|i\rangle|^2 \delta(\epsilon - \epsilon_{0i}), \tag{2.1}$$

where α is the fine structure constant, 0 is the ground state, i is the final state of interest, ϵ is the eigenvalue and $\epsilon_{0i} = \epsilon_0 - \epsilon_i$; this sum was computed using configurations drawn every 10 fs from 40-ps equilibrium production runs with a bin size of 0.15 eV.

The main text focuses on the absorption spectra obtained for the hydrated electron at different temperatures when the density of water is held constant at 0.997 g/mL. The resulting spectra (see Figs. 2.2 and 2.3 in Section 2.3.1) clearly indicate that only the non-cavity LGS model is able to capture the red-shift of the optical absorption spectra with increasing temperature at fixed density, a result we attributed to the attractive features included in our LGS pseudopotential. For the sake of completeness, we also decided to investigate the effects of changing density along with changing temperature on the calculated absorption spectrum. To do this, we conducted simulations at ∼300 K and 0.997 g/mL, ∼325 K and 0.987 g/mL, ∼350 K and 0.974 g/mL, and ∼370 K and 0.961 g/mL, which are the experimental densities for liquid water at 1 atm. The resulting absorption spectra are shown in Figure 2.5 and the change in $E_{\max}$ with temperature found from fitting the curves of Figure 2.5 to a Gauss-Lorentzian form are displayed in Figure 2.6. As evidenced in Figure 2.6, both the TB (blue solid curve) and SR (green solid curve) models do a reasonable job of predicting the experimental shift in $E_{\max}$ (black solid curve, see Ref [27]) at the 1-atm experimental density of water, while the LGS model (purple solid curve) somewhat overestimates the shift. This is not surprising since, as mentioned in the main text, the LGS pseudopotential is somewhat overly attractive as seen in the fact that it overestimates the red-

shift with increasing temperature at fixed density. What is clear from all of these simulations is that in order to recreate the temperature-dependent redshift of $E_{\max}$ at constant density, the cavity models require more attraction in the electron-water interaction than is present in the SR and TB models. Conversely, less attraction is needed in the LGS electron-water interaction in order to have better quantitative agreement with the redshift in $E_{\max}$ at both the 1-atm experimental densities and at constant density. As mentioned in the main text, the behavior of the hydrated electron depends sensitively on the balance between the attractive and repulsive features of the electron-water pseudopotential, and apparently the perfect balance has not yet been found in any of the one-electron models explored to date.

2.5.1.2 Electric field strength vs. O–H stretch frequency for flexible SPC water

Resonance Raman spectra were calculated taking advantage of a semiclassical method introduced by Corcelli and Skinner, who found that the instantaneous quantum vibrational frequency and polarizability of a water molecule in liquid water is strongly correlated with the amplitude of the electric field on the hydrogen atom of that water molecule in a classical MD simulation:[38, 39, 40]

$$\omega_{10} = 3761.6 \text{ cm}^{-1} - 5060.4 \text{ cm}^{-1} E - 86225 \text{ cm}^{-1} E^2 \tag{2.2}$$

where E is defined as the electric field along the OH bond evaluated at the H atom in atomic units,

$$E = \hat{\mathbf{r}}_{\mathrm{OH}} \cdot \sum_{i=1}^{3n} \frac{q_i \hat{\mathbf{r}}_{i\mathrm{H}}}{r_{i\mathrm{H}}^2} + \hat{\mathbf{r}}_{\mathrm{OH}} \cdot \sum_{i=1}^{n_{grid}} \frac{-\Psi_i^2 \hat{\mathbf{r}}_{i\mathrm{H}}}{r_{i\mathrm{H}}^2} \tag{2.3}$$

$\hat{\mathbf{r}}_{\mathrm{OH}}$ is the unit vector that points from O to H along the OH bond of interest, q_i is the charge on site i, $\hat{\mathbf{r}}_{i\mathrm{H}}$ is the unit vector that points from site i to the H atom

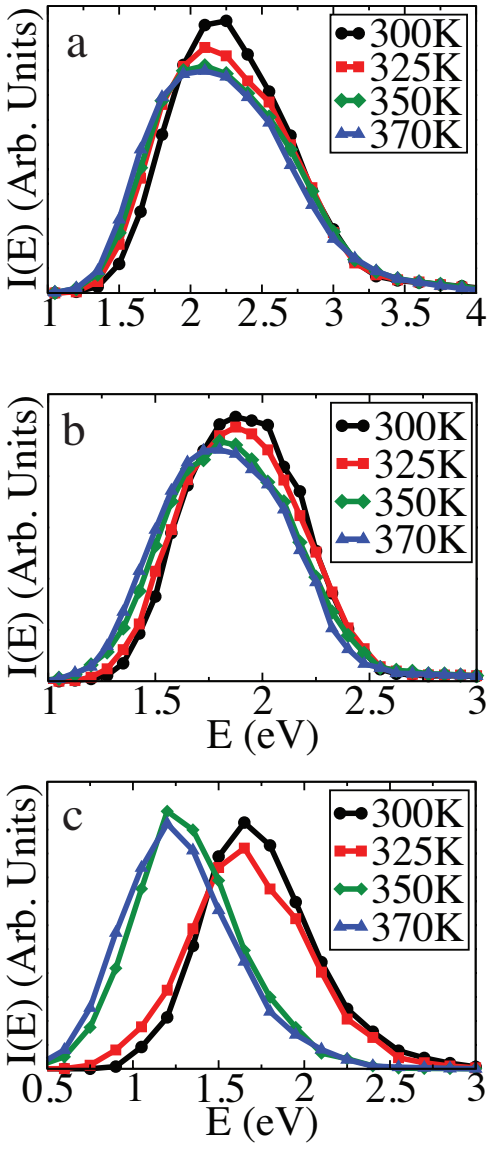

Figure 2.5: Calculated absorption spectra for the (a) SR, (b) TB, and (c) LGS models of the hydrated electron at ∼300 K (black circles), ∼325 K (red squares), ∼350 K (green diamonds), and ∼370 K (blue triangles) at the 1-atm experimental densities. The SR, TB, and LGS models all capture the experimentally observed red-shift with increasing temperature; see also Fig. 2.6.

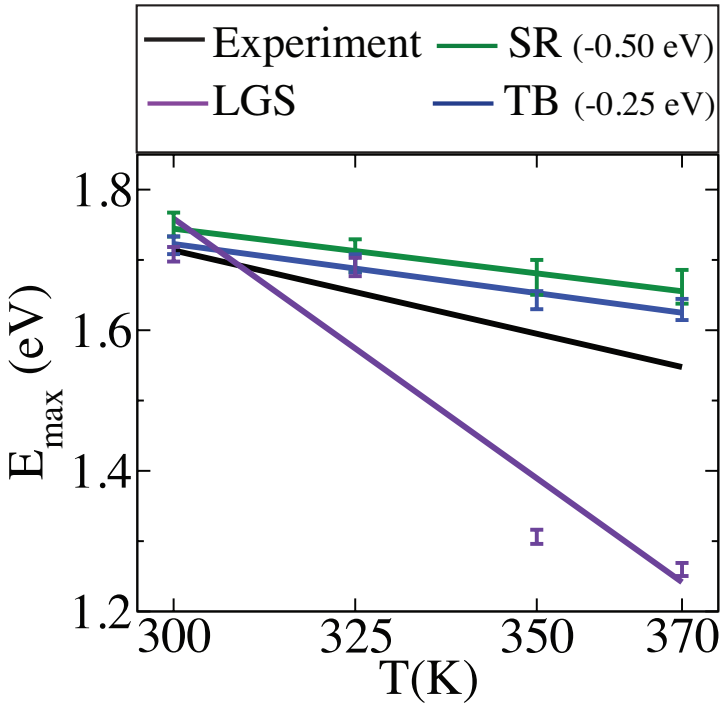

Figure 2.6: The peak of the hydrated electron's absorption spectrum, $E_{\max}$ plotted against temperature with the water density changing as if the pressure were held constant at 1 atm. The black curve shows the experimentally measured results, see Ref. [27]. For the different simulation models, $E_{\max}$ and the error bars (which represent 95% confidence intervals) were determined by fitting the data in Fig. 2.5 to the standard Gauss-Lorentz form, yielding values for the SR model (green curve), TB model (blue curve) and LGS model (purple curve). The SR and TB models predict a slope in reasonable agreement with experiment while the LGS model somewhat overestimates the shift.

of interest, $r_{i\mathrm{H}}$ is the distance between site i and the H atom of interest, and Ψ_i^2 is the electron density at gridpoint i.

The first term in Eq. 2.3 describes the electric field along the O-H bond on a given H atom from the neighboring classical water molecules, while the second term is the electric field from the hydrated electron's charge density summed over each gridpoint. The electric field on each H atom thus enables us to calculate the Raman spectrum of the water in the presence of the excess electron, but the experiment to which we wish to compare is a measurement of the *resonance* Raman spectrum. This means that only the OH vibrations that are displaced upon electronic excitation of the hydrated electron should contribute to the measured spectrum. To account for this, we used the correlation of the local E-field with stretching frequency, Eq. 2.2, along with the fact that the resonance Raman intensity for a given water molecule is proportional to the square of the force difference felt by that water upon excitation of the electron,[47, 48] to construct the resonance Raman spectrum using each of the 998 H atoms in our simulations. Using this prescription, we found that only the closest water molecules to the hydrated electron contributed significantly to the calculated resonance Raman spectra, and that the Raman spectra all were well in the inhomogeneous limit (discussed in more detail below).

The relationship between the electric field on a given H atom and the stretching frequency of the corresponding O–H bond (Eq. 2) was originally developed for the SPC/E water model.[38, 39, 40] All of the simulations performed in this work utilized the flexible version of the SPC water model (SPC/F).[32] The primary differences between these two models are first, the flexible SPC waters undergo dynamic O–H stretching (although these stretching motions are unrelated to the calculated O–H stretch frequencies) while SPC/E water molecules are rigid,[32, 49] and second, there is a tiny difference in the values of the point charges on the O and H sites in the two models. Because both SPC/E and SPC/F are variations of the

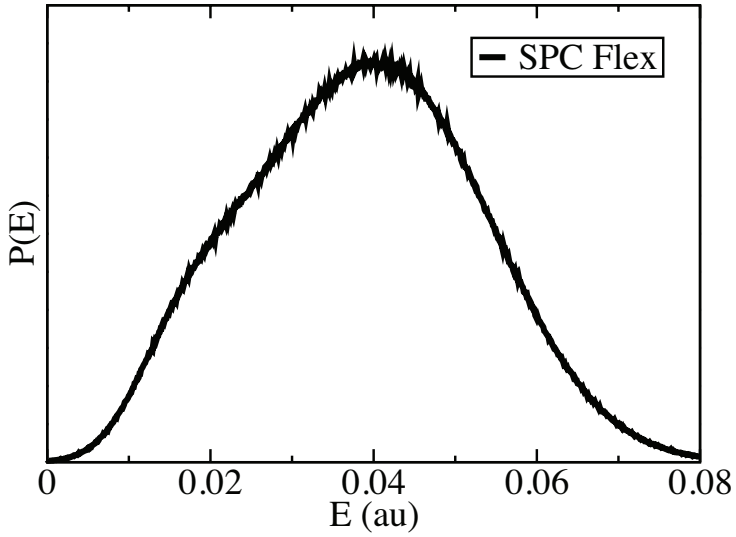

Figure 2.7: The electric field distribution experienced by Hydrogen atoms in bulk flexible SPC water. The distribution matches that for SPC/E water (see Figure 6 in Ref. [38]), indicating that the relationships developed by Corcelli and Skinner for SPC/E water can be used for flexible SPC water as well.

original SPC water model,[50] it seems logical that the electric fields experienced by the water molecules in the different variants would be similar. To test this, we ran a classical simulation consisting of 499 flexible SPC waters in a periodic box of size 24.64 Å. We then calculated the electric fields on the hydrogen atoms according to:

$$E = \hat{\mathbf{r}}_{OH} \cdot \sum_{i=1}^{3n} \frac{q_i \hat{\mathbf{r}}_{iH}}{r_{iH}^2}, \tag{2.4}$$

which led to the electric field distribution shown in Figure 2.7. A comparison of this electric field distribution to that originally published by Corcelli and Skinner (see Figure 6 in Ref. [38]) shows that the two distributions are nearly identical. This gives us confidence that we can use the relationship derived by Corcelli and Skinner for SPC/E water molecules for the flexible SPC water molecules used in our simulations.

2.5.1.3 Generating resonance Raman spectra using inhomogeneous frequency distributions

In order to calculate the isotropic Raman spectrum of water from a classical MD simulation, Corcelli and Skinner developed a correlation between the electric field experienced by a hydrogen atom and both the isotropic transition polarizability and the vibrational coordinate of the O–H stretch between the ground and first excited states;[39] the Raman spectrum is then determined as the Fourier transform of the appropriate polarizability correlation function. The fact that we wished to calculate *resonance* Raman spectra associated with excitation of a particular aqueous solute (the hydrated electron in our case) instead of the bulk water Raman spectrum required us to weight the contributions of each water molecule by the square of the force difference it experiences upon excitation of the solute, as discussed further below. The use of the force weighting method, however, prevents us from using Corcelli and Skinner's method to generate the isotropic Raman line shapes. This is because we cannot construct meaningful correlation functions since the force weighting for each water molecule is constantly fluctuating as waters move closer to or farther from the solute, leading to an artificial decay of the polarizability correlation function. Instead, in the main text we assumed that the resonance Raman spectra are well in the inhomogeneous broadening limit, and that we can accurately construct such spectra by simply looking at the force-weighted frequency distribution averaged over an ensemble of representative configurations. We tested this assumption by comparing our inhomogeneous frequency distribution for bulk flexible SPC water (Figure 2.8) to the Raman spectrum of bulk SPC/E water calculated by Corcelli and Skinner (see Figure 4b of Ref. [39]) and found near quantitative agreement. Moreover, the inhomogeneous O–H stretch frequency distribution we calculated for SPC/F water actually better resembles the experimental Raman spectrum for pure water since the blue shoulder found in the inhomogeneous frequency distribution is slightly

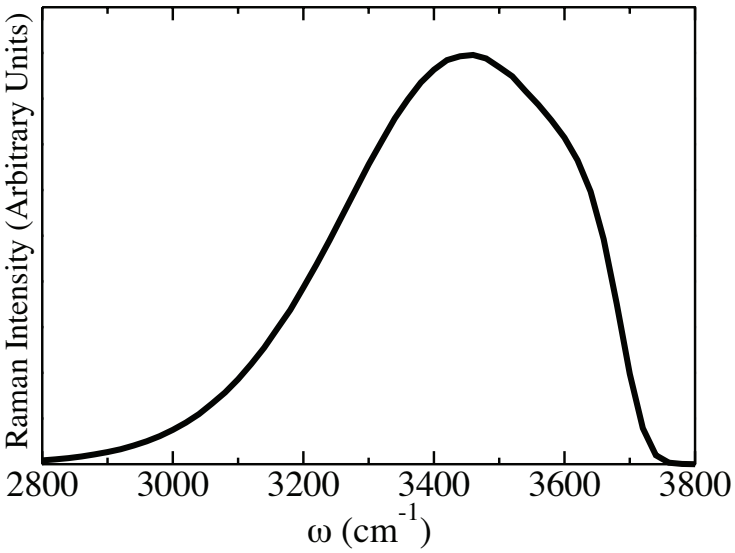

Figure 2.8: The frequency distribution of O-H stretches in bulk flexible SPC water. The distribution closely matches the experimental Raman spectrum of bulk water, indicating that the Raman spectrum is within the inhomogeneous broadening limit.

smaller than that in the spectrum calculated from the correlation function method (see Figure 4a of Ref. [39]).

Our assumption of using the inhomogeneous limit to calculate the resonance Raman spectrum of the hydrated electron is further validated by some recent work by Smith, Saykally, and Geissler (SSG).[33] SSG compared the Raman spectra of water in the presence of alkali halides to the frequency distributions of these same systems obtained from Monte Carlo simulations. Like Corcelli and Skineer,[38] SSG also found that there was a strong correlation between the electric fields on the hydrogen atoms and the corresponding inhomogeneous frequency distribution.

Finally, and perhaps most importantly, we note that even if the experimental resonance Raman spectrum of the hydrated electron has a significant homogeneously broadened component, in the main text we use the same force-weighted inhomogeneous frequency distributions to calculate the resonance Raman spectra

for all three models of the hydrated electron. Thus, any error introduced by using the inhomogeneous limit should enter on the same footing when comparing the resonance Raman spectra of the SR, TB and LGS models.

2.5.1.4 Simulation and force-weighting details for calculating resonance Raman spectra of the hydrated electron

In this work, we are specifically interested in calculating *resonance* Raman spectra. For any solute, the vibrational modes that contribute most to a resonance Raman spectrum are those that have the largest displacement between the excited state and the ground state.[47, 48]. This is because a large displacement results in a stronger transition dipole between the displaced vibronic wavefunctions. The degree of displacement of a vibronic motion is simply related to the difference in slope along the ground and excited-state potentials at the point where the Franck-Codon excitation takes place (see Figure 2.9). Thus, for our mixed quantum/classical simulations of the hydrated electron, we determined the displacement of each of the neighboring water molecule's O–H bonds by examining how the force the hydrated electron exerts on each bond changed when the electron was promoted from its ground to its first excited state. To do this, we ran 40-ps ground-state production trajectories for each of the three hydrated electron models. Every 10 fs along these trajectories we took configurations for which we also calculated the hydrated electron's lowest excited-state wavefunction, which in turn enabled us to calculate the Hellmann-Feynman forces exerted by the electron along each of the classical water O–H bonds for both the ground and excited states. We then calculated the force difference on each classical water from excitation of the quantum mechanical electron as:

$$\mathbf{f}_{\text{ground}} = \mathbf{f}_{\text{H,ground}} - \mathbf{f}_{\text{O,ground}} \tag{2.5}$$

$$\mathbf{f}_{\text{excited}} = \mathbf{f}_{\text{H,excited}} - \mathbf{f}_{\text{O,excited}} \tag{2.6}$$

$$\Delta\mathbf{f} = (\mathbf{f}_{\text{excited}} - \mathbf{f}_{\text{ground}}) \cdot \hat{\mathbf{r}}_{\text{OH}} \tag{2.7}$$

The theory of resonance Raman spectroscopy tells us that the intensity of each displaced mode is proportional to the square of the force difference, $\Delta\mathbf{f}^2$.[47, 48] Thus, in all of our resonance Raman calculations, we weighted the contribution of each molecule's O–H stretching frequency (determined by the value of the electric field on the H atom) by the square of the force difference felt along that bond when the electron is placed into its first excited state. This ensures that only water molecules that are appropriately displaced upon excitation of the electron (*i.e.* those that are closest to the electron's charge density; see below) contribute to the calculated resonance Raman spectrum; molecules that are far from the electron's charge density experience no change in force when the electron is excited, and thus do not contribute to the calculated spectrum.

2.5.2 The origins of the resonance Raman spectra of different hydrated electron models

2.5.2.1 The electric field distributions in the non-cavity and cavity models of the hydrated electron

As described above, we used the distribution of electric fields on each classical H atom in the simulation to determine the resonance Raman frequency distribution for the different models of the hydrated electron (and then weighted the contribution of each water molecule by its displacement upon excitation of the electron). Figure 2.10 shows the raw electric field distributions as a function of distance from the electron center of mass (COM) for the SR, TB, and LGS models. The electric fields experienced by hydrogen atoms in the first solvent shell (defined as 3.0 Å from the COM for SR, 2.7 Å from the COM for TB, and 2.6 Å from the COM for

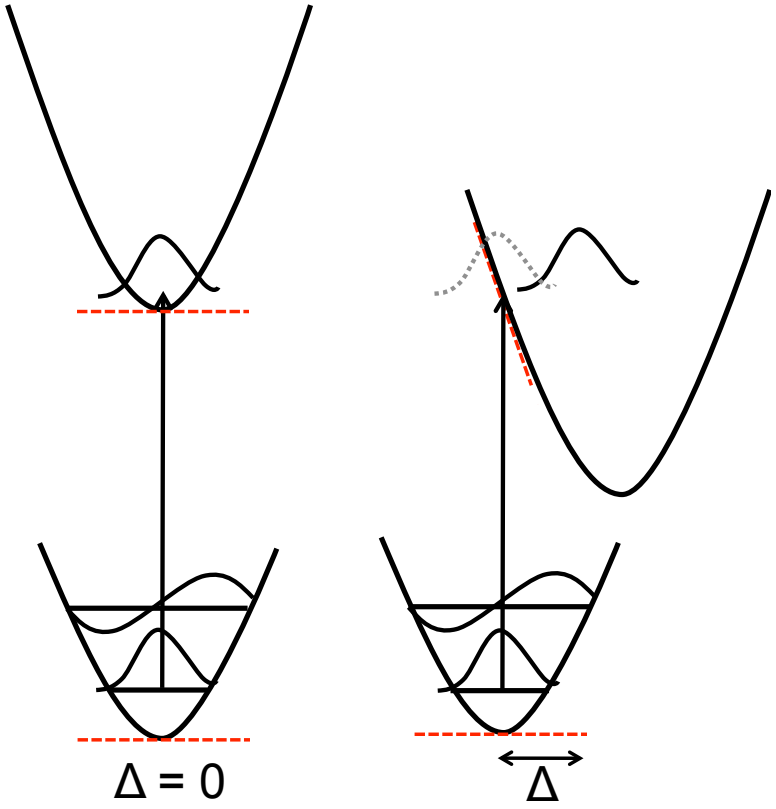

Figure 2.9: Illustration of the origin of resonance Raman signal intensity. The initial ground-state wavefunction is excited, where it becomes a moving wavepacket. If the initial and final states are orthogonal (as shown in the image to the left), there is no resonance Raman intensity. A large displacement between the ground and excited state (as shown in the image to the right) results in an intense resonance Raman signal. The strength of the signal is related to the displacement of the O-H bond upon excitation, which can be approximated by the differences in slope along the ground and excited state potentials where the Frank Condon excitation takes place (represented by red dashed lines).

LGS) are highlighted in red. The figure makes clear that the water H atoms in the first shell of the cavity SR and TB models experience a range of electric fields that is quite different than the electric fields experienced by water molecules in the bulk. The distribution of electric fields for these first-shell water molecules is much narrower than seen in the bulk and the values of the electric field felt by the first-shell water molecules are on average much smaller than the bulk. This is because the cavity electron resides approximately 2.5 Å away from the first-shell water molecules, so the electron provides a smaller electric field for the first-shell H atoms than would an H-bonded water molecule. As discussed in Section 2.3.2, this type of disruption of the local H-bond network is similar to the structure breaking induced by dissolving anions such as the halides in water. Since the dissolution of anions in water leads to a narrowing and blue-shift of the water O–H stretching band, it is not surprising to see this same effect for a cavity solvated electron that breaks the local water structure in a similar way. In contrast, our non-cavity LGS model shows a wider range of electric fields experienced by the H atoms closest to the electron COM. The magnitude of the electric fields of these water molecules inside the LGS electron are significantly greater than those in bulk water because these water molecules are still H-bonded to other waters. Thus, these interior water molecules feel electric fields from both the high-density surrounding water molecules and the gradient of the surrounding non-cavity electron's charge density. As discussed in the main text, only a non-cavity model that does not break the local H-bond structure of the water is able to capture the large distribution of electric fields necessary to generate a broad Raman spectrum that is consistent with experiment.

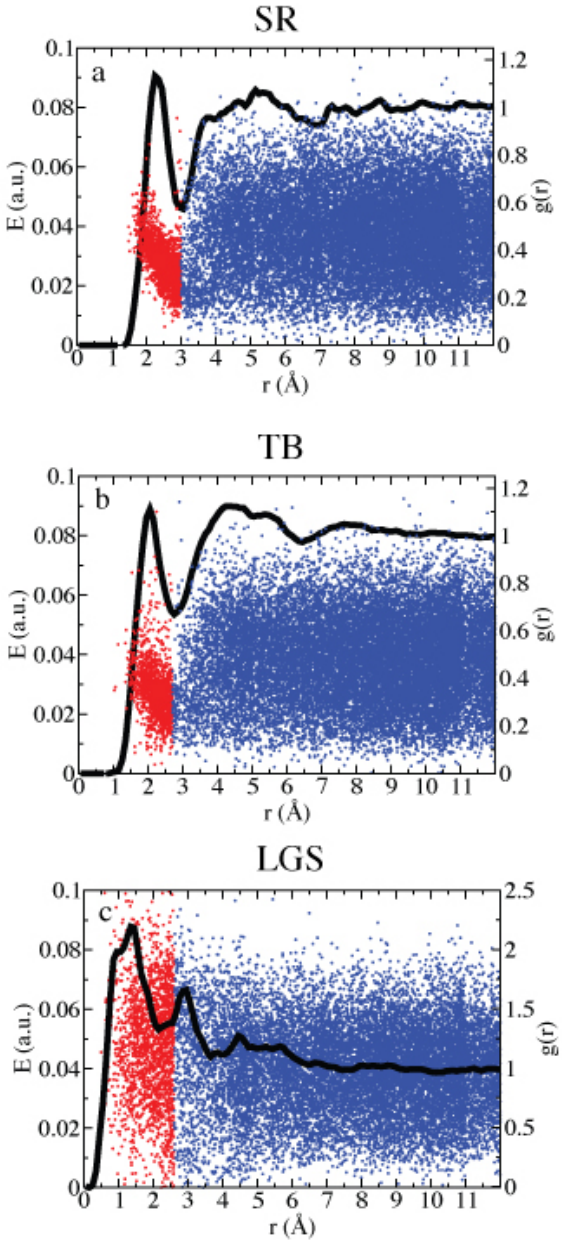

Figure 2.10: The raw distribution of electric fields experienced by H atoms plotted against the distance the specific H atom is from the electron center of mass for the (a) SR, (b) TB, and (c) LGS models. The red points indicate hydrogen atoms that are within the first solvent shell around the electron (defined as 3.0 Å for SR, 2.7 Å for TB, and 2.6 Å for LGS). The radial distribution function is provided to emphasize the range of electric fields experienced by first shell hydrogen atoms. We have arbitrarily reduced the density of points at different distances for clarity of presentation.

2.5.2.2 Molecules that contribute to the Raman spectrum come from first two solvation shells

We already argued above that our force-weighting method used to calculate the resonance Raman spectrum of the hydrated electron tends to emphasize the O–H stretches of water molecules within the first two solvation shells because these are the waters that experience the largest force difference upon electronic excitation of the hydrated electron. This is because for all three models, the excitation of the hydrated electron from its *s*-like ground state to its *p*-like first excited state causes molecules near the *p*-state lobes to suddenly have increased overlap with the electron wavefunction while water molecules near the node in the *p*-like excited-state wavefunction may suddenly have less overlap, either of which could result in large changes in the force experienced by those water molecules. This idea is quantified in Figure 2.11, which examines the magnitude of the force-weighting of the water H atoms based on the distance each H atom is from the electron COM. The H atoms that contribute most to the resonance Raman spectrum (those that experience the greatest changes in force upon electron excitation) are marked in red. For the cavity SR and TB models, the water molecules that most heavily influence the spectrum are all within 4 Å of the electron COM, a distance that is similar to the radius of gyration for the *excited state* of the hydrated electron.[9] In contrast, for our non-cavity LGS model, the water molecules that experience the greatest force differences tend to lie within 1.5 Å of the electron COM, although most of the water molecules within the LGS electron experience some change in force upon excitation and thus have some contribution to the calculated spectrum. Since all three hydrated electron models produce similar first excited state radii of gyration, the main difference between them results from the fact that for the LGS model, water molecules residing 4 Å away from the electron COM still have significant overlap with LGS ground-state electron density.[12] Thus, many of the water molecules between 1.5 and 4 Å of the COM of the LGS hydrated electron

have similar overlap with the electron's wavefunction in both the ground and first excited states, causing these water molecules to have a somewhat smaller weighting in the resonance Raman spectrum.

Even though we felt that an accurate treatment of the resonance Raman spectrum of the hydrated electron should include the appropriate force weighting, we also noted that it might be acceptable to simply approximate the resonance Raman spectrum by equally weighting all of the important molecules near the electron's COM. To test this idea, we generated frequency distributions to approximate the electron's Raman spectrum by equally weighting the contributions from all water molecules that were within 4 Å of the electron COM for each of the SR, TB, and LGS models, as shown in Figure 2.12. We find that there is excellent qualitative and near-quantitative agreement between these approximate spectra and the fully force-weighted spectra shown in the main text. In particular, for the cavity SR and TB models, the distance cut-off spectra are slightly blue-shifted relative to the force-weighted spectra. This is because the 4 Å distance cut-off includes water molecules in the first shell that are not included in the force-weighting method. These first-shell water molecules experience electric fields that are much weaker than those experienced by bulk water molecules (*cf.* Figure 2.10) for the reasons discussed above and in the main text, thus producing an even further blue-shifted spectrum that would be in further disagreement with experiment. When we changed the distance cut-off to 3 Å, the calculated SR and TB Raman spectra were still blue-shifted relative to the force-weighed spectra, but were also narrower than the force-weighted spectra; this is because there are second-shell water molecules (which are included in the 4 Å cut-off calculation) that help contribute to the width of the spectrum. In contrast, the non-cavity LGS Raman spectrum generated with the 4 Å cut-off actually matches the experimental resonance Raman spectrum better than the force-weighted spectrum. This is because the 4 Å cut-off more heavily weights the molecules that are slightly fur-

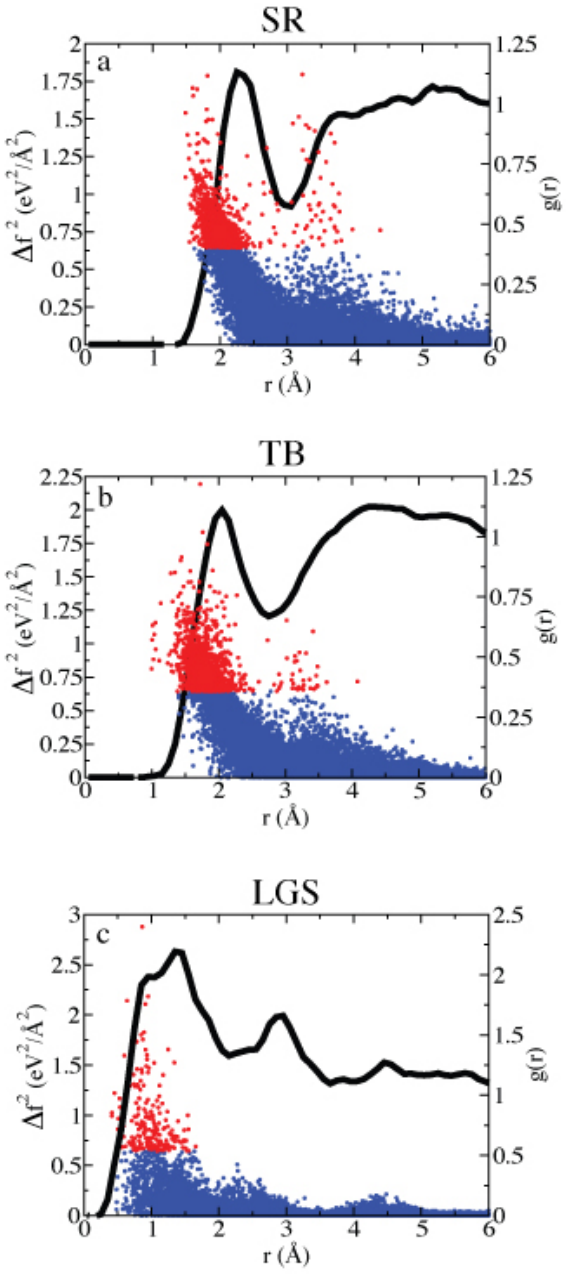

Figure 2.11: The force weighting of each hydrogen atom plotted against the distance the specific H atom is from the electron center of mass for the (a) SR, (b) TB, and (c) LGS models. The red points indicate H atoms that experience a force weighting of 0.64 $eV^2/Å^2$ or greater. The radial distribution function is provided to demonstrate where the largest force differences occur. We have arbitrarily reduced the density of points at different distances for clarity of presentation.

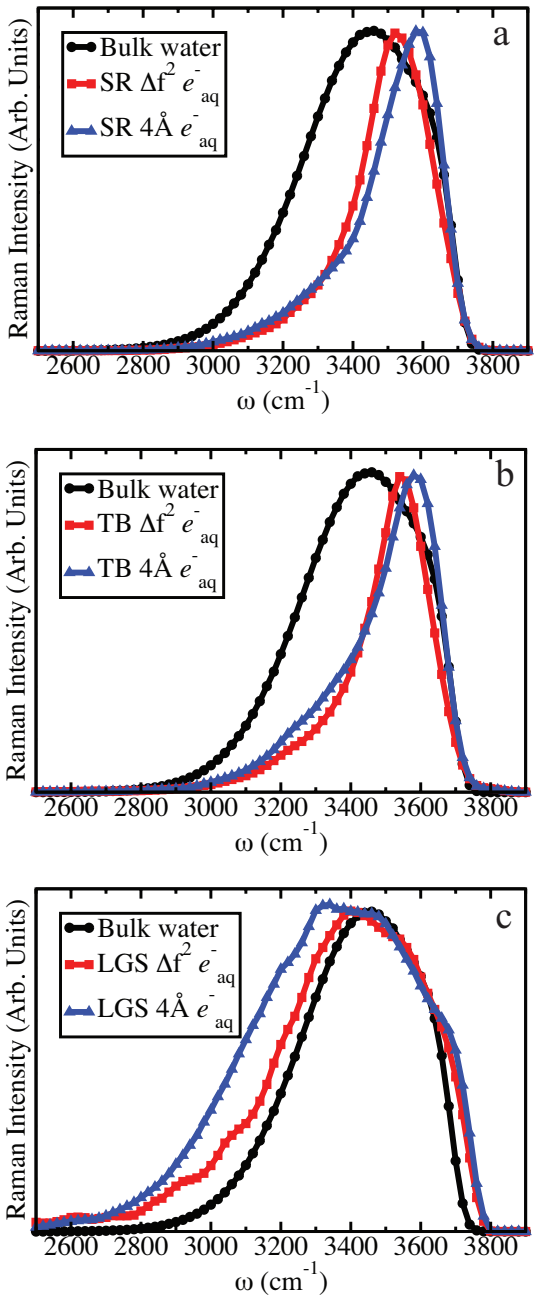

Figure 2.12: The calculated Raman spectrum of bulk flexible water (black circles) compared to the hydrated electron's force-weighted resonance Raman spectrum (red squares) and the resonance Raman spectrum generated by all water-molecules within a 4 Å cutoff of the electron center of mass (blue triangles) for the SR (a), TB (b), and LGS (c) models. The 4 Å cutoff provides a surprisingly good approximation to the force-weighting method, leading to spectra that are in qualitative agreement.

ther from the electron's COM compared to the force-weighting calculation. Since these water molecules experience a wide variety of different local electric fields (see Figure 2.10), including all of them creates a broader spectrum that matches better with experiment. Changing the LGS cut-off to 3 Å leads to almost no differences relative to the 4 Å LGS spectrum.

CHAPTER 3

An investigation into the properties that dictate cavity and non-cavity character in hydrated electron models

3.1 Abstract

The hydrated electron – the species that results from the addition of a single excess electron to liquid water – has been the focus of much interest both because of its role in radiation chemistry and other chemical reactions, and because it provides for a deceptively simple system that can serve as a means to confront the predictions of quantum molecular dynamics simulations with experiment. Despite all this interest, there is still considerable debate over the molecular structure of the hydrated electron: does it occupy a cavity, have a significant number of interior water molecules, or a structure somewhere in between? The reason for all this debate is that different computer simulations have produced each of these different structures, yet the predicted properties for these different structures are still in reasonable agreement with experiment. In this Chapter, we explore the reasons underlying why different structures are produced when different pseudopotentials are used in quantum simulations of the hydrated electron. We also show that essentially all the different models for the hydrated electron, including those from fully *ab initio* calculations, have relatively little direct overlap of the electron's wavefunction with the nearby water molecules. Thus, a non-cavity hydrated electron is better thought of as an 'inverse plum pudding' model, with interior waters

that locally expel the surrounding electron's charge density. Finally, we also explore the agreement between different hydrated electron models and certain key experiments, such as resonance Raman spectroscopy and the temperature dependence and degree of homogeneous broadening of the optical absorption spectrum, in order to distinguish between the different simulated structures. Taken together, we conclude that the hydrated electron likely has a significant number of interior water molecules.

3.2 Introduction

The hydrated electron, which is a single excess electron in electrically neutral liquid water, is an important chemical species in areas of science ranging from biological processes to radiation chemistry. Yet, despite years of intense study using both theoretical and experimental techniques,[1] there is still not universal consensus on the molecular structure of this simplest of quantum mechanical solutes. The theoretical methods most commonly used to model the hydrated electron involve mixed quantum/classical (MQC) simulations, where the excess electron is treated quantum mechanically and the surrounding water molecules are treated classically. One of the key features of the one-electron approximation inherent in MQC approaches is the use of an electron-water pseudopotential. As we discuss further below, it turns out that the molecular structure of the hydrated electron obtained from MQC simulations is extremely sensitive to the choice of this pseudopotential – the sensitivity is so high that small changes in the functional form of the potential can literally turn the hydrated electron's molecular structure inside out. Since experiments have not been able to conclusively determine a structure for the hydrated electron, in this Chapter, we explore the questions of what exactly the hydrated electron looks like and how physically reasonable are the various proposed structures.

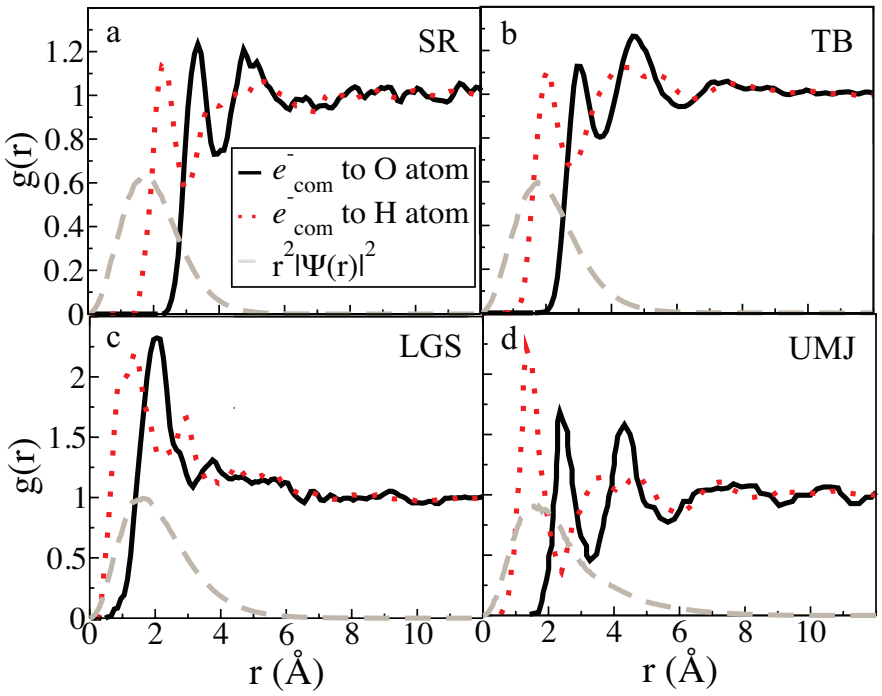

Figure 3.1: The radial distribution functions of the electron center-of-mass to water O atoms (black, full) and H atoms (red, dotted), along with the electron density (gray, dashed) for the (a) SR, (b) TB, (c) LGS, and (d) UMJ models. The SR and TB models show a clear cavity occupied by the electron, while no cavity is present in the LGS model and a very small cavity is present in the UMJ model.

Instinctively, one would expect the hydrated electron to be repelled by each of the surrounding water molecules; after all, the Pauli exclusion principle tells us that the excess electron cannot occupy the same regions of space that are already occupied by the electrons residing in the water molecules' molecular orbitals (MOs). Based on this idea, the early picture that emerged was that of a hydrated electron which expelled the nearby solvent molecules and occupied a cavity in the water.[51] From this perspective, the hydrated electron is expected to act like an aqueous halide, midway in size between chloride and bromide,[6] but with a structure that is softer and more flexible than that of the halides due to the highly polarizable nature of the electron. This cavity picture was reinforced by early MQC simulation studies.[21, 52] For example, Schnitker and Rossky (SR), who used a pseudopotential that was later found to contain an error,[28] performed MQC simulations that indicated that the hydrated electron resides in a cavity that is surrounded by six bond-oriented water molecules.[5, 6, 7] This structure, which is shown in Figure 3.1a, was quite reminiscent of the structure suggested in earlier EPR experiments performed on excess electrons in aqueous alkaline glassy matrices.[4] Later, Turi, Borgis, and their co-workers (TB) ran MQC molecular dynamics (MD) simulations that also suggested that the hydrated electron occupied a cavity in the water, although the particular structure (with only roughly four first-shell water molecules, Figure 3.1b) was different than that suggested by SR.[8, 9] More recently, the effects of water polarization on the hydrated electron's structure and energetics was explored by Jacobson and Herbert [10, 11]. Some amount of electronic polarization is included in the SR, TB, and LGS models as well, but in a mean-field manner,[53] whereas Jacobson and Herbert treated water polarization explicitly and self-consistently. They found that the inclusion of self-consistent polarization is important to obtaining meaningful ionization potentials and capturing the blue tail in the optical absorption spectra, yet while the calculated energetics were affected, the structure of the hydrated electron was only

slightly modified from that seen by TB. The Jacobson and Herbert model for the hydrated electron still resides in a cavity which is surrounded by approximately four water molecules, although the cavity is slightly smaller than the TB cavity. Finally, recent MQC simulations performed by Larsen, Glover, and Schwartz (LGS) have suggested a completely different picture for the hydrated electron; rather than dwelling in a cavity, LGS suggested that the hydrated electron occupies a region of enhanced water density ($\rho \approx 1.2$ g/cm^3), with many water molecules residing in the interior of the excess electron's charge density (Figure 3.1c).[12]

3.3 Controversy over one-electron hydrated electron MD simulations

Even though the calculated properties of the LGS non-cavity hydrated electron agreed as well with experiment as predictions from cavity models,[12, 15, 54] the idea of a hydrated electron with interior waters quickly met with significant resistance.[13, 14, 31] This lack of acceptance for a non-cavity electron partially stems from the fact that the calculated properties of the hydrated electron depend sensitively on the nature of the pseudopotential chosen for the simulation. Both TB and LGS derived their pseudopotentials from the Phillips-Kleinman (PK) formalism, which provides a prescription for calculating a potential that guarantees that the wavefunction of the excess electron is orthogonal to the wavefunctions of all the electrons in the water MOs (as calculated at the Hartree-Fock level of theory).[19, 20] Even when constructed for expressed use in the condensed phase, these pseudopotentials are based on calculations of an electron with a single, gas-phase molecule. This presents a problem for the case of water, as a single, gas-phase water molecule does not bind an electron. This can be dealt with in a number of ways: by the addition of a confinement potential meant to constrain

the excess electron in the vicinity of the water molecule, or by the implementation of a basis set with finite range. The consequences of each of these methods is not obvious and an evaluation of how sensitive the resulting potential is to the chosen method of electron confinement is underway. Regardless of the details behind the development of a PK pseudopotential, it is not computationally feasible to use the full numerical PK potential in a MQC simulation; the standard procedure has been to fit this potential with an analytic function. TB decided to fit the PK potential with a very simple function. They adjusted the parameters of their fit to guarantee that the eigenenergy would be correct, but the functional form they chose missed many of the physical features of the pseudopotential. For example, the full, exact PK potential for an excess electron interacting with a water molecule has an attractive region behind the water O atom (opposite the H atoms) and a strongly repulsive region between the H atoms (Fig. 3.2a) that are missed by the TB fit (cf. Fig. 3.2e). LGS, on the other hand, decided to fit this same PK pseudopotential in such a way as to retain these distinct features, but at the cost of changing the eigenenergy by $\sim$0.1 eV (Fig. 3.2b). Perhaps even more surprising, small changes in the shape of the fitting function can change the behavior of the simulated hydrated electron from cavity to non-cavity or back again.[15, 13] Thus, starting with identical formalism, TB and LGS have produced two very different pictures of the hydrated electron, all because of subtle details in the way that the numerical PK psuedopotential was analytically fit.

Another issue with the implementation of pseudopotentials in hydrated electron simulations is the fact that such potentials have strongly varying features on length scales short compared to the water O–H bond. This means that the basis sets used in simulations using such potentials must be extensive enough to capture spatial variation in the wavefunction on the same length scale as the variations in the potential. Since it is impractical to use more than $\sim 10^4$ basis functions in dynamical simulations (as would be required to calculate the hydrated electron's

wavefunction both on top of and between the water molecules), the standard practice is to spatially smooth the potential to remove the finer features.[8, 12]. Figure 3.2 also shows plots of the numerically exact PK pseudopotential after having been smoothed (via convolution of the PK pseudoorbital with a Gaussian before calculation of the pseudopotential) at several different spatial resolutions. Figure 3.2a shows the pseudopotential in its least adulterated form, while Figs. 3.2c and 3.2d show that the effects of increased smoothing wash out many prominent features of the numerically exact potential, as expected. It is worth noting that although the LGS potential has been criticized for being overly attractive in the region behind the water O atom,[13] a comparison of the left column of Figs. 3.2a and 3.2b shows that the LGS fit actually underestimates the attraction in this region that is present in the full potential. As the magnitude of the smoothing increases, this attractive feature is essentially completely removed, as is the repulsive feature between the H atoms. What makes the loss of these features interesting is that the TB potential, Fig. 3.2e, bears a striking resemblance to the pseudopotential that has been smoothed to such an extent that most of the features have been washed out. Thus, when evaluating the accuracy of the PK-derived pseudopotentials that have been presented in the literature, one has to compare a potential that has the correct eigenenergy but none of the physical features needed to ensure orthogonality with the electrons in the water MOs (TB), to a potential that has the correct calculated shape but misses the eigenenergy by an amount less than $k_{\mathrm{B}}T$ at room temperature (LGS). This obvious sensitivity to the details of the construction of the pseudopotential make it abundantly clear that a more rigorous, dynamical approach to the construction of a water pseudopotential that responds to a changing environment may be necessary to shed light on the simulation of this system.[44]

The other reason that the LGS non-cavity picture of the hydrated electron has not been well received lies in the fact that it initially appears counterintuitive. Because scientists studying solvated electrons have spent decades developing the idea

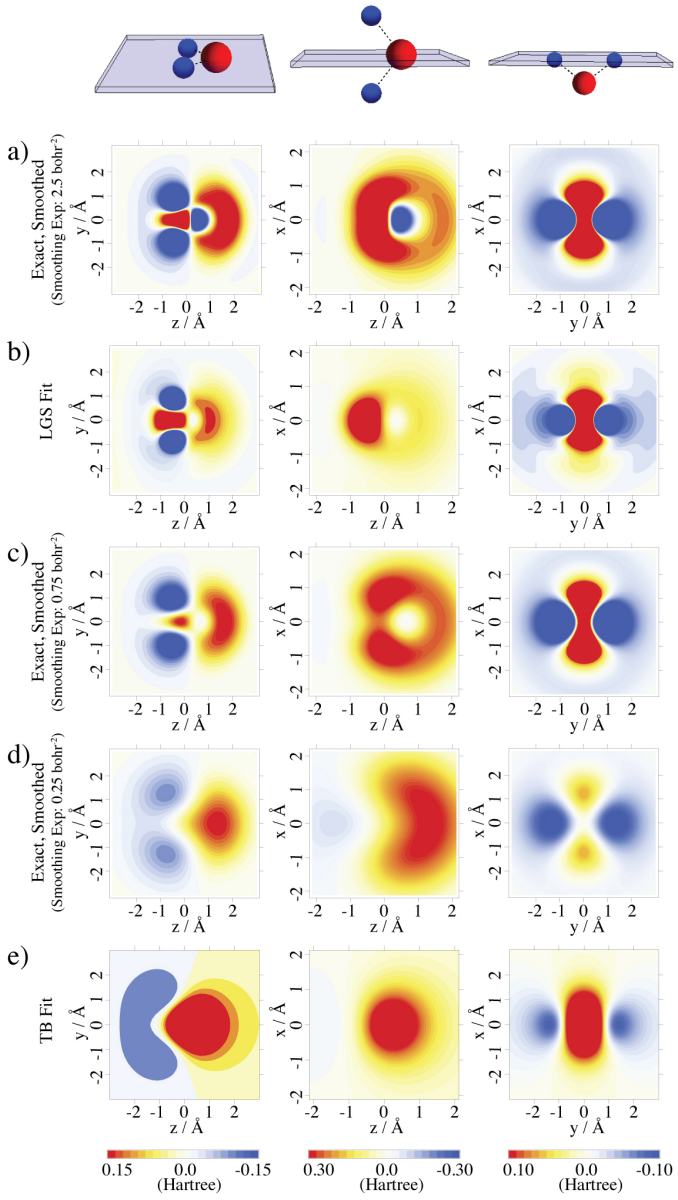

Figure 3.2: Cuts of the full, exact PK electron-water pseudopotential, after smoothing the corresponding pseudoorbital with a Gaussian with an exponent of (a) 2.5 bohr^{-2}, (c) 0.75 bohr^{-2}, (d) 0.25 bohr^{-2}, and the (b) LGS and (e) TB fits to the exact (smoothed) pseudopotential. The water molecule lies in the y-z plane with the dipole pointing along the z-axis. The O atom is located at (0.0 Å, 0.0 Å, 0.11663 Å), and the H atoms are located at (0.0 Å, 0.76001 Å, -0.46654 Å) and (0.0 Å, -0.76001 Å, -0.46654 Å). The left panels show a cut parallel to the molecular y-z plane with $x = 0.0$ Å, the middle panels show a cut perpendicular to the plane of the molecule with $y = 0.0$ Å, and the right panels show a cut perpendicular to the molecular plane through the H atoms. The energy scales are in units of Hartree.

that closed-shell molecules are intrinsically repelled by excess electrons, the idea of an electron that completely overlaps with these molecules seems to go against our very instinct on the matter. But as we show below, the LGS non-cavity electron does not have significant direct overlap between the excess electron's charge density and the interior water molecules; instead, it simply has a different arrangement of the water molecules associated with the charge density. The hydrated electron is a purely quantum mechanical object, capable of significant distortion – contrary to the simple pictures prevalent in the literature, it is not and does not have to behave like a halide ion. In fact, the idea of a non-cavity hydrated electron was explored over twenty years ago by Tuttle and Golden, who compared the absorption spectra of solvated electrons to solvated halide ions and determined that a cavity model for the hydrated electron is inconsistent with the experimental absorption spectra.[55] Instead, they proposed that the spectroscopy of the hydrated electron was more consistent with a solvent-anion complex, a structure which shares many features in common with the LGS simulations.[55] Indeed, moment analysis of the hydrated electron's absorption spectrum tells us that the hydrated electron's charge density has a radius of gyration of 2.4 Å,[56] but nothing in the spectrum directly indicates whether the water molecules are primarily inside or outside of the charge density.

One might think that the question of the structure of the hydrated electron could be easily settled from fully *ab initio* calculations, but here again the results have been ambiguous. Most *ab initio* work on the hydrated electron has been performed on small gas-phase water anion clusters.[29, 57, 58] The clusters in these studies are usually cold, so the calculated structures are often those of metastable states.[59] In addition to occupying surface states, most water anion cluster studies have shown cavity-type bound states for the excess electron,[60, 59] although some also have started with structures that are predisposed to cavity formation rather than to enhanced interior density. The one-electron LGS simulations suggest that

the non-cavity structure is stable only in the presence of a sufficient number (of order hundreds) of water molecules so that the interior of the electron is filled and there are several additional surrounding solvent shells.[12] This places *ab initio* calculations at the limit of what is computationally feasible for density functional theory (DFT) and out of range for more accurate quantum chemistry methods. We note that when the limits are pushed, however, recent cluster calculations based on DFT have shown water density penetrating deep into the electron's center, even for room temperature water (e.g., see Fig. 2 of Ref. [61]). And when extending such calculations to bulk liquid water, Uhlig, Marsalek, and Jungwirth (UMJ) have found a hydrated electron that has both cavity and non-cavity characteristics.[17] In UMJ's picture, there is a small central cavity at the center of the hydrated electron's wavefunction, but over half of the charge density resides amongst the solvent in a manner reminiscent of that proposed by LGS (Fig. 3.1d).

3.4 Quantifying the extent of electron–water overlap in different hydrated electron models

Although *ab initio* calculations support the idea that there can be significant electron-water overlap, we are still left with the conundrum of whether or not the hydrated electron occupies a cavity, encompasses a region of enhanced water density, or has a structure that is some hybrid mixture of the two. To better understand what it really means to have water molecules inside of the hydrated electron, and to help determine whether or not a hydrated electron with interior waters is consistent with our physical instincts, we have investigated the amount of electron–water overlap in the SR, TB, LGS, and UMJ models. Once we have a better understanding of what makes these models quantitatively different from each other, we can then focus on how these differences relate to the extent of agreement each of these models have with experiment.

The difficulty in quantifying the extent of electron–water overlap in different models of the hydrated electron is that there is not a unique way to define what is meant by 'overlap.' In this work we define two types of overlap: radial and direct. Radial overlap is what we believe most scientists think about when confronted with the idea of waters interior to the charge density of the hydrated electron; we define the radial overlap Φ as the extent to which the average electron charge density at a given distance from the electron's center of mass falls on top of an average number of water molecules that are present at that same distance:

$$\Phi = 4\pi \int r^2 g(r) |\Psi(r)|^2 dr \tag{3.1}$$

where r is the distance between the electron center of mass (COM) and the O atom on a given water molecule, $g(r)$ is the e^--oxygen radial distribution function, and $|\Psi(r)|^2$ is the hydrated electron's charge density. Table 3.1 shows the value of Φ for each of the four hydrated electron models considered here. Not surprisingly, the two cavity models show relatively little radial overlap of the electron with the nearby waters: the SR model has 16.9% overlap while the slightly softer TB model has 31.1% radial overlap. It is important to note that even cavity models still have appreciable radial overlap between the electron density and water density; as shown in Figure 3.1, the 'tail' of the electron's wavefunction extends through the first solvent shell and beyond in both of these models. The LGS non-cavity model, in contrast, has a radial overlap of 122%. This >100% overlap is not unphysical; it arises because the average density of the water molecules inside the hydrated electron's charge density is ∼1.22 g/mL,[12] and the electron's wavefunction has perfect radial overlap with all of the interior waters. Finally, the UMJ hybrid model has 63.1% radial electron-water overlap, roughly half-way between the cavity and non-cavity hydrated electron models.

Although Φ tells us a great deal about where the water molecules reside relative

to the electron's charge density, the radial overlap does not provide a good measure of how much of the excess electron's charge lies physically on top of the water molecules. Thus, we can define another measure of overlap, the direct overlap Θ, as the fraction of the hydrated electron's density that resides inside of spheres centered at the geometric center of mass of each water molecule. This definition depends on the cutoff radius chosen for the sphere, r_c, with the direct overlap given by:

$$\Theta = \left\langle \sum_{i=1}^{n_{molcs}} 4\pi \int_0^{r_c} r_i^2 |\Psi(r_i)|^2 dr_i \right\rangle \tag{3.2}$$

where the sum runs over all of the water molecules in the simulation and the result is averaged over a large number of trajectories. We examined several choices for the value of r_c, and decided that a value of 1.0 Å was the most appropriate, since this size roughly represents the core orbitals of the water molecule: smaller sizes led to negligible values of Θ, while larger sizes led to similar values for all the various hydrated electron models (see Figure 3.3). Table 3.1 shows the calculated direct overlap for the four hydrated electron models considered here with this choice of r_c: the SR cavity model has a direct overlap of 1.0% while the TB cavity model has a higher direct overlap of 5.7%. Interestingly, the LGS non-cavity model and the UMJ hybrid model have similar direct overlaps of 17.0% and 17.9%, respectively. These latter values are both very close to the ∼20% direct overlap estimated in previous *ab initio* studies.[62, 63] The fact that the LGS non-cavity model shows similar amounts of direct overlap to the UMJ and other *ab initio* calculations suggests that a small amount of direct overlap between the excess electron and the water molecules is indeed physically reasonable. Thus, the LGS model is the only MQC model that appears to give a 'correct' estimate for the amount of direct electron-water overlap. The various cavity models of the hydrated electron may in fact have too little direct overlap to be physically

Hydrated Electron Model	Φ	Θ
SR (cavity)	16.9%	1.0%
TB (cavity)	31.1%	5.7%
LGS (non-cavity)	122%	17.0%
UMJ (hybrid)	63.1%	17.9%

Table 3.1: Calculated percent radial (Φ) and direct (Θ) overlap for the SR, TB, LGS, and UMJ models. Direct overlap percentages were obtained by averaging over 400 trajectories containing 499 water molecules.

meaningful, as the amount of overlap they show is much more reminiscent of what is seen for $Cl^-(H_2O)_n$.[63] And, as we argue further below, the experimental resonance Raman spectrum shows that the hydrated electron cannot have a structure like that of a chloride ion.

Perhaps the most interesting aspect of the overlap data in Table 3.1 is that there is relatively little direct electron-water overlap in all of the various hydrated electron models; most of the electron density resides between the water molecules rather than on top of them, even in the LGS non-cavity and UMJ hybrid models. This idea suggests that the descriptor 'non-cavity' may not be ideal for the LGS model of the hydrated electron; despite the fact that there is no single large cavity to which the electron is confined, the label 'non-cavity' does not provide an accurate description as to where exactly the electron does reside. In light of our new calculations and reanalysis, we now feel that the LGS hydrated electron is better described as being an 'inverse plum pudding' model: the electron is a diffuse ball of charge which occupies multiple interstitial voids present between the water molecules, thus resulting in relatively little direct electron-water overlap (See Fig. 3.4). This picture is reminiscent of a kind of inverse Thompson 'plum pudding' model of the atom, which had electrons embedded as 'plums' inside a diffuse and spatially extended positive nucleus 'pudding.' When viewed this way, it is clear that the LGS and UMJ models of the hydrated electron simply provide an alternative way to arrange the water molecules around the charge density of

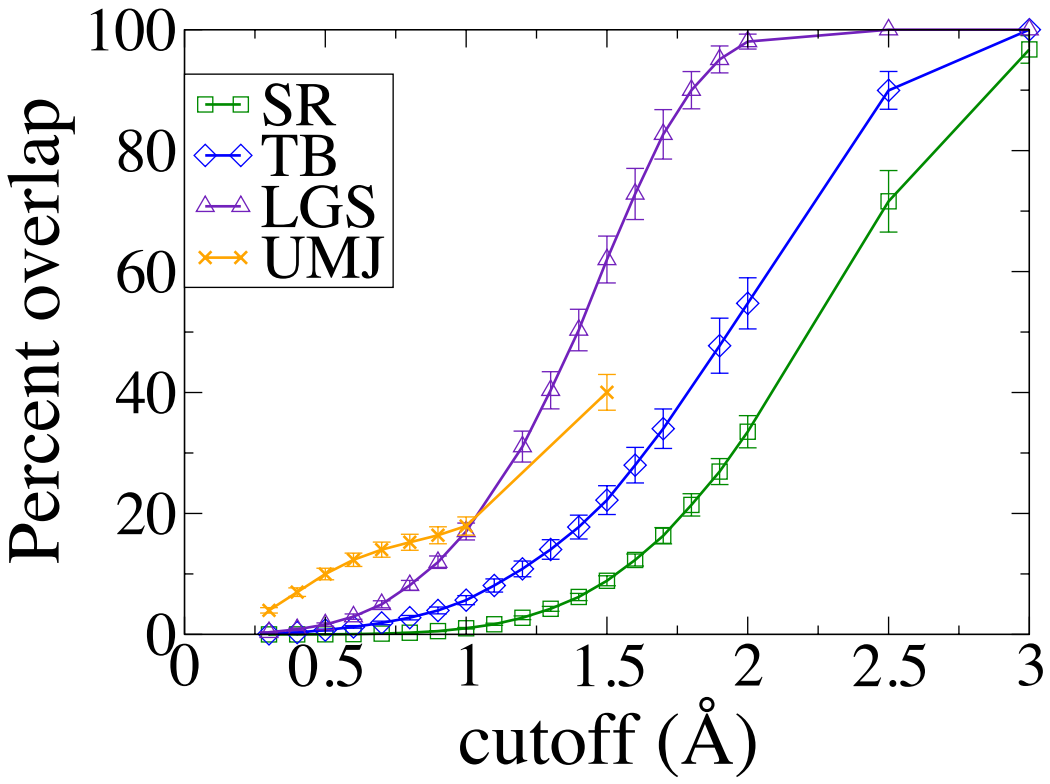

Figure 3.3: Calculated percent direct overlap between electron density and water density using different cutoff values (r_c) for the SR (green curve, squares), TB (blue curve, diamonds), LGS (purple curve, triangles), and UMJ (orange curve, crosses) models. Error bars represent one standard deviation.

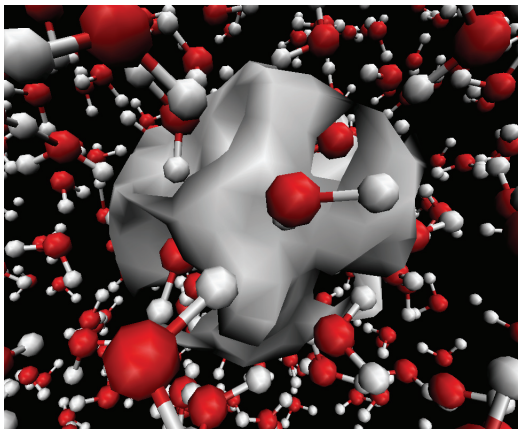

Figure 3.4: LGS water configuration from MD simulation, with exaggerated electron density contours for clearer illustration of inverse plum pudding effect.

the excess electron while minimizing the entropic cost of creating a cavity and disrupting liquid water's strong H-bonding network. In the end, all of the models have the electron density being repelled from the water molecules' core MOs, in accord with our intuition based on the Pauli exclusion principle. The main difference between the SR, TB, LGS, and UMJ pictures of the hydrated electron is the amount of radial overlap in each model. Thus, we now turn towards understanding how different amounts of radial overlap determine the level of agreement each model has with various experiments.

3.5 Comparing different hydrated electron models to experiment

Despite the differences in direct and especially radial overlap between the cavity, inverse plum pudding, and hybrid models of the hydrated electron, all of them do a decent job at predicting basic experimental observables, making it difficult to immediately eliminate any one model. For example, experiment has shown that the hydrated electron has a radius of gyration of 2.45 Å,[56] while the SR, TB, and LGS hydrated electrons have radii of gyration of 2.25 Å,[64] 2.42 Å,[9] and

2.5 Å,[12] respectively. The UMJ hydrated electron, on the other hand, shows large fluctuations in the radius of gyration ranging from 2.4 Å to 4.5 Å, with a mean value of 2.8 Å.[17] Thus, even though it has not yet been calculated, the large average value and spread in the radius of gyration of the UMJ model suggests that its optical absorption spectrum would be broadened and red-shifted compared to experiment. It should be noted that all of the values for the radius of gyration reported here were obtained by the minimum-image convention, as the radius of gyration is dependent on the way in which the long-range interactions are treated, i.e. whether one chooses to use minimum-image convention or Ewald summation.[14] Given that the SR, TB, and LGS one-electron models all have roughly the correct radius of gyration, they all predict an optical absorption spectrum of the hydrated electron in reasonable agreement with experiment. The SR cavity model predicts an optical absorption band that is blue-shifted relative to the experimental band by about 0.7 eV,[64] but the absorption band shifts into significantly better agreement with experiment when a mathematical error in the derivation of the SR pseudopotential is corrected.[28] The TB cavity model and the LGS inverse plum pudding model both predict an optical absorption spectrum of the hydrated electron that agrees very well with what is seen experimentally, although the calculated absorption maximum is slightly too blue for the TB model and slightly too red for the LGS model.[9, 12]

To further investigate the relationship between different models' predicted optical absorption spectrum and experiment, Herbert and Jacobson used long-range-corrected time-dependent density functional theory (TD-DFT) to take many-electron effects into account when calculating the absorption spectrum for configurations extracted from various one-electron simulation models of the hydrated electron.[31] What these authors found from their TD-DFT calculations is that the TB model has an absorption spectrum that is in excellent agreement with experiment, whereas the LGS model gives a spectrum that is $\sim$0.5 eV too red,

and the authors' polarizable model (which they call PWEP-2) gives a spectrum that is ∼0.4 eV too blue. Although we understand the impetus for grafting many-electron effects onto calculated properties of the hydrated electron, we note that the configurations used as input for these calculations were still generated from one-electron calculations (which themselves are based on pseudopotentials that are derived either empirically or at the Hartree-Fock level of theory), so that it is not clear that the calculations themselves are internally consistent. Moreover, because of the computational expense involved, these authors were able to explicitly include only a few tens of the closest water molecules to the electron's COM in their TD-DFT calculations. This limitation puts the LGS model at a distinct disadvantage since the calculation includes mostly the interior waters, and not the large number of exterior waters whose polarization helps to bind the electron and reduce the radius of gyration to what is seen experimentally, explaining why the spectrum calculated this way is overly red-shifted.

So it seems that no matter what the level of theory, any calculation that gives an electron with a radius of gyration close to 2.45 Å will give an absorption spectrum that is reasonably consistent with experiment, whether or not the electron has interior water molecules. It is for this reason why we turned to the experimentally known temperature dependence of the hydrated electron's absorption spectrum to distinguish between these different models. Experiments have shown that the maximum of the hydrated electron's optical absorption spectrum undergoes a roughly linear red-shift with increasing temperature (2.2 meV/K), even when the water density is held constant.[26, 27] Based on our calculated optical absorption spectra of the SR, TB, and LGS hydrated electrons at fixed density as a function of temperature (see Chapter 2), we found that the LGS inverse plum pudding model was able to capture the red-shift with increasing temperature, but the calculated slope was about a factor of 2.4 larger than experiment. In contrast, the SR and TB cavity models showed no spectral shift with changing temperature

at constant density, giving a slope of zero or an effective error of infinity relative to the experimental slope. Thus, the calculated temperature dependence suggests that an inverse plum pudding picture is more consistent with experiment than a cavity picture of the hydrated electron. We attribute this agreement between the inverse plum pudding picture and experiment to the attractive features found in the LGS pseudopotential that were effectively smoothed away in the TB and other potentials.[54]

Another important feature of the hydrated electron's optical absorption spectrum is whether it is homogeneously or inhomogeneously broadened. For systems like the hydrated electron, which have the bulk of their absorption between a ground state and three quasi-degenerate and orthogonal excited states, polarized hole-burning experiments can be used to determine the degree of homogeneous broadening.[65] Early calculations based on the SR cavity model of the polarized hole-burning experiment predicted a clear polarized hole-burning signature and a homogeneous linewidth that is about half of the full linewidth.[66] Subsequent calculations using different cavity models, however, have been less clear about what the polarized hole-burning experiment should show for the hydrated electron.[67, 68, 11] The LGS model predicts a homogeneously broadened line; in this inverse plum pudding picture, librational motions of the interior waters cause the orientations of the three excited states to quickly rotate, so that absorption to each of the three states has the same width as the full spectrum.[12] The experimental results of the polarized hole-burning experiment on the hydrated electron also have not been clear-cut. Early experiments showed a clear polarized hole-burning signature,[69] suggesting an inhomogeneously broadened line, but the preponderance of later experiments have found no polarized hole-burning and thus conclude that the spectrum is homogeneously broadened.[70, 71, 72] Similar experiments have also concluded that the absorption spectrum of the solvated electron in methanol is homogeneously broadened.[70] Recently, Doan

and Schwartz discovered that there is a clear polarized hole-burning signature for solvated electrons in liquid acetonitrile; the spectroscopy indicates that the homogeneous linewidth is about half of the full linewidth.[73] Doan and Schwartz have argued that solvated electrons in acetonitrile must therefore occupy cavities, and that by extension, hydrated electrons (as well as solvated electrons in methanol and other solvents that are similar in polarity to acetonitrile but in which the solvated electron's absorption is homogeneously broadened) do not. Moreover, these authors have speculated that H-bonding solvents are less likely to form cavity solvated electrons than non-H-bonding solvents, because the free energetic cost to break up the H-bond network is simply too high to form a cavity.[73]

Beyond the optical absorption spectrum, probably the best experimental indicator of the structure of the hydrated electron comes from resonance Raman spectroscopy, which provides a direct measure of the changes in the local H-bonding environment associated with electronic excitation of the electron. Tauber and Mathies,[22, 23, 25] as well as Tahara and co-workers,[37] have measured the resonance Raman spectrum of the hydrated electron, and found that the O–H stretching band is red-shifted and broadened compared to that of bulk liquid water. In Chapter 2, we extended a semiclassical theory developed by Skinner and coworkers, which relates the O–H stretching frequency of a condensed-phase water molecule to the local electric field experienced by the water H atom,[38, 39, 40] to calculate the resonance Raman spectrum of the hydrated electron with the SR, TB, and LGS models (see Figure 2.4). We found that both of the cavity models predict resonance Raman spectra that are in qualitative disagreement with experiment: the cavity models predict O–H stretching bands that are narrower and blue-shifted relative to that of bulk water. In fact, the resonance Raman spectra of the SR and TB hydrated electrons are very reminiscent of the larger halides dissolved in water.[33, 34] Thus, the local breaking of water's H-bonding structure that is seen in cavity models of the hydrated electron is inconsistent with

the experimental resonance Raman spectrum. In contrast, the LGS inverse plum pudding model is able to correctly capture the red-shift and broadening of the O–H stretch seen experimentally. This is because the water molecules inside of the LGS electron density experience a variety of environments and orientations, leading to a broader spectrum than seen in pure water, and the higher density of water inside the electron leads to stronger H-bonding that helps contribute to the red-shift.[54]

To better understand how the hybrid picture of the hydrated electron compares to experiment, we also have calculated the resonance Raman spectrum for the UMJ model. Unfortunately, the DFT calculation performed by UMJ does not give information on the electronic excited states that are needed to calculate the displacement of the water O–H stretches upon excitation. Consequently, we used the approximation outlined in Chapter 2.5.2 to calculate the Raman spectrum, where instead of using the force-weighting method to calculate the contribution of each water molecule to the resonance Raman spectrum, we instead took advantage of the fact that equally weighting all molecules within 4 Å of the electron's center of mass provides a good approximation to the true resonance Raman spectrum.[54] We recognize that we are applying a correlation intended for classical water molecules to the quantum water molecules used by UMJ, and to ensure that this is an appropriate approximation, we plotted the electric field distribution of the pure quantum water molecules and found it to be very similar to the electric field distribution seen with the SPC/Flex water model. Because the electric field distribution seems to be relatively unchanged, we feel that it is acceptable to use this correlation to construct the resonance Raman spectrum for the UMJ hydrated electron. The orange crosses and curve in Figure 3.5 show the results, indicating that the UMJ model of the hydrated electron predicts a broader and more red-shifted O–H stretch than the cavity models, but is still unable to capture the experimental red-shift and broadening of the O-H stretch

compared to that of the pure water spectrum. This is because the presence of even a small central cavity breaks the local H-bond structure of the water, producing a qualitatively incorrect predicted Raman spectrum.

3.6 Conclusions

In this Chapter, we have reflected on the nature of the structure of the hydrated electron. Although there has been a lot of resistance to the idea that there may be water molecules in the interior of the electron's charge density, we have seen that in fact, there is relatively little direct overlap of the electron's wavefunction with the interior water molecules. Considering this idea in combination with the fact that *ab initio* calculations also suggest that there can be interior waters with a small amount of direct overlap, it seems that inverse plum pudding and hybrid structures must be considered with at least equal weight alongside the more traditional cavity models. Even the traditional cavity models have a significant amount of their charge density outside the first solvation shell, while the LGS inverse plum pudding model still has a deficit of water density right at the electron's center of mass (cf. Fig. 3.1 and Table 3.1), so distinguishing cavity vs. inverse plum pudding models involves a continuum more than a two-state approach. It is important to note that none of the models discussed here show perfect quantitative agreement with experiment, so the exact average structure of the hydrated electron is still unknown. Thus, the question we are asking in many ways is a semantic one: do we want our zeroth order picture for the structure of the hydrated electron to have a significant number of interior water molecules, or not? And how should we weigh the evidence from different one-electron and *ab initio* simulations to help us decide?

All of the models considered here provide good agreement with the experimental absorption spectrum and most of the pump-probe transient absorption

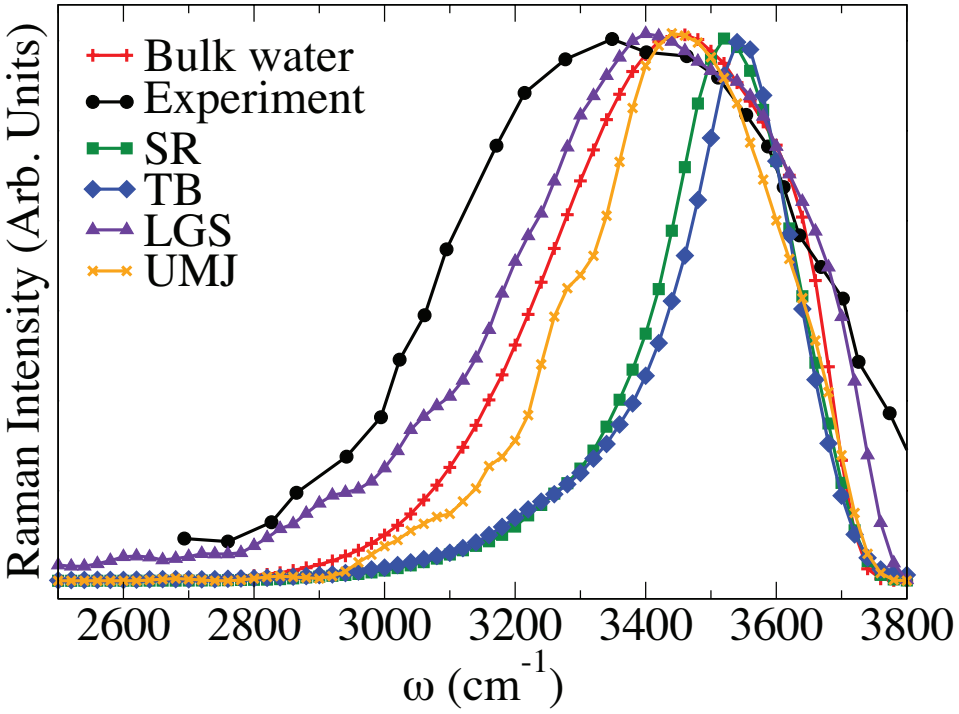

Figure 3.5: The experimental resonance Raman spectrum of the hydrated electron (black circles/curve, from Ref. [25]) compared to the calculated Raman spectrum for bulk SPC/Flex water (red plus signs/curve), the force-weighted calculated resonance Raman spectrum of the SR (green squares/curve), TB (blue diamonds/curve), and LGS (purple triangles/curve) models, and the 4 Å-cutoff calculated resonance Raman spectrum of the UMJ (orange crosses/curve) model of the hydrated electron. Both the SR and TB models produce Raman spectra that are blue-shifted and narrowed compared to the bulk spectrum, in stark contrast to the experiment, while the LGS model correctly predicts that the resonance Raman spectrum of the hydrated electron should be both broader and red-shifted relative to that of bulk water. The UMJ hybrid model's spectrum is broader and more red-shifted than the SR and TB cavity models spectra, but is still unable to capture the broadening and red-shift compared to the pure spectrum that is seen experimentally.

experiments[56, 69, 70, 74] that have been performed on the hydrated electron.[11, 66, 67, 68, 75] But given the variety of models that produce such similar predictions on this front, the question of whether or not there should be interior waters depends on the details of the potential between a water molecule and the excess electron. Figure 3.2 shows that based on quantum chemistry calculations, there should be attractive regions (beyond the simple Coulomb attraction of the excess electron to the positively-charged H atoms) in this interaction potential, at least at the one-electron level. These attractive features are entirely ignored in the TB and SR cavity models and are included to some extent in the LGS model, but the 'true' potential, if such a thing exists, appears to be right at the tipping point where interior waters become stable.[15, 13] *Ab initio* calculations aimed at this problem are also at their limits as it is a challenge to find functionals and basis sets that can describe the structure of an excess unpaired electron whose density resides almost entirely between the hundreds of water molecules that are needed to provide a converged structure. Thus, the best we can do at this point is examine how well each model can predict observables for the few experiments where the subtle differences between the various models can be discerned.

Perhaps the most sensitive measure of the balance between the attractive and repulsive terms in the electron-water interaction comes in the temperature dependence of the hydrated electron's optical properties. So far, none of the various cavity models have been able to reproduce the known red-shift of the experimental spectrum with increasing temperature at constant density, whereas the LGS inverse plum pudding model is in qualitative agreement with experiment, but overestimates the magnitude of the shift. The LGS model is also the only one that is able to capture both the red-shift and broadening of the resonance Raman O–H stretch spectrum of the hydrated electron relative to that of bulk water. Models that break the local H-bond structure of the water molecules nearby the electron, such as the cavity and hybrid models explored here, provide qualitatively incor-

rect predictions of the shape of the resonance Raman O–H stretching band (cf. Fig. 3.5). Thus, even though the LGS model does not provide quantitative agreement with experiment, it appears that its inverse plum pudding picture provides the most reasonable general agreement with experiment.

Given that there still is not consensus on the nature of the hydrated electron's structure, where can we go from here in terms of trying to further distinguish the various models against experiment? One example of potential interest is the behavior of the hydrated electron at interfaces. Our intuition says that the cavity and inverse plum pudding models of the hydrated electron should make dramatically different predictions as to whether or not the electron prefers to reside at the interface. For example, one might expect a cavity hydrated electron, which prefers to expel water molecules from its center, to preferentially localize at an interface, much like the larger halides.[76, 77, 78] Placing a cavity electron at the interface would limit the structure breaking effects of the hydrated electron, and make it easier for such an electron to locally expel the water molecules. On the other hand, a hydrated electron that contains a significant number of interior water molecules likely prefers to avoid the interface. This is because it would be difficult for an inverse plum pudding electron to have an increased interior water density at an interface where water molecules are scarce. Although there is not an abundance of experimental data on the behavior of hydrated electrons at interfaces, there is some indirect evidence that hydrated electrons prefer the bulk to the interface. For example, interface-sensitive second harmonic generation (SHG) experiments show no signals from samples in which hydrated electrons have been generated in the interior.[79] Moreover, pulse radiolysis experiments in silica pore glasses with $\sim$1-nm channel diameters have found no changes in the hydrated electron's absorption spectrum relative to that in bulk water,[80] again suggesting that the electron is avoiding the interface. There is some simulation work exploring the behavior of cavity electrons at air/water interfaces,[29, 60, 81]

and in Chapter 4, we make a detailed comparison between the behavior of cavity and inverse plum pictures of the hydrated electron at the air/water interface that provide yet another direct confrontation with experiment. Overall, even though the inverse plum pudding picture of the hydrated electron seems unconventional at first, the idea certainly has merit in that this model has proven to be more consistent with experiment than the traditional cavity picture.

CHAPTER 4

Exploring the Behavior of Cavity and Non-cavity Hydrated Electron at the Air/Water Interface

4.1 Abstract

As theory and experiment attempt to determine the true structure of the hydrated electron, many competing models have emerged. It has become imperative that we distinguish between these various models to determine the most accurate representation of the hydrated electron. In this Chapter, we explore the behavior of one-electron models in the presence of an air/water interface. Experimental work on interfacial hydrated electrons has been under debate recently, and we provide predictions as to what might be expected for cavity and non-cavity electrons. Through construction of Potentials of Mean Force, we have determined a complete picture of electron solvation in the bulk and at the interface. We find that while all one-electron models prefer bulk solvation (in large part due to the polarization potential), the TB cavity electron has a free energy local minimum located near the interface, allowing for some population of interfacial electrons to exist. These interfacial electrons have properties that are quite different from the bulk, which would lead to unique experimental signatures. The non-cavity electron's strong desire for enhanced water density prevents it from approaching the interface, resulting in bulk-like properties as close as 1 nm below the air/water surface.

4.2 Introduction

The hydrated electron, which is a free electron solvated by liquid water, has recently been at the center of much debate. This simplest of quantum mechanical solutes was first discovered by Hart and Boag in the early 1960s,[82] and has since proven to be an important reactant in many scientific fields, ranging from radiation chemistry to biochemistry.[1, 2] Although many spectroscopic signatures of the hydrated electron have been found, there is very little direct experimental evidence for the structure of this prominent species. One experiment that is often referenced is an Electron Paramagnetic Resonance (EPR) experiment performed by Kevan on alkaline glassy matrices held at 77 K.[4] This experiment produced the well-known 'Kevan structure,' where the hydrated electron occupies a cavity that is surrounded by six water molecules in an octahedral fashion.

This picture of the hydrated electron has prevailed for many decades, and was only recently challenged in light of new theoretical work on the hydrated electron.[12] Early mixed-quantum/classical (MQC) molecular dynamics (MD) simulations performed by Schnitker and Rossky (SR) found a cavity-bound electron that was reminiscent of the Kevan structure mentioned above (see Fig. 1.1 and Fig. 1.2A).[5, 6, 7] Turi and Borgis (TB) developed another MQC MD psuedopotential for the hydrated electron and found the structure of the hydrated electron to be similar to what was seen by SR. The TB hydrated electron resides in a smaller, four-coordinated cavity, but the general picture did not change. More recently, our group developed a more rigorous pseudopotential, yet saw completely different behavior from all previous one-electron calculations. We found that the electron resides in a region of enhanced water density, so that instead of carving out a cavity in the local water structure, the electron actually pulls water molecules into itself.[12] This non-cavity model is referred to as the LGS hydrated electron, and we find that its structure is best thought of as an inverse

plum pudding, where water molecules are embedded within the electron density (see Figure 3.4).[83]

Despite how different the cavity and non-cavity pictures are, each model has generally good agreement with various experimental observables that probe electronic structure, such as the optical absorption spectrum. The hydrated electron cavity and non-cavity models predict very similar electronic properties yet the non-cavity model still has met with significant resistance,[13, 14, 15] primarily based on its extreme sensitivity to subtle features in the psuedopotential.[83] We decided to test the robustness of cavity and non-cavity models by seeing how well they predict experimental observables that are sensitive to local water structure, such as the resonance Raman and the temperature-dependent optical absorption spectra. We discovered that the LGS non-cavity model is able to find qualitative agreement with these two experiments while the SR and TB cavity models cannot.[54] In this Chapter, we work to further distinguish between cavity and non-cavity models by exploring the hydrated electron at the air/water interface.

The air/water interface is a region of great interest as chemistry in this region is prominent in fields such as biochemistry and atmospheric chemistry.[2] In particular, there has been an interest in halide behavior at the air/water interface, and it was not until recently that both theory and experiment verified that certain anions do prefer solvation at the interface over solvation in the bulk.[84] Larger, more polarizable anions such as iodide prefer the interface while smaller, harder anions such as fluoride are found almost exclusively in the bulk. Anions of intermediate size, such as bromide, are sometimes predicted to be at the interface, although this depends heavily on the force-field used, with polarizable force fields leading to increased adsorption at the interface.[84] Based on the resonance Raman, cavity-bound electrons behave similarly to anions such as bromide, while the non-cavity electrons behave more like fluoride. If this is the true for the case of the air/water interface, then there should be significantly different signatures

between cavity and non-cavity electrons.[6, 54]

A common experiment utilized to study (potential) interfacial hydrated electrons is photoelectron spectroscopy (PES). Such experiments indicate that the hydrated electron is not found at the air/water interface.[85, 86, 87, 88] Siefermann et al. reported two ionization energies for the electron, one at 1.6 eV and one at 3.3 eV, which they attributed to the presence of both a surface bound and an interior hydrated electron.[89] No other experiment has been able to verify this finding, and so the consensus still is that the electron is absent from the air/water interface. The hydrated electron also has been probed with second harmonic generation (SHG) by Verlet and co-workers,[79] who used different surfactants to determine the possible location of electrons near the interface. They determined that the electron was not at the surface, but resided at least 1-2 nm below the surface, at which distance it retains its bulk-like properties. Another experiment of interest is pulse-radiolysis of water confined in 1 nm diameter silica pore glasses, from which it was discovered that hydrated electrons in 1 nm pores have the same absorption spectrum as electrons in bulk water.[80] This result also indicates that the electron avoids the interface. Although further experimental work is still being done, there is substantial evidence that the hydrated electron would not be found at the interface.

Theoretical studies have been performed by Madarasz and coworkers, who investigated the localization of the TB electron in the presence of an air/water interface.[90]. They found that the hydrated electron would initially localize at the interface, but would eventually move to the bulk after $\sim$10 ps. They also investigated temperature effects and found that at 0°C, the surface-bound state persists for hundreds of picoseconds. Jungwirth and coworkers examined their *ab inito* hybrid model near an air/water interface and found that the electron did reside at the surface, with some electron density protruding into the vacuum (usually below 10%, but sometimes as high as 30%).[81] Despite being at the

interface, they found that the election maintained many of its bulk properties such as structure and binding energy. Although these simulations give some idea of how the different hydrated electron models behave near an interface, we wanted to go a step further and calculate Potentials of Mean Force (PMF) and detailed structural characterization for the SR, TB, and LGS hydrated electrons. From the PMF, we can determine the relative stability of interfacial electrons compared to bulk, and we can understand what specifically makes solvation in different regions favorable.

4.3 Methods

4.3.1 Simulation details

We performed mixed quantum/classical (MQC) molecular dynamics (MD) simulations on one quantum mechanical electron and 499 SPC-Flex water molecules.[32] In order to create an interface, the x- and y-axis lengths of the simulation box were kept at $L = 24.64$ Å, while the z-axis was extended to $5L$. The quantum mechanical wavefunction was represented on a Fourier grid, whose size was altered to account for the increased size of the electron at the interface. We found that for the SR and LGS electrons, 32^3 grid points with a spacing of 0.56 Å were sufficient. For the TB electron, we chose a grid of size 18 Å $\times$18 Å $\times$ 20 Å for umbrella windows centered between 9 Å and 1 Å below the interface and a grid of size 20 Å $\times$ 20 Å $\times$ 20 Å for windows where the electron was at or above the interface; all TB grids have a grid spacing of 1.12 Å. Periodic boundary conditions were applied in all directions, and electrostatic interactions were calculated using 3D Ewald summation (EW3D), with $z = 5L$. In the past, we have used tapered spherical cutoffs centered at the oxygen atom to account for electrostatic interactions (see Chapters 2 and 3), and we will address the reason for our switch in methodology in Section 4.3.2. The adiabatic eigentstates were found at every

time step using the Lanczos algorithm,[91] and the quantum forces were evaluated using the Hellmann-Feynman Theorem with the Verlet algorithm used to propagate dynamics with a 1.0-fs time step.

It is common practice for the interface to be defined by the Gibbs dividing surface (GDS), which is the height where the average water density is equal to half the bulk density value. Recently, Willard and Chandler presented the idea of an instantaneous interface[92], which is based on a coarse-graining method that can be used to determine the local density in MD simulations. The instantaneous interface is defined as the two-dimensional surface where the local density is equal to half of the bulk density. The density is calculated through the following equation:

$$\tilde{\rho}(\mathbf{r}) = \sum_{i=1}^{N} \phi(|\mathbf{r} - \mathbf{r}_i|) \tag{4.1}$$

where N is the number of water molecules, $\{\mathbf{r}_i\}$ are the water oxygen atom positions, and $\phi(r)$ is a Gaussian-like smoothing function that comes from stitching together two cubic functions of r at $r = r_c$ under the following conditions: (a) $\phi(r)$, $\phi'(r)$, and $\phi''(r)$ are continuous at $r = r_c$; (b) $\phi(3\xi) = 0$; (c) $\phi'(0) = \phi'(3\xi) = 0$; (d) $\phi''(3\xi) = 0$; and (e) $\int_0^\infty 4\pi r^2 \phi(r) dr = 1$.[93] Like Varilly and Chandler, we chose r_c to be 2.1ξ, where ξ is the width of the represented Gaussian. We set ξ equal to 2.117 Å for water. We chose to include the electron in the definition of the instantaneous interface as well. It has been shown that while including the solute in the definition does not change the resulting PMF in a qualitative way, it can change it quantitatively.[94] The ξ parameters used for the SR and TB electrons are 2.404 Å and 2.444 Å, respectively. Because LGS does not approach the interface (as will be demonstrated later), there was no need to include it in the definition of the interface.

To construct Potentials of Mean force, we biased the distance between the electron and the point on the interface directly above the electron. Because the

electron's wavefunction cannot be directly biased due to the noncommutation of the Hamiltonian and umbrella potential, we used a method created by Borgis and Staib that instead allows us to bias the expectation value of the electron's position.[95] The umbrella potential used had the following form:

$$U = \frac{k}{2}(h(x_e, y_e; \mathbf{r}^N) - z_e - \widetilde{a})^2 \tag{4.2}$$

where k, the spring constant, is equal to 0.1 eV/Å^2, h is the z-coordinate of the point on the interface above the electron (it depends on both the position of the x and y coordinate of the electron center-of-mass, x_e and y_e, and the positions of all of the oxygen atoms which make up the interface, $\mathbf{r}^N$), z_e is the z-coordinate of the electron center-of-mass, and $\widetilde{a}$ is the biasing distance. Because the umbrella potential depends on the electron center-of-mass and the interface, both of which are dictated by the solvent molecules, the umbrella forces ultimately get applied only to the solvent molecules:

$$\begin{aligned} F^U_{\alpha i} = -k(h(x, y; \mathbf{r}^N) - z_e - \widetilde{a}) \cdot \Bigg[& \left(\frac{\partial h(x, y; \mathbf{r}^N)}{\partial x_e} + \left.\frac{\partial h(x, y; \mathbf{r}^N)}{\partial x}\right|_{x_e} \right) \\ & \cdot \frac{\partial x_e}{\partial r_{\alpha i}} + \left(\frac{\partial h(x, y; \mathbf{r}^N)}{\partial y_e} + \left.\frac{\partial h(x, y; \mathbf{r}^N)}{\partial y}\right|_{y_e} \right) \cdot \frac{\partial y_e}{\partial r_{\alpha i}} \\ & + \left(\frac{\partial h(x, y; \mathbf{r}^N)}{\partial z_e} - 1 \right) \frac{\partial z_e}{\partial r_{\alpha i}} + \frac{dh(x, y; \mathbf{r}^N)}{dr_{\alpha i}} \Bigg] \end{aligned} \tag{4.3}$$

where $\alpha = x, y, z$, and

$$\frac{dh(x, y; \mathbf{r}^N))}{d\mathbf{r}_i} = -\frac{\partial \widetilde{\rho}}{\partial \mathbf{r}_i} \Big/ \frac{\partial \widetilde{\rho}}{\partial z} \tag{4.4}$$

where

$$\widetilde{\rho}(x_e, y_e, h(x_e, y_e; \mathbf{r}^N); \mathbf{r}^N) = (1/2)\rho_l \tag{4.5}$$

Staib and Borgis used a perturbative approach to solve for terms like $\frac{\partial x_e}{\partial r_{\alpha i}}$, which then requires many electronic states to be calculated during the simulation and still does not guarantee an exact solution.[95] We found that the number of states

required (especially as the electron approached the interface) made the MQC simulations infeasible. Fortunately, an exact solution that does not require excited states exists for such expressions, which is what we utilized in this work.[96] We performed a minimum of 80 ps for each umbrella sample window, biasing to distances ranging from 1 Å above the interface to 9 Å below the interface for the case of SR and TB, and 4 Å to 9 Å below the interface for LGS. The decreased range for the LGS electron is a result of our inability to pull the LGS electron any closer to the interface without having the electron tear the interface apart in an attempt to keep increased water density inside of the electron. We performed the umbrella simulations at every 1 Å, resulting in a total of 11 simulation windows for SR and TB, and 6 simulation windows for LGS. These conditions guaranteed good sampling of our data. We then used the Multistate Bennett Acceptance Ratio (MBAR) method to properly unbias and stitch together the umbrella sampling windows.[97] We also used MBAR to properly weight samples when constructing radial distribution functions and optical absorption spectra.

4.3.2 The use of Ewald Summation versus spherical truncation for long-range electrostatics

As mentioned previously, we have used EW3D to account for our long-range electrostatic interactions. It has been well established that spherical truncation methods can lead to quantitative differences when investigating interfaces, in particular with regards to the electrostatic potential.[98, 99] We also have found that the use of spherical truncation can lead to a dramatically different PMF. We calculated the PMF for the test case of iodide in the presence of an air/water interface using both spherical truncation and EW3D with an extended z-coordinate of $5L$. We used the same simulation parameters as those outlined above for the electron case. We decided to include iodide in the definition of the interface, and we used $\xi = 2.117$ Å for Iodide (the ξ parameter remained the same for water). The iodide

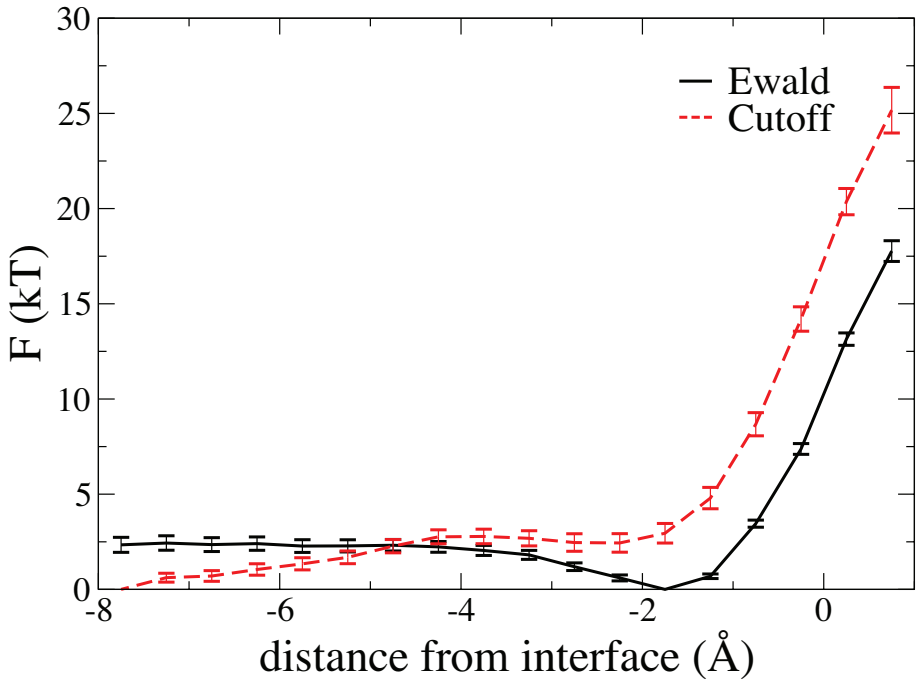

Figure 4.1: The Potential of Mean Force between iodide and the instantaneous interface when using 3D Ewald summation (black, solid curve) and spherical truncation (red, dashed curve) for the treatment of long-range electrostatics. All error bars presented represent one standard deviation.

Lennard-Jones parameters came from work done by Koneshan and coworkers.[100] We used 50-ps equilibrated umbrella sampling runs, with windows ranging from 8.5 Å below the interface to 0.5 Å above the interface. Our results using EW3D and spherical truncation are shown in Figure 4.1. The use of spherical truncation leads to iodide being preferentially solvated in the bulk, while the use of EW3D shows preferential solvation of iodide near the interface. The interfacial PMF is sensitive enough to the electrostatics of a system that we obtain a qualitatively incorrect PMF when using the spherical truncation scheme, as it has been well established that iodide is preferentially solvated at the interface.[94]

We should also address the fact that we used EW3D rather than 2D Ewald

summation (EW2D). This is common practice in the literature [90, 94], as EW2D is prohibitively expensive given the quantum mechanical nature of our system. Fortunately, EW3D does a good job of approximating EW2D if the z-coordinate is elongated by a factor of 5.[98] The small differences in the electrostatic potential found when using EW2D and EW3D have to do with the fact that with EW3D, there is an unphysical coupling between replicas of the interfacial dipole. A correction for this has been proposed (which we will refer to as EW3DC), and we have tested it on the iodide case mentioned above.[99] As can be seen from Figure 4.2, there are very slight differences in the PMF when we include this correction, although barely outside the noise of our calculation. The bulk becomes slightly destabilized with respect to the interface when the correction term is included, although it would seem that removing the artificial interface dipole interaction might stabilize the bulk solvation of iodide. Because the system is not neutral though, the added correction term requires that neutralization of the system is accounted for by two charged walls, which draws the iodide closer to the interface.[101] Ultimately, the correction makes a minor difference, and for the electron case, we decided it was best to follow precedent and use EW3D. We thus compare the SR, TB, and LGS models on an equal footing as far as electrostatics are concerned.

It should be noted that the use of Ewald summation causes a general red-shift in the LGS electron optical absorption spectrum, as pointed out by Herbert and Jacobson.[31] This red-shift seems to arise from large fluctuations in the radius of gyration, as indicated by the purple, dashed curve in Figure 4.7. Because of the extreme sensitivity of the interfacial PMF to the treatment of the long-range electrostatics (see Figure 4.1), it is critical that we use Ewald summation at the cost of the LGS optical absorption spectrum. In this study, we are interested in the differences between observables when the electron is at the interface versus the bulk, so we comment on relative differences between the interface and bulk

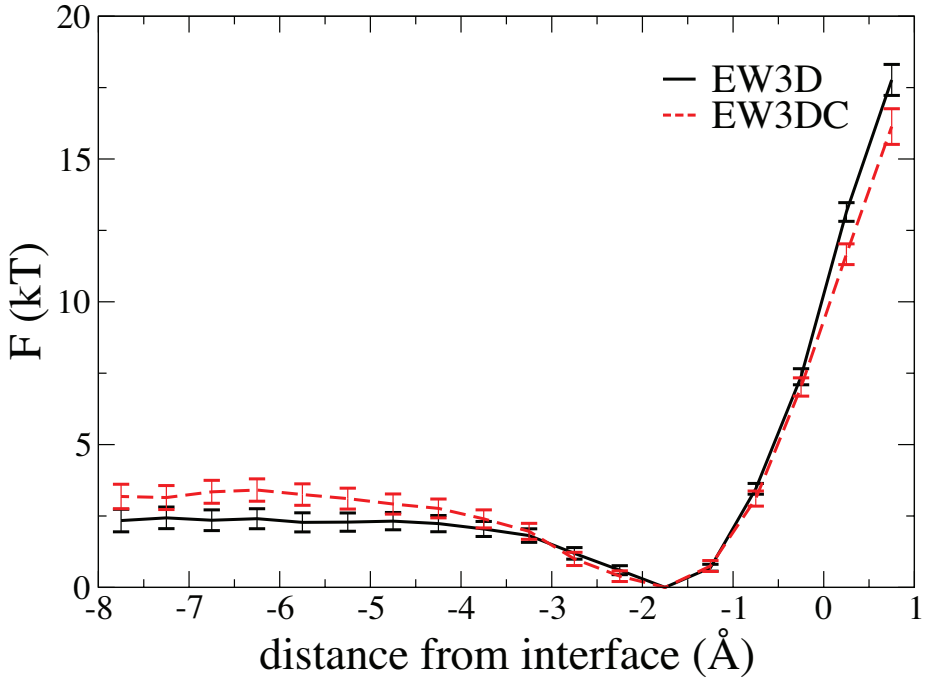

Figure 4.2: The Potential of Mean Force between iodide and the instantaneous interface when using 3D Ewald summation (black, solid curve) and a correction to the 3D Ewald summation (red, dashed curve).

that would be expected in experiments.

4.4 Results

4.4.1 Energetic properties of hydrated electron models relative to the air/water interface

The PMFs for the SR, TB, and LGS electrons relative to the instantaneous air/water interface are plotted in Figure 4.3. As expected, the LGS electron (blue, dashed curve) prefers to remain far from the interface. The LGS electron encounters a huge barrier to get to the air/water interface; to pull the LGS electron to within 5 Å of the interface costs almost 9 $k_{\mathrm{B}}T$. We were unable to bias

the LGS electron any closer than 4 Å below the interface or else the interface collapsed as the LGS electron pulled interfacial waters into itself; there is a strong desire for the LGS electron to maintain significant electron-water density overlap, as we discuss in Section 4.4.2.

From Figure 4.3, it is clear that the SR electron (black, dot-dashed curve) also prefers the bulk, although it is more likely to be found near the interface than the LGS electron. It at first seemed surprising that the SR electron would remain in the bulk despite its disruption to the local water structure, but this finding actually fits with what has been discovered about hard anions at the air/water interface.[84] Anion adsorption to the air/water interface is highly model dependent, with more polarizable force fields leading to greater stability at the surface. As mentioned above, Br^- is stable at the interface if polarizable force fields are used, and unstable if nonpolarizable force fields are used.[84] It makes sense then that the hard SR electron, which is dominated by repulsive interactions and is similar in size to a Cl^- or Br^- atom, is not found at the interface.

The TB electron also prefers bulk solvation, but unlike LGS, there only is a very small barrier and a local free energy minimum near the interface. The barrier to get to the interface is about 2 k_BT, while the barrier to return to the bulk from the interface is about 1 k_BT. The free energy maximum near 4 Å is related to the difficulty water has with solvating both the electron and the interface. As can be seen in Figure 4.4A, when the TB electron is around 5 Å from the interface, there are a few water molecules at the interface that can help solvate the electron, yet doing so disrupts their ability to favorably solvate the interface since water molecules within the first layer of the interface prefer to have one OH bond pointing into the vapor phase, leaving only one OH bond available for hydrogen bonding.[92] When the TB electron is ∼2 Å below the interface, as seen in Figure 4.4B, it has broken through the surface of the water layer, making it possible for interfacial water molecules to solvate both the electron and other

surface water molecules.

Because the TB electron is more polarizable and has a softer overall potential compared to SR, we find that the TB electron favors the interface more than the SR electron does. This implies that even though the SR and TB models are both cavity electrons, they are not equivalent when it comes to absorptivity to the interface. We noted some differences between the two models in Chapter 3 with our investigation into electron-water overlap and now we have another way in which the two cavity models differ. Previous experimental studies (such as the resonance Raman and temperature-dependent optical absorption) have indicated that the two cavity models are essentially the same, but we now have a way to potentially distinguish between cavity models.

In Figure 4.5, we have plotted the eigenvalue, E^Q (blue, solid curve), and the electron-water polarization energy, E^{POL} (red, dashed curve), for the TB (top panel, A) and LGS (bottom panel, B) models (further analysis will be done only on the TB and LGS models, as these are the two one-electron models heavily utilized in the field after a mistake was found in the derivation of the SR potential[28]). E^{POL} represents the polarization experienced by the water molecules due to the hydrated electron density, and it takes the form of $V_{pol} = -f(r)/2\alpha r^4$, where $f(r)$ is a short-range damping function that is slightly different for the TB and LGS models.[9, 12] As can be seen in Figure 4.5, E^Q and E^{POL} follow the same trend, indicating that it is the polarization energy that makes the bulk so favorable. This is an interesting point as the polarization models used in these MQC MD simulations are *ad hoc* and well-known to overestimate the water polarization due to a neglect of dipole induced-dipole interactions that effectively screen the polarization felt by the water molecules.[102, 103] By using this specific form of V_{pol}, we favor bulk solvation over interfacial solvation since E^{POL} is strictly attractive, thus causing preferential solvation in regions of higher water density. The TB and SR electrons might thus have a higher propensity to reside at the

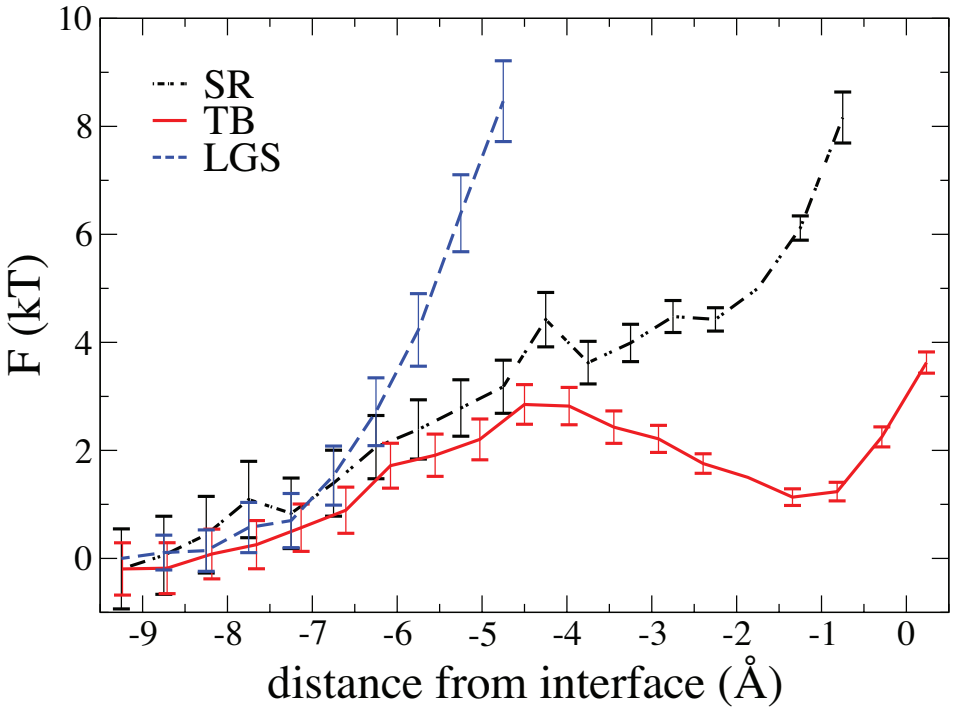

Figure 4.3: The Potential of Mean Force (Helmholtz Free Energy) between the SR (black, dot-dashed curve), TB (red, solid curve), and LGS (blue, dashed curve) hydrated electrons and the instantaneous interface. Negative distances indicate the height below the instantaneous interface.

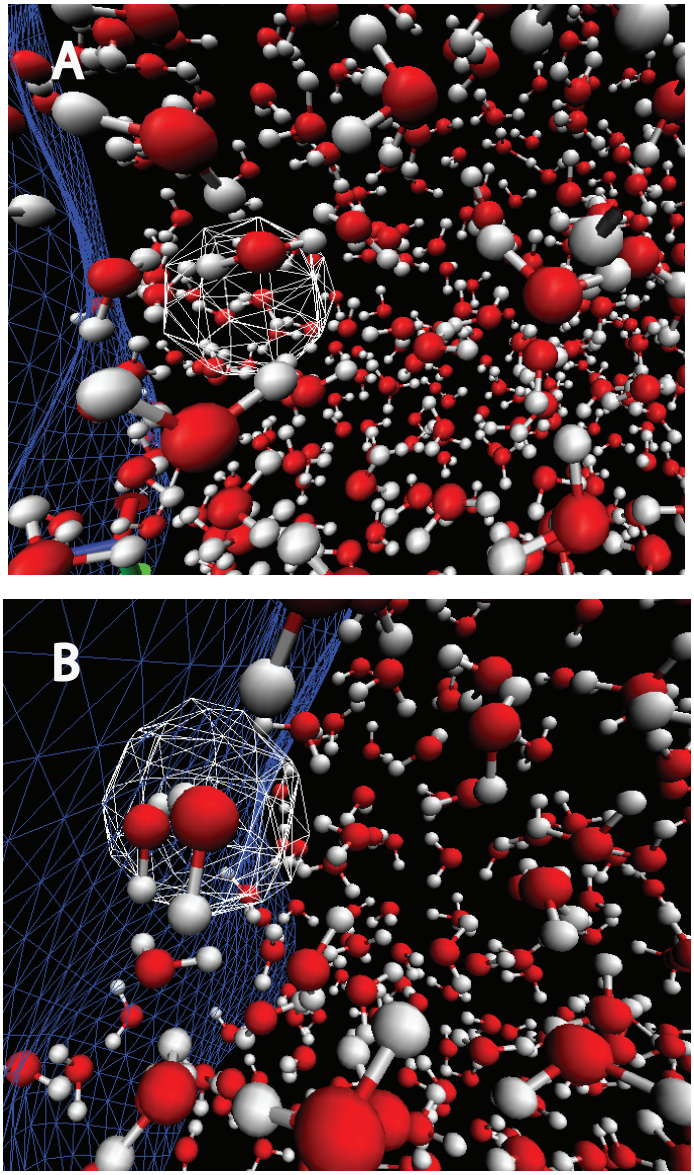

Figure 4.4: Snapshot of the TB electron within 5Å (A) and within 2Å (B) of the instantaneous interface.

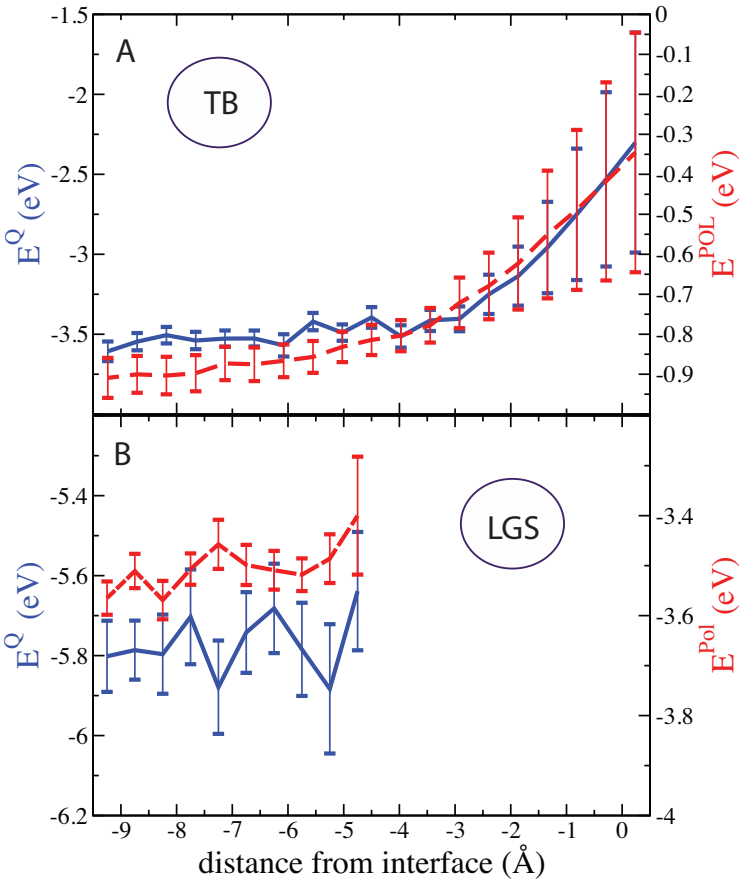

Figure 4.5: The TB (A, top panel) and LGS (B, bottom panel) electrons' quantum energy eigenvalue(right axis, blue solid curve) and electron-solvent polarization energy (left axis, red dashed curve). The LGS energies are only plotted up to 4 Å below the interface as that is as close as we can bias the LGS electron, see Section 4.3.1.

surface than indicted by our study, although we expect that the LGS electron will still strongly prefer the bulk as it is unable to get close to the surface, to keep its solvation intact. In the future, a more rigorous electron-water polarization is warranted for quantitative results. Because our simulations treat all three electron models with similar electron-water polarization potentials, we can safely make qualitative comparisons and predictions amongst the three models.

4.4.2 Effects on the radial distribution function as a function of distance from the air/water interface

We examined the radial distribution functions (rdfs) for the TB and LGS electrons at various distances along the PMF curve, as shown in Figure 4.6. Specifically, we plotted the rdfs for the TB electron (top panels, A and B) at the local minimum (1 Å below the interface, black curves), the maximum (4 Å below the interface, red curves), and global minimum (9 Å below the interface, blue curves) and we plotted the rdfs for the LGS electron (bottom panels, C and D) at the global minimum (9 Å below the interface, blue curves) and 5 Å below the interface (black curves). As can be seen in Figures 4.6C and 4.6D, there is no significant change in the oxygen and hydrogen rdfs when the LGS electron is 9 Å and 5 Å below the interface. The LGS electron remains similarly solvated regardless of its distance to the interface. We calculated the number of water molecules within 6 Å of the electron center of mass to see if the LGS electron still occupies a region of enhanced water density, even near the surface. We found that at 9 Å, 34.6 ± 0.8 waters occupied that volume while at 4 Å, 33.4 ± 0.9 occupied that volume. For this volume and normal density, only 30 water molecules are expected. Thus, there is still a higher density of water molecules inside of the LGS electron density, even when the electron is only 5 Å below the surface. Since we examined the number of water molecules within a radius of 6 Å from the electron center of mass, our calculation should encompass some part of the interface if the electron is biased to 5 Å. Yet the LGS electron still manages to pull enough waters into itself to keep its preferred solvation. This finding fits with our inability to pull the electron any closer than 4 Å to the interface, as such distances would make it impossible for the LGS electron to maintain its ideal water structure.

As for the the TB electron, it becomes substantially less solvated as it approaches the air/water interface, which is indicated by the rdf no longer approaching unity at long distances. As there are fewer water molecules near the surface, it

seems obvious that the interfacial TB electron would be less solvated than when in the bulk. The more interesting question is how the coordination number changes as the TB electron moves closer to the interface. We calculated the coordination number based on a first solvent shell size of 3.7 Å and found a coordination number of 4.5 ± 0.3, 4.1 ± 0.3, and 2.3 ± 0.3 water molecules for 9 Å, 4 Å, and 1 Å below the interface, respectively. From the TB oxygen rdf (see Fig. 4.6A), it is clear that the size of the first solvent shell also changes with the TB electron's distance to the interface, so to account for that, we calculated the coordination number using a cutoff value of 4.0 Å when the TB electron was 1 Å below the surface and found a value of 3.1 ± 0.4 first shell waters. Regardless of our definition, the TB electron has fewer coordinating water molecules when it resides at the interface. Another noticeable difference between the solvation of an interfacial and bulk TB electron is the size of the cavity. For all three distances from the interface examined here, the oxygen rdf turns on at approximately the same distance of 2 Å, yet the oxygen peak of the interfacial TB electron is shifted to a higher value. The increased cavity size is consistent with the increase in radius of gyration seen as the TB electron approaches the interface (see Figure 4.7). The TB electron's first solvation shell also becomes less structured when near the surface (see Figure 4.6B), which fits with the idea that the first solvation shell is severely disrupted.

4.4.3 Behavior of the optical absorption spectrum as a function of distance from the air/water interface

The optical absorption spectra for the TB (top panel, A) and LGS (bottom panel, B) electrons along various positions of the PMF are plotted in Figure 4.8. As in the case with the rdfs, we have looked at the TB electron at the local minimum (1 Å below the interface, black dashed curve), local maximum (4 Å below the interface, red dot-dashed curve), and global minimum (9 Å below the interface, blue solid curve) and the LGS electron at the global minimum (9 Å below the in-

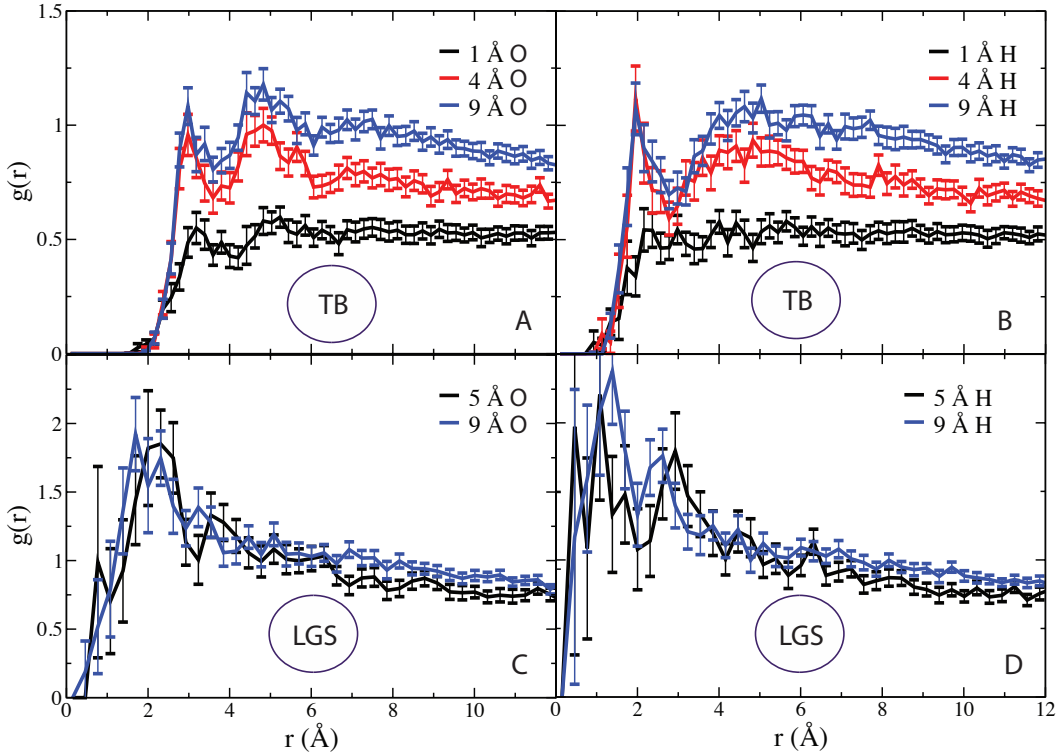

Figure 4.6: The radial distribution function (rdf) of the electron center of mass to the water Oxygen atoms (panels A and C) and to the Hydrogen atoms (panels B and D) for the SR (panels A and B) and LGS (panels C and D) hydrated electron models. For TB, the rdfs have been plotted for 1 Å below the interface (black and gray curves), 4 Å below the interface (red and pink curves), and 9 Å below the interface (blue and teal curves). For LGS, the rdfs have been plotted for 5 Å below the interface (black and gray curves) and 9 Å below the interface (blue and teal curves).

terface, blue solid curve) and 5 Å below the interface (black dashed curve). What is immediately obvious is the strong dependence both models' optical absorption spectra have on the location of the electron from the interface. The absorption spectrum of the TB electron undergoes a dramatic redshift as the electron approaches the interface. This result is consistent with the large fluctuations seen in the radius of gyration of the TB electron when it is near the interface (see Figure 4.7, blue curve). The TB electron goes from an average size of ∼2.5 Å to ∼3 Å, and the size fluctuations increase as the electron moves towards the interface. The LGS electron's optical absorption spectrum shows the opposite behavior, and a slight blue-shift is seen as the electron gets closer to the interface. This finding may also be consistent with a change in radius of gyration of the LGS electron as it approaches the interface, although the fluctuations in the radius of gyration are so large that is difficult to tell if the LGS electron is actually getting smaller within the noise. The size of the fluctuations makes it very difficult to know if the blue-shift is even physical.

These optical absorption results have important implications for experiment. Because the TB electron's optical absorption spectrum shifts by ∼1 eV, we would not expect TB electrons near the interface to behave like TB electrons in the bulk. In the SHG experiment performed by Verlet and co-workers,[79] they concluded that electrons might be present in the first layers of water, but that those electrons have the same properties as a bulk electron. The TB electron is inconsistent with these results, as we would expect some population of the TB electrons to be within 1 Å of the surface, which would lead to shifts of the optical absorption spectrum. The LGS electron is consistent with the experimental findings thus far, as it can be found within 9 Å of the interface yet retains its bulk properties. It seems that a TB cavity electron is too sensitive to the dramatic changes in solvation that are undergone from going to the bulk to the surface.

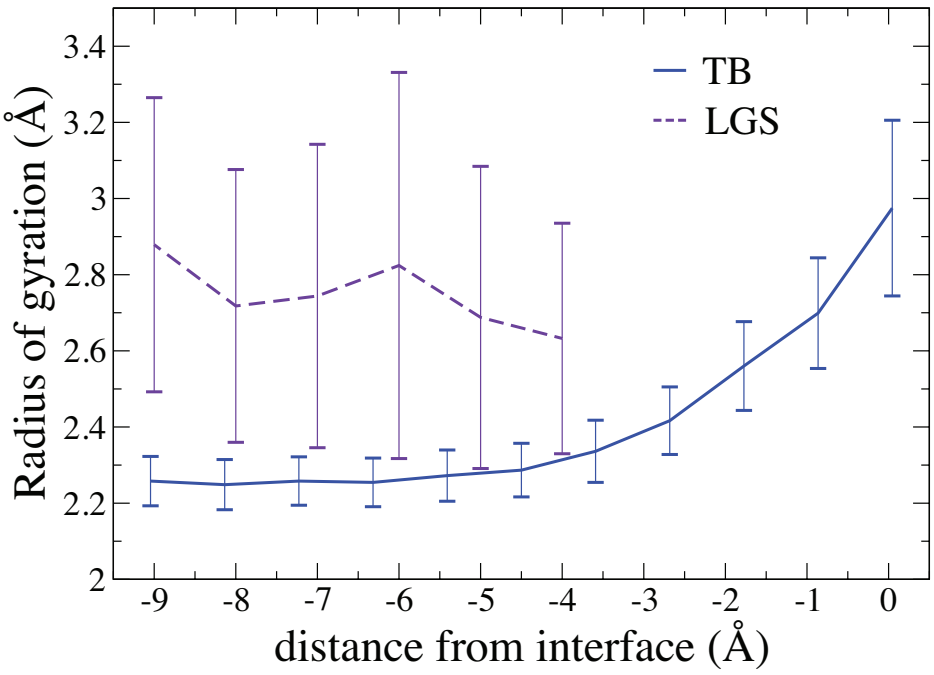

Figure 4.7: The radius of gyration of the TB (blue, solid curve) and LGS (purple, dashed curve) hydrated electron models plotted as a function of distance from the interface.

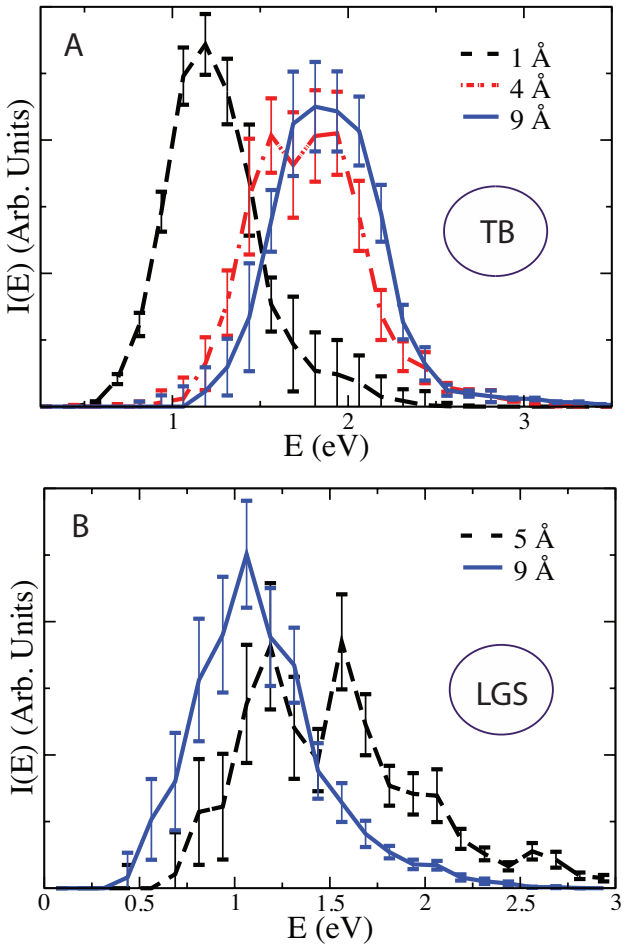

Figure 4.8: The optical absorption spectrum of the TB (top panel, A) and LGS (bottom panel, B) hydrated electron models at various distances along the Potential of Mean Force. The TB electron's optical absorption spectrum is plotted for 1 Å below the interface (black dashed curve), 4 Å below the interface (red dot-dashed curve), and 9 Å below the interface (blue solid curve) while the LGS electron's optical absorption spectrum is plotted for 5 Å below the interface (black dashed curve) and 9 Å below the interface (blue solid curve).

4.4.4 Determining the partial molar volume of one-electron models

With the implementation of the instantaneous interface, we are able to simulate quasi-constant pressure simulations, which can be used to determine the partial molar volume of the hydrated electron. Two experiments have been done to obtain this value, a radiolysis experiment at high pressures and a time-resolved photoacoustic study.[104, 105] The first experiment found the partial molar volume of the electron to be -5.9 cm^3/mol, while the second experiment found a value of +26 cm^3/mol, making it unclear as to even what the sign of this quantity should be. To calculate the partial molar volume of the electron, we used unbiased simulations of 50 ps and represented the interfaces on a grid of 100×100, with a grid spacing of 0.243 Å. We found a molar solvation volume of +29 ± 12 cm^3/mol, +31 ± 12 cm^3/mol, and -116 ± 27 cm^3/mol for the SR, TB, and LGS electrons respectively. These values agree with our intuition: the cavity electrons exclude water, resulting in an increased volume of the water slab, while the LGS electron pulls waters into itself, which should decrease the overall volume of the slab. The SR and TB partial molar volumes agree well with the photoacoustic experimental results. The LGS electron's partial molar volume has the same sign as the radiolysis experiments, but the magnitude is much greater. This fits with previous work done on the LGS non-cavity model. For example, the LGS electron overestimates the shift of the temperature-dependent optical absorption spectrum due to its overly attractive nature (see Chapter 2). This significant amount of attraction is manifest in our PMF calculation, as we find that the LGS electron always resides in a region of enhanced water density. The electron's partial molar volume is a very difficult number to obtain experimentally, and it is currently unclear as to what the true experimental value is. Regardless, the cavity models do find experimental agreement while the LGS model does not.

4.5 Conclusions

Through the construction of PMFs between various one-electron models and the instantaneous interface, we have provided another potential way to distinguish between the cavity and non-cavity pictures. The LGS non-cavity electron is very unlikely to be found at the interface, although it can be found around 1 nm away from the interface, at which point it retains its bulk properties. The TB cavity electron also favors bulk solvation, but there is a local free energy minimum around 1 Å below the surface, which is consistent with studies performed by Madarasz, Rossky, and Turi.[90] When the TB electron resides at the interface, its properties vary from those found in the bulk. The SR cavity electron resides primarily in the bulk with no local free energy minimum near the surface. These findings agree with work done on halides that show the extreme sensitivity of interfacial adsorption to electronic polarization.[84] Since the SR electron is defined by a more repulsive potential than the TB electron, we would expect the TB electron to have a greater propensity for interfacial solvation. This provides us with a way to distinguish between various cavity models, as differences between cavity pseudopotentials leads to different behavior at the air/water interface.

The treatment of water polarization in these one-electron MQC MD simulations is primarily responsible for the strong preference seen for bulk solvation. The polarization potentials used in these one-electron models are *ad hoc* and tend to overestimate the water-electron attraction, so we would actually expect to find more stability for interfacial electrons than presented here. In the future, it seems that a more robust treatment of water polarization is required to obtain quantitatively meaningful results.

Current experimental data seems to indicate that the hydrated electron is not solvated at the interface, or if it is, it retains its bulk-like properties.[88, 79] The TB electron disagrees with experimental findings, as when the TB electron

is near the interface, the optical absorption spectrum undergoes a dramatic red-shift. As for the vertical binding energy (VBE), it appears that the TB electron experiences little change from its bulk value of $\sim$3 eV. The LGS electron does fit with current experimental findings (except for the molar solvation volume), as the LGS electron avoids the interface, yet it is able to get within 1 nm of the surface. But unlike the TB electron, the LGS electron retains its bulk-like properties. From our results, a non-cavity electron is more fitting with what is seen experimentally. Taken together with other experiments which are sensitive to the local water structure around the electron (such as the resonance Raman spectrum or temperature dependent optical absorption spectrum),[54] it appears that the LGS non-cavity model is still the most appropriate one-electron picture we have of the hydrated electron.

APPENDIX A

Appendix

A.1 Information about source code

The source code I used for this work can be found on Bitbucket, which is a code repository located at https://bitbucket.org/. The code is entitled Na0_H2o. The source code is capable of outputting the necessary parameters for generation of optical absorption spectra (onedips.out). The parameters for the absorption spectrum print as long as the parameter *nstates* is greater than 1. The resonance Raman parameters (specifically the electric field on the H atoms, O-H stretch frequency, vibrational coordinate matrix element, transition dipole moment, isotropic transition polarizability, and force-weighting) are output to the file out.raman. In order to print these values, the parameter *raman_print* needs to be set to true. The parameter *nstates* needs to be set to a value greater than 1 for the Raman calculation in order for the force-weighting to be meaningful.

The instantaneous interface is turned on if the parameter *interface* is set to true. This extends the z-axis by *scalez*, another parameter than can be set. The instantaneous interface is printed out to out.intf_pos and out.intf_neg if the parameter *intf_print* is set to true. This will also print out the distance between the solute and the point on the interface directly above it to out.h_intf, regardless if an umbrella potential is being applied. The gridpoints that the interface are calculated over are defined by *grdwd* and *grdwdz*.

To perform umbrella sampling between the interface and a classical solute, set

the parameter *iumb* to 2. The parameter *const* sets the desired biasing distance (in Å) while the parameter *gk* defines the spring constant (in kJ/mol·nm^2). For a quantum mechanical solute, set *iumb* equal to 3. The parameter *uk* sets the spring constant (in eV/Å^2) while *uzeta* sets the biasing distance (in Å). To include the solute in the definition of the interface, set *interi* to true. The distance between the solute center of mass and the point directly above it on the instantaneous interface is output to out.h_intf, while out.h_intf_close gives the point closest to the solute on the instantaneous interface if *print_close* is set to true.

A.2 Information about analysis

The simulation output for the temperature-dependent optical absorption spectra can be found on the UCLA chemistry lead server under:

/mnt/fce1/schwartz/jrcasey/PROJECT_hydrated_electron/TD_Abs

The simulation output for the resonance Raman can be found on the UCLA chemistry lead server under:

/mnt/fce1/schwartz/jrcasey/PROJECT_hydrated_electron/Raman

The simulation output for the LGS, TB, and SR interface biasing windows can be found on the Schwartz storage under:

/volume1/homes/jrcasey/hydrated_electron_interface_LGS_PMF_NEW_1

/volume1/homes/jrcasey/hydrated_electron_interface_TB_PMF_NEW_1

/volume1/homes/jrcasey/hydrated_electron_interface_SR_PMF_NEW_1

The code used for analysis can also be found on Bitbucket, under Util. The absorption spectrum is calculated with absspec.f90, the electric field, O-H stretch frequency, and weighted O-H stretch frequency distributions are calculated by raman_plot.f90, and the radial distribution functions for the bulk and slab are calculated with rdfsol.f90 and rdfsol_intf.f90 respectively. The Potential of Mean

Force is calculated by umbrella-pmf.py, while umbrellaexpec.py calculates an unbiased expectation value from the biased umbrella windows. The code umbrella-expechist.py calculates unbiased histograms which can be used for the calculation of radial distribution functions or the optical absorption spectrum. When interested in another coordinate, indirect umbrella sampling can be done using umbrella-indirect-pmf.py and umbrella-indirect-expechist.py.

References

[1] L. Turi and P. J. Rossky. Theoretical studies of spectroscopy and dynamics of hydrated electrons. *Chem. Rev.*, 112:5641–5674, 2012.

[2] B. Abel. Hydrated interfacial ions and electrons. *Annu. Rev. Phys. Chem.*, 64:533–552, 2013.

[3] K. R. Siefermann and B. Abel. The hydrated electron: A seemingly familiar chemical and biological transient. *Angew. Chem., Int. Ed.*, 50:5264–5272, 2011.

[4] L. Kevan. Solvated electron structure in glassy matrices. *Acc. Chem. Res.*, 14:138–145, 1981.

[5] J. Schnitker and P. J. Rossky. An electron-water pseudopotential for condensed phase simulation. *J. Phys. Chem.*, 86(6):3462–3469, 1987.

[6] J. Schnitker and P. J. Rossky. Quantum simulation study of the hydrated electron. *J. Chem. Phys.*, 86(6):3471–3485, 1987.

[7] J. Schnitker and P. J. Rossky. The hydrated electron: Quantum simulation of structure, spectroscopy, and dynamics. *J. Phys. Chem.*, 92:4277–4285, 1988.

[8] L. Turi, M. P. Gaigeot, N. Levy, and D. Borgis. Analytical investigations of an electron-water pseudopotential. 1. Exact calculation on a model. *J. Chem. Phys.*, 114:7805–7815, 2001.

[9] L. Turi and D. Borgis. Analytical investigations of an electron-water molecule pseudopotential. 2. Development of a new pair potential and molecular dynamics simulations. *J. Chem. Phys.*, 117:6186–6195, 2002.

[10] L. D. Jacobson, C. F. Williams, and J. M. Herbert. The static-exchange electron-water pseudopotential, in conjecture with a polarizable water model: A new hamiltonian for hydrated-electron simulations. *J. Chem. Phys.*, 130:124115/1–124115/18, 2009.

[11] L. D. Jacobson and J. M. Herbert. A one-electron model for the aqueous electron that includes many-body polarization: Bulk equilibrium structure, vertical electron binding energy, and optical absorption spectrum. *J. Chem. Phys.*, 133:154506/1–154506/19, 2010.

[12] R. E. Larsen, W. J. Glover, and B. J. Schwartz. Does the hydrated electron occupy a cavity? *Science*, 329:65–69, 2010.

[13] L.Turi and A. Madarasz. Comment on Does the hydrated electron occupy a cavity?". *Science*, 331:1387c, 2011.

[14] L. D. Jacobson and J. M. Herbert. Comment on Does the hydrated electron occupy a cavity?". *Science*, 331:1387–d, 2011.

[15] R. E. Larsen, W. J. Glover, and B. J. Schwartz. Response to comments on Does the hydrated electron occupy a cavity?". *Science*, 331:1387e, 2011.

[16] T. R. Tuttle and S. Golden. Solvated electrons: What is solvated? *J. Phys. Chem.*, 95:5725–5736, 1991.

[17] F. Uhlig, O. Marsalek, and P. Jungwirth. Unraveling the complex nature of the hydrated electron. *J. of Phys. Chem. Lett.*, 3:3071–3075, 2012.

[18] D. Frenkel and B. Smit. *Understanding Molecular Simulation: From Algorithms to Applications*. Academic Press, 2001.

[19] J. C. Phillips and L. Kleinman. New method for calculating wave functions for crystals and molecules. *Phys. Rev.*, 116:287, 1959.

[20] C. J. Smallwood, R. E. Larsen, W. J. Glover, and B. J. Schwartz. A computationally efficient exact pseudopotential method 1. Analytical reformulation of phillips-kleinman theory. *J. Chem. Phys.*, 125:074102, 2006.

[21] A. Wallqvist, G. Martyna, and B. J. Berne. Behavior of the hydrated electron at different temperatures: Structure and absorption spectrum. *J. Phys. Chem.*, 92:1721–1730, 1988.

[22] M. J. Tauber and R. A. Mathies. Fluorescence and resonance Raman spectra of the aqueous solvated electron. *J. Phys. Chem. A*, 105:10952–10960, 2001.

[23] M. J. Tauber and R. A. Mathies. Resonace Raman spectra and vibronic analysis of the aqueous solvated electron. *Chem. Phys. Lett.*, 354:518–526, 2002.

[24] C. Nicolas, A. Boutin, B. Levy, and D. Borgis. Molecular simulation of a hydrated electron at different thermodynamic state points. *J. Chem. Phys.*, 118:9689–9696, 2003.

[25] M. J. Tauber and R. A. Mathies. Strucuture of the aqueous solvated elecron from resonance Raman spectroscopy: Lessons from isotopic mixtures. *J. Am. Chem. Soc.*, 125:1394–1402, 2003.

[26] D. M. Bartels, K. Takahashi, J. A. Cline, T. W. Marin, and C. D. Jonah. Pulse radiolysis of supercritcal water. 3. Spectrum and thermodynamics of the hydrated electron. *J. Phys. Chem. A*, 109:1299–1307, 2005.

[27] Y. Du, E. Price, and D. M. Bartels. Solvated electron spectrum in supercooled water and ice. *Chem. Phys. Lett.*, 438:234–237, 2007.

[28] R. E. Larsen, W. J. Glover, and B. J. Schwartz. Comment on An electron-water pseudopotential for condensed phase simulation". *J. Chem. Phys.*, 131:037101/1–037101/2, 2009.

[29] M. Boero, M. Parrinello, K. Terakura, T. Ikeshoji, and C. C. Liew. First-principles molecular-dynamics simulations of a hydrated electron in normal and supercritical water. *Phys. Rev. Lett.*, 90:226403/1–226403/4, 2003.

[30] D. M. Neumark. Spectroscopy and dynamics of excess electrons in clusters. *Mol. Phys.*, 106:2183–2197, 2008.

[31] J. M. Herbert and L. D. Jacobson. Sturcture of the aqueous electron: Assessment of one-electron pseudopotential models in comparision to experimetnal data and time-dependent density functional theory. *J. Phys. Chem. A*, 115:14470–14483, 2011.

[32] K. Toukan and A. Rahman. Molecular-dynamics study of atomic motions in water. *Phys. Rev. B: Condens. Matter Mater. Phys.*, 31:2643–2648, 1985.

[33] J. D. Smith, R. J. Saykally, and P. L. Geissler. The effects of dissolved halide anions on hydrogen bonding in liquid water. *J. Am. Chem. Soc.*, 129:13847–13856, 2007.

[34] P. N. Perera, B. Browder, and D. Ben-Amotz. Perturbations of water by alkali halide ions measured using multivariate Raman curve resolution. *J. Phys. Chem. Lett. B*, 113:1805–1809, 2009.

[35] H. C. Andersen, D. Chandler, and J. D. Weeks. Roles of repulsive and attractive forces in liquids: The equilibrium theory of classical fluids. *Adv. Chem. Phys.*, 34:105–156, 1976.

[36] F. Y. Jou and G. R. Freeman. Temperature and isotope effects on the shape of the optical absorption spectrum of solvated electrons in water. *J. Phys. Chem.*, 83:2383–2387, 1979.

[37] M. Mizuno and T. Tahara. Novel resonance Raman enhancement of local structure around solvated electrons in water. *J. Phys. Chem. A*, 105:8823–8826, 2001.

[38] S. A. Corcelli, C. P. Lawrence, and J. L. Skinner. Combined electronic structure/molecular dynamics approach for ultrafast spectroscopy of dilute HOD in liquid H_2O and D_2O. *J. Chem. Phys.*, 120:8107–8117, 2004.

[39] S. A. Corcelli and J. L. Skinner. Infrared and Raman line shapes of dilute HOD in liquid H_2O and D_2O from 10 to 90°C. *J. Phys. Chem. A*, 109:6154–6165, 2005.

[40] B. Auer, R. Kamar, J. R. Schmidt, and J. L. Skinner. Hydrogen bonding and Raman, IR, and 2D-IR spectroscopy of dilute HOD in liquid D_2O. *Proc. Natl. Acad. Sci. U.S.A.*, 104:14215–14220, 2007.

[41] W. H. Robertson and M. A. Johnson. Molecular aspects of halide ion hydration: The cluster approach. *Annu. Rev. Phys. Chem.*, 54:173–213, 2003.

[42] W. H. Thompson and J. T. Hynes. Frequency shifts in the hydrogen-bonded OH stretch in halide-water clusters. The importance of charge transfer. *J. Am. Chem. Soc.*, 122:6278–6286, 2000.

[43] D. Y. Wu and et al. Theoretical study of binding interactions and vibrational Raman spectra of water in hydrogen-bonded anion complexes: $(H_2O)^{-n}$ (n = 2 and 3), H_2O-X^- (X = F, Cl, Br, I), and $H\dot{}_2O$-M^- (M = Cu, Ag, Au). *J. Phys. Chem. A*, 112:1313–1321, 2008.

[44] A. Kahros and B. J. Schwartz. Going beyond the frozen core approximation: Development of coordinate-dependent pseudopotentials and application to Na^{2+}. *J. Chem. Phys.*, 138:054110/1–054110/9, 2013.

[45] D. Laria and M. S. Skaf. Path integral-molecular dynamics study of electronic states in supercritical water. *J. Phys. Chem. A*, 106:8066–8069, 2002.

[46] A. Madarasz, P. J. Rossky, and L. Turi. Interior and surface bound excess electron states in large water cluster anions. *J. Chem. Phys.*, 130:124319/1–124319/7, 2009.

[47] E. J. Heller. The semiclassical way to molecular spectroscopy. *Acc. Chem. Rev.*, 14:368–375, 1981.

[48] A. B. Myers. Resonace Raman intensities and charge-transfer reorganization energies. *Chem. Rev.*, 96:911–925, 1996.

[49] H. J. C. Berendsen, J. R. Grigera, and T. P. Straatsma. The missing term in effective pair potentials. *J. Phys. Chem.*, 91:6269–6271, 1987.

[50] H. J. C. Berendsen, J. P. M. Postma, W. F. van Gunsteren, and J. Hermans. *Intermolecular Forces*. Reidel, Dordrecht, 1981.

[51] R. A. Ogg. Physical interaction of electrons with liquid dielectric media. The properties of metal-ammonia solutions. *Phys. Rev.*, 69:668–669, 1946.

[52] R. N. Barnett, Uzi Landman, and C. L. Cleveland. Electron localization in water clusters. II. Surface and internal states. *J. Chem. Phys.*, 88:4429–4447, 1988.

[53] V. K. Voora, J. Ding, T. Sommerfeld, and K. D. A. Jordan. A self-consistent polarization potential model for describing excess electrons interacting with water clusters. *J. Phys. Chem. B*, 117:4365–4370, 2013.

[54] J. R. Casey, R. E. Larsen, and B. J. Schwartz. Resonance Raman and temperature-dependent electronic absorption spectra of cavity and noncavity models of the hydrated electron. *Proc. Natl. Acad. Sci. U.S.A.*, 110:2712–2717, 2013.

[55] T. R. Tuttle and S. Golden. Solvated electrons: What is solvated? *J. Phys. Chem.*, 95:5725–5736, 1991.

[56] D. M. Bartels. Moment analysis of hydrated elecron cluster spectra: Surface or internal states? *J. Chem. Phys.*, 115:4404–4405, 2001.

[57] J. M. Herbert and M. Head Gordon. Penetration and the origin of large O-H vibrational red-shifts in hydrated electron clusters, $(H_2O)^{-n}$. *J. Am. Chem. Soc.*, 128:13932–13939, 2006.

[58] Ondrej Marsalek, Frank Uhlig, and Pavel Jungwirth. Electrons in cold water clusters: An *ab initio* molecular dynamics study of localization and metastable states. *J. Phys. Chem. C*, 114:20489–20495, 2010.

[59] O. Marsalek, F. Uhlig, T. Frigato, and B. Schmitdt, and P. Jungwirth. Dynamics of electron localization in warm versus cold clusters. *Phys. Rev. Lett.*, 105:043002, 2010.

[60] A. Madarasz, P. J. Rossky, and L. Turi. Excess electron relaxation dynamics at water/air interfaces. *J. Chem. Phys.*, 126:234707/1–234707/11, 2007.

[61] O. Marsalek, F. Uhlig, J. Vandevondele, and P. Jungwirth. Structure, dynamics, and reactivity of hydrated electrons by *ab initio* molecular dynamics. *Acc. Chem. Res.*, 45:23–32, 2012.

[62] I. A. Shkrob, W. J. Glover, R. E. Larsen, and B. J. Schwartz. The structure of the hydrated electron. Part 2. A mixed quantum/classical molecular dynamics embedded cluster density functional theory: Single-excitation configuration interaction study. *J. Phys. Chem. A*, 111:5232–5243, 2007.

[63] J. M. Herbert and M. Head-Gordon. Charge penetration and the origin of large O-H vibrational red-shifts in hydrated-electron clusters, $(H_2O)^{n-}$. *J. Am. Chem. Soc.*, 128:13932–13939, 2006.

[64] J. Schnitker, K. Motakabbir, P. J. Rossky, and R. Friesner. A priori calculation of the optical-absorption spectrum of the hydrated electron. *Phys. Rev. Lett.*, 60:456–459, 1988.

[65] J. Yu and M. Berg. Local anisotropy and structural and phonon dynamics of permanganate (MnO_4^-) in glassy and liquid lithium chloride hexahydrate by ultrafast transient hole burning. *J. Phys. Chem.*, 97:1758–1764, 1993.

[66] P. J. Rossky and B. J. Schwartz. Pump-probe spectroscopy of the hydrated electron: A quantum molecular dynamics simulation. *J. Chem. Phys.*, 101:6917–6926, 1994.

[67] I. A. Shkrob. Pump-probe polarized transient hole-burning (PTHB) dynamics of the hydrated electron revisted. *Chem. Phys. Lett.*, 467:84–87, 2008.

[68] S. Bratos and J. C. Leicknam. Pump-probe absorption anisotropy of the hydrated electron. *Chem. Phys. Lett.*, 291:496–500, 1998.

[69] P. J. Reid, C. Silva, P. K. Walhout, and P. F. Barbara. Femtosecond absorption anisotropy of the aqueous solvated electron. *Chem. Phys. Lett.*, 228:658–664, 1994.

[70] M. C. Cavanagh, I. B. Martini, and B. J. Schwartz. Revisiting the pump-probe polarized transient hole-burning of the hydrated electron: Is its absorption spectrum inhomogeneously broadened? *Chem. Phys. Lett.*, 396:359–366, 2004.

[71] M. Assei, R. Laenen, and A. Laubereau. Dynamics of excited solvated electrons in aqueous solution monitored with femtosecond-time and polarizaiton resolution. *J. Phys. Chem. A*, 102:2256–2262, 1998.

[72] A. Baltuska, M. F. Emde, M. S. Pshenichnikov, and D. A. Wiersma A. Early-time dynamics of the photoexcited hydrated electron. *J. Phys. Chem. A*, 103:10065?10082, 1999.

[73] S. C. Doan and B. J. Schwartz. Nature of excess electrons in polar fluids: Anion-solvated electron equilibrium and polarized hole-burning in liquid acetonitrile. *J. Phys. Chem. Lett.*, 4:1471?1476, 2013.

[74] K. Yokoyama, C. Silva, D. H. Son, P. K. Walhout, and P. F. Barbara. Detailed investigation of the femtosecond pump-probe spectroscopy of the hydrated electron. *J. Phys. Chem. A*, 102:6957–6966, 1998.

[75] B. J. Schwartz and P. J. Rossky. Hydrated electrons as a probe of local anisotropy: Simulations of ultrafast polarization-dependent spectra hole burning. *Phys. Rev. Lett.*, 72:3282?3285, 1994.

[76] L. X. Dang. Characterization of water octamer, nanomer, decamer, and iodide-water interactions using molecular dynamics techniques. *J. Chem. Phys.*, 110:1526?1532, 1999.

[77] P. Jungwirth and D. J. Tobias. Ions at the air/water interface. *J. Phys. Chem. B*, 106:6361–6373, 2002.

[78] J. Rodriguez and D. Laria. Electronic states at the water/air interface. *J. Phys. Chem. B*, 109:6473?6478, 2005.

[79] D. M. Sagar, C. D. Bain, and J. R. R. Verlet. Hydrated electrons at the air/water interface. *Journal of American Chemical Society*, 132:6917, 2010.

[80] R. M. Musat, A. R. Cook, J. P. Renault, and R. A. Crowell. Nanosecond pulse radiolysis of nanoconfined water. *J. Phys. Chem. C*, 116:13104–13110, 2012.

[81] F. Uhlig, O. Marsalek, and P. Jungwirth. Electron at the surface of water: Dehydration or not? *J. Phys. Chem. Lett.*, 4:338–343, 2013.

[82] E. J. Hart and J. W. Boag. Absorption spectrum of the hydrated electron in water and aqueous solutions. *J. Am. Chem. Soc.*, 84:4090–4095, 1962.

[83] J. R. Casey, A. Kahros, and B. J. Schwartz. To be or not to be in a cavity? The hydratd electron dilemma. *J. Phys. Chem. B*, 117:14173–14182, 2013.

[84] D. J. Tobias, A. C. Stern, M. D. Baer, Y. Levin, and C. J. Mundy. Simulation and theory of ions at atmospherically relevant aqueous liquid-air interfaces. *Annu. Rev. Phys. Chem.*, 64:339–359, 2013.

[85] A. Lubcke, F. Buchner, N. Heine, I. Hertel, and T. Schultz. Time-resolved spectroscopy of solvated electrons in aqueous NaI solutions. *Phys. Chem. Chem. Phys.*, 12:14629–14634, 2010.

[86] Y. Tang, H. Shen, K. Sekiguchi, N. Kurahashi, T. Mizuno, and et al. Direct measurement of vertical binding energy of a hydrated electron. *Phys. Chem. Chem. Phys.*, 12:3653–3655, 2010.

[87] A. T. Shreve, T. A. Yen, and D. M. Neumark. Photoelectron spectroscopy of hydrated electrons. *Chem. Phys. Lett.*, 493:216–219, 2010.

[88] F. Buchner, T. Schultz, and A. Lubcke. Solvated electrons at the water-air interface: Surface versus bulk signal in low kinetic energy photoelectron spectroscopy. *Phys. Chem. Chem. Phys.*, 14:5837–5842, 2012.

[89] K. R. Siefermann, Y. Liu, E. Lugovoy, O. Link, M. Faubel, U. Buck, B. Winter, and B. Abel. Binding energies, lifetimes and implications of bulk and interface solvated electrons in water. *Nat. Chem.*, 2:274–279, 2010.

[90] A. Madarasz, P. J. Rossky, and L. Turi. Excess electron relaxation dynamics at water/air interfaces. *J. Chem. Phys.*, 126:234707, 2007.

[91] R. E. Larsen, M. J. Bedard-Hearn, and B. J. Schwartz. Exploring the role of decoherence in condensed-phase nonadiabatic dynamics: A comparison of different mixed quantum/classical simulation algorithms for the excited hydrated electron. *J. Phys. Chem. B*, 110:20055, 2006.

[92] A. P. Willard and D. Chandler. Instantaneous liquid interfaces. *J. Phys. Chem. B*, 114:1954–1958, 2010.

[93] P. Varilly and D. Chandler. Water evaporation: A transition path sampling study. *J. Phys. Chem. B*, 117:1419–1428, 2013.

[94] A. C. Stern, M. D. Baer, C. J. Mundy, and D. J. Tobias. Thermodynamics of iodide adsorption at the instantaneous air-water interface. *J. Chem. Phys.*, 138:114709, 2013.

[95] D. Borgis and A. Staib. Quantum adiabatic umbrella sampling: The excited state free energy surface of an electron-atom pair in solution. *J. Chem. Phys.*, 104:4776–4783, 1996.

[96] W. J. Glover, J. R. Casey, and B. J. Schwartz. Chemistry by fiat: The coupled-perturbed quantum umbrella sampling method. *Manuscript submitted*, 2014.

[97] M. R. Shirts and J. D. Chodera. Statistically optical analysis of samples from multiple equilibrium states. *J. Chem. Phys.*, 129:124105/1–124105/10, 2008.

[98] E. Spohr. Effect of electrostatic boundary conditions and system size on the interfacial properties of water and aqueous solutions. *J. Chem. Phys.*, 107:6342–6348, 1997.

[99] I. C. Yeh and M. L. Berkowitz. Ewald summation for systems with slab geometry. *J. Chem. Phys.*, 111:3155–3162, 1999.

[100] S. Koneshan, Jayendran C. Rasaiah, R. M. Lynden-Bell, and S. H. Lee. Solvent structure, dynamics, and ion mobility in aqueous solutions at 25°C. *J. Phys. Chem. B*, 418:4193–4204, 1998.

[101] V. Ballenegger, A. Arnold, and J. J. Cerda. Simulations of non-neutral slab systems with long-range electrostatic interactions in two-dimensional periodic boundary conditions. *J. Chem. Phys.*, 131:094107/1–094107/10, 2009.

[102] P. Stampfli. Theory for the electron affinity of clusters of rare gas atoms and polar molecules. *Phys. Rep.*, 255:1–77, 1995.

[103] V. K. Voora, J. Ding, T. Sommerfeld, and K. D. Jordan. A self-consistent polarization potential model for describing excess electrons interacting with water clusters. *J. Phys. Chem. B*, 117:4365–4370, 2012.

[104] R. R. Hentz and D. W. Brazier. Radiolysis of liquids at high pressures. X. The reaction H + OH^- and the partial molal volume of the hydrated electron. *J. Chem. Phys.*, 54:2777–2780, 1971.

[105] C. D. Borsarelli, S. G. Bertolotti, and C. M. Previtali. Thermodynamic changes associated with the formation of the hydrated electron after photoionization of inorganic anions: A time-resolved photoacoustic study. *Photochem. Photobio. Sci.*, 2:791–795, 2003.